Characterising the function of the systemic right ventricle in hypoplastic left heart syndrome using cardiac magnetic resonance imaging

Wong, James Kai-Bun

Awarding institution:
King's College London

Characterising the function of the systemic right ventricle in hypoplastic left heart syndrome using cardiac magnetic resonance imaging

Dr. James Kai-Bun Wong

Kings College London

Supervisors

Prof. Reza Razavi and Prof. Tobias Schaeffter

Thesis submitted to the University of London for the degree of *Doctor of Philosophy*

June 2017

Abstract

Background

Children born with hypoplastic left heart syndrome (HLHS) have a LV too small to support the circulation. They undergo surgery resulting in the right ventricle (RV) supporting the systemic circulation. Accurately assessing systemic RV function is challenging but important as patients experience early circulatory failure. MRI is well established as a tool for assessing congenital heart disease. The technology is advancing allowing us to study the impact of energy, motion and shape on ventricular function. Characterising these factors in relation to HLHS might provide new insights into this condition.

Methods

A stepwise approach was used:

1. Ventricular work and function were studied at varying heart rates using MRI catheterisation techniques to study the work of the heart and understand the causes of exercise intolerance.
2. Continuing the energetic theme; a non-invasive 4D flow MRI sequence was translated into a tool to study intra-cardiac kinetic energy (KE) a measure of the useful work of the heart. This metric was used to devise a new biomarker based on the ratio of ejected to total systolic KE -the particle energy ejection fraction (PE EF).
3. Finally, computational processing tools were employed to study how differ-

ent operations effect the shape and motion of the RV.

Results

The major findings were:

1. The systemic RV displayed good contractility and relaxation but preload (p <0.008) and stroke volume fell at higher heart rates indicating a limitation of blood flow due to the absence of a sub-pulmonary ventricle.
2. Early diastolic KE was adversely affected in HLHS by the presence of a larger left ventricle (LV) remnant which acts as a stiff non-compliant structure impeding relaxation. Altered KE indices meant we attempted to study a new metric of function based on KE - PE EF - which was lower in those with single ventricles (p <0.001) and LV dysfunction (p =0.01).
3. HLHS subjects receiving RV-to-pulmonary artery conduits compared to those receiving shunts demonstrated ventricular dilatation (p =0.001), increased sphericity (p =0.006) and reduced multi-axial strain which is a sensitive measure of function.

Conclusions

Novel MRI approaches were used to assess energy, shape and motion in the systemic RV. Characterising ventricular function in these terms provided new insights into HLHS pathophysiology. Refining and implementing these MRI techniques could help guide management of this difficult condition.

Table of Contents

List of Tables

List of figures

Acknowledgements

Firstly I would like to thank the children and families from the Evelina London Children's Hospital who so kindly agreed to be involved in this research. I am impressed by your bravery and willingness to help contribute towards our understanding of congenital heart disease. In return, I hope the results of this work will help to improve the care and treatment you receive.

Next I would like to thank my colleagues. I am indebted to my supervisors, Prof. Reza Razavi and Prof. Tobias Schaeffter for their invaluable help and support in bringing this work to a conclusion. The members of the Imaging Sciences Team at King's College London who collaborated to help translate the science and the ideas into clinical practice, including but certainly not limited to: Dr. Gerald Greil and Dr. Tarique Hussain for their encouragement and advice; Dr. Kuberan Pushparajah for his patience and experience and; Dr. Radomir Chabiniok for seeing the potential in this project and willingness to explore new ideas. Thank you also to the staff at the Evelina Hospital who allowed me to acquire additional research data.

Finally I dedicate this thesis to my parents, Holly and Danny, to my wife Philippa and our children Alexander and Caspar. Your love, support and patience made this possible.

J. Wong, June 2017

Abbreviations

2D	Two-dimensional
3D	Three-dimensional
4D	Four-dimensional
ANOVA	Analysis of Variance
ccTGA	congenitally corrected Transposition of the Great Arteries
CHD	congenital heart disease
CI	cardiac index
CO	cardiac output
CMR	cardiac magnetic resonance
DCM	dilated cardiomyopathy
Ea	arterial elastance or afterload
ECG	electrocardiogram
Ees	ventricular elastance or contractility
EF	Ejection Fraction
EDPVR	end diastolic pressure volume relationship
EDV	end diastolic volume
ESV	end systolic volume
ESPVR	end systolic pressure volume relationship
HLHS	hypoplastic left heart syndrome
KE	kinetic energy
kt-PCA	kt-principal component analysis
LAD	left anterior descending artery

LV	left ventricle
mBT shunt	modified Blalock-Taussig shunt
MRI	magnetic resonance imaging
PC	phase contrast
PE	particle energy
PV loop	pressure-volume loop
PVR	pulmonary vascular resistance
Qp:Qs	pulmonary to systemic blood flow ratio
RCA	right coronary artery
rf	radiofrequency
RV	right ventricle
RV-PA conduit	right ventricle to pulmonary artery conduit
SV	stroke volume
SVC	superior vena cava
SSFP	steady state free precession
TCPC	total cavo-pulmonary connection
TGA	transposition of the great arteries
TR	tricuspid regurgitation
VENC	velocity encoding
VSD	ventricular septal defect
VV EF	Ventricular Volumetric Ejection Fraction
XMR	magnetic resonance imaging with catheterization

Publications arising from this thesis

1. **Wong J,** Pushparajah K, de Vecchi A, Ruijsink B, Greil GF, Hussain T, Razavi R. Pressure-volume loop derived cardiac indices during dobutamine stress; a step towards understanding limitations in cardiac output in children with hypoplastic left heart syndrome. International Journal of Cardiology. International Journal of Cardiology 230 (2017) 439–446
2. **Wong J,** Lamata P, Rathod RH, Bertaud S, Dedieu N, Bellsham-Revell H, Pushparajah K, Razavi R, Hussain T, Schaeffter T, Powell AJ, Geva T, Greil GF. Right ventricular morphology and function following stage I palliation with a modified Blalock-Taussig shunt versus a right ventricle-to-pulmonary artery conduit. European Journal of Cardio-Thoracic Surgery (2016) 1–8
3. **Wong J,** Chabiniok R, Tibby SM, Pushparajah K, Sammut E, Celermajer D, Giese D, Hussain T, Greil GF, Schaeffter S, Razavi R. Exploring kinetic energy as a new marker of cardiac function in the single ventricle circulation. *J Appl Physiol* 125: 889–900, 2018.

Related work

Wong J, Chabiniok R, de Vecchi A, Dedieu N, Sammut E, Schaeffter T, Razavi R. Age-related changes in intra-ventricular kinetic energy: a physiological or pathological adaptation? Am J Physiol Heart Circ Physiol. 2016 Mar 15;310(6):H747-55.

Statement of conjoining work

Subchapters 4.1 and 5.1 contain brief descriptions of work that form the background prologue to the studies described in the remainder of each chapter.

Chapter 2.6

Giese D, **Wong J,** Greil G, Buehrer M, Schaeffter T and Kozerke S. Towards highly accelerated Cartesian time-resolved 3D flow MRI in a clinical setting. JCMR. 2014 16:42

Dr Giese is primary author. As second author my contribution was study planning, data collection, analysis and manuscript editing. Findings relevant to this thesis are described briefly in chapter 2.6.

Chapter 3.1

Pushparajah K, **Wong J,** Bellsham-Revell H, Hussain T, Valverde I, Bell A, Tzifa A, Greil G, Simpson J, Kutty S, Razavi R. Magnetic resonance imaging

catheters stress haemodynamics post-Fontan in Hypoplastic left heart syndrome. Eur Heart J Cardiovasc Imaging. 2016 Jun;17(6):644-51.

Dr Pushparajah is primary author. As second author my contribution was study planning, data collection, analysis and manuscript editing. Findings relevant to this thesis are described briefly in chapter 3.1.

Chapters 4

Chabiniok R, **Wong J,** Giese D, Nordsletten D, Shi W, Greil G, Rueckert D, Razavi R, Schaeffter T, Smith N. Flow analysis in cardiac chambers combining phase contrast, 3D tagged and cine MRI. Functional Imaging and Modelling of the Heart (FIMH): Lecture notes in Computer Science. 2013. Vol 7945: 360-369.

Dr Chabiniok is primary author. As second author my contribution was study planning, data collection and manuscript editing. The findings of this paper are not included in this thesis but represent the background work towards developing the computational analysis of kinetic energy described in chapter 5.2 and chapter 5.3.

Foreword

characterise

ˈkarəktərʌɪz/

verb

verb: **characterise**; 3rd person present: **characterises**; past tense: **characterised**; past participle: **characterised**; gerund or present participle: **characterising**;

1 describe the distinctive nature or features of.

2 (of a feature or quality) be typical or characteristic of.

The modern usage of the verb "*to characterise*" *arose* in the late 16th century from French *caractériser* or medieval Latin *characterizare* meaning ‘engrave' or 'inscribe’. Its true origin may extend as far back as the ancient Greek *kharaktērizein*, from *kharaktēr* ‘a stamping tool’

This thesis sets out to *characterise* the distinctive patterns and features that predominate in systemic right ventricles. Using a translational approach the work, energy and shape of the ventricle will be related to its function.

1. Introduction

1.1 Rationale

Single ventricle hearts are a rare but serious form of congenital heart disease (CHD). A healthy heart has two ventricles but patients with this condition have a heart that contains only one normal sized ventricle typically because the other is underdeveloped. One of the severest forms is hypoplastic left heart syndrome (HLHS) in which the left sided heart structures are too small to support the systemic circulation.[1] Underlying the severity of the condition is that it is uniformly fatal unless patients undergo a series of surgical operations starting soon after birth resulting in the right ventricle (RV) being used to support the systemic circulation, in place of the under-developed left ventricle (LV).[2 3]

As our experience of looking after children with this condition has improved increasing numbers of these children are surviving into early adulthood. However despite improvements in care they still experience a higher morbidity and a lower life expectancy compared to healthy children. This is even more pronounced in those with single RV hearts compared to single LV hearts where outcomes are markedly worse [4] and children with HLHS have the highest reported incidence of exercise intolerance. [5, 6] The adverse prognosis of patients with HLHS makes accurate characterisation of cardiac function and detection of early deterioration especially important in order to plan treatment strategies.

Many of our methods of functional assessment in this group of patients are insensitive to early dysfunction.[7] Patients experience significant symptoms including reduced exercise tolerance, fatigue and breathlessness before cardiac dysfunction is detected. In HLHS the absence of one ventricle combined with the necessary surgical procedures[2, 8] that are performed to save the lives of these children has the unintended consequence of altering the shape and motion of the heart.[9] Changes in cardiac shape and motion alter the normal path of blood through the chambers of the heart which in turn affect how the heart transfers its energy to the flowing blood. Energetic inefficiencies accumulate over thousands of heart beats. Studying the function of the heart in terms of shape, motion, blood flow and energy transfer and linking it to established methods of assessment may provide new insights into the pathophysiology underpinning this condition. This premise led to the development of this thesis to investigate the interplay of energy, motion and shape on ventricular function in those with hypoplastic left heart syndrome (HLHS) through the application of CMR techniques.

1.2 Structure of the thesis

The thesis is divided into 6 chapters.

Chapter 1 covers the necessary background to understanding this piece of work. It starts with the context of the research outlining the role of the healthy RV and how it differs to the LV and the physiological alterations and complications following surgical palliation for HLHS. The challenges of assessing RV

function are described and this leads onto how CMR techniques could be applied towards our understanding of cardiac shape, motion and energy. There is a critical appraisal of the application of these technique and their relationship to this thesis.

Chapter 2 outlines the research methodology. It provides justification for the techniques chosen including assumptions and limitations of the chosen methods. It links back into the background covered in the previous chapter.

Chapters 3, 4 and 5 are based around a number of published pieces of work or work in progress. Chapter 3 covers the assessment of ventricular work using XMR techniques and the unmasking of dysfunction through the use of pharmacological stress. The theme of cardiac energetics is further explored in Chapter 4. It outlines the validation of a new accelerated 4D flow MRI sequence, its application towards measuring intra-cardiac kinetic energy in HLHS, and the rationale for developing a new measure of function based around KE. Chapter 5 utilises computational processing and modelling techniques to build a cardiac atlas of ventricular shape in HLHS. Single institution datasets for rare conditions such as HLHS are often small in size. Through a collaboration with Boston Children's Hospital, the effects of the choice of surgical Norwood palliation on the three dimensional shape, motion and function of the ventricle is explored.

Chapter 6 brings together the individual concepts discussed in earlier chapters. It outlines: the contribution this thesis makes towards our understanding of the constraints imposed upon the systemic RV; contextualises the limitations of the data and; makes suggestions for future directions.

1.3 Background

This section provides an overview of the normal heart and the morphological differences between the right and left ventricles. As an introduction to the topic of single right ventricle physiology one must first appreciate the specificity of the right ventricle to pump to the pulmonary circulation and the adaptations of pumping under high pressure are incomplete. An overview of the different surgical stages of the Norwood procedure are provided. The burden of cardiovascular failure in patients with HLHS is described and the challenges of assessing function in this group of patients is provided with comments on key papers that have shaped our idea of cardiac function in this group of patients.

1.3.1 The normal heat

The normal heart is divided into a right and left side, each composed of an upper chamber known as an atrium and a lower chamber called a ventricle. Deoxygenated blood returns from the body and enters the right atrium, it fills the right ventricle which supports the low pressure pulmonary circulation. Oxygenated blood from the lungs returns to the left atrium, this in turn fills the left ventricle which supports the high pressure systemic circulation.

1.3.2 Differences between the right ventricle and left ventricle

The healthy RV and healthy LV are morphologically different and an understanding of these is important prior to exploring the changes that occur when the RV is used in place of the systemic LV. A healthy RV sits anteriorly in the chest behind the mediastinum. It is thin walled and crescenteric in shape with a sharp apex and curves over the ellipsoid shape of the LV. The RV pumps efficiently to the low-pressure pulmonary circulation. It has low wall mass and a large radius of curvature resulting in low wall tension. It is composed of three parts, the inlet and outlet portions and the apical trabecular section. Morphological classification (Table 1) is dependent on the apical section which is the most constant of these parts as the inlet and outlet portions can be malformed or absent in various forms of CHD. The ventricle is identified based on the pattern of the apical trabeculations. The RV has coarse trabeculations in contrast to the fine trabeculations of the LV. It has been postulated that thick trabeculations trap blood particularly in the apex, helping to smooth the intra-ventricular blood flow, and conserving momentum of blood. [10] The flow of blood moves in a gradual curvature between the basal and mid-ventricular portions before being ejected from the RV. This is in contrast to the LV where there is a more acute turn at the apex. [11] [12] This has no energetic advantages but acts to ensure blood is moved in and out of the ventricle in a “first-in first-out” model. The filling of the RV is more dependent on valve plane motion sweeping over blood whilst LV filling relies more on a suction-recoil effect which generates

more energetic momentum. As a consequence the LV, compared to the RV, has a larger early diastolic kinetic energy (KE) peak corresponding with the E wave inflow. [13] This point is explored further in Chapter 1.4.4.4 - Kinetic work.

The RV has two layers of fibres making up its myocardial wall. The subendocardial layer is responsible for longitudinal shortening and the subepicardial layer for circumferential shortening. The RV relies on longitudinal shortening for ejection. In comparison the LV has three layers allowing torsion, longitudinal and radial shortening to occur. The LV primarily contracts in a twisting motion to eject blood. Individual fibres shorten by only 10-15% however the LV is able to eject almost two-thirds of its end-diastolic volume. The muscle layers, fibre orientation and motion of the LV result in a more energetically effective process for pumping under high pressure. In healthy children and adults the RV afterload from the pulmonary artery pressure is much less than the LV afterload from the systemic blood pressure. This allows the RV to be energetically efficient despite the RV possessing a thinner wall and less layers of fibres than the LV. [14] The RV and LV are well designed for their respective jobs.

Anatomic Features	Right Ventricle	Left Ventricle
Trabeculations	Coarse	Fine
	Few	Numerous
	Straight	Oblique
Moderator band	Present	Absent
Papillary muscles	Variable	Two
	Small	Large
	Attach to septum	Attach to free wall
Atrioventricular valves	Apically offset	Basally sited
	Three leaflets	Two leaflets
Infundibulum	Well developed	Absent
Coronaries	One (RCA)	Two (LAD + circumflex)
Conduction system radiations	One	Two

Table 1: Anatomic features of the right and left ventricle. Adapted from Nadas' Pediatric Cardiology, 1992. [15] Where RCA is right coronary artery, LAD is left anterior descending artery.

1.3.3 Incidence of congenital heart disease

Congenital heart disease (CHD) represents a spectrum of conditions characterised by the abnormal development and maturation of the heart. It has a reported incidence of 0.8%, affecting about 7 cases in every 1000 life births. [16]

The causes of CHD are often multi-factorial comprising a complex interplay between genes and the environment. [17]

Congenital heart defects are typically divided into: (Figure 1)

1. lesions that cause abnormal *mixing* of blood between the right and left sided circulations
2. *obstructive* lesions that prevent the egress of blood from the heart or vessels
3. *cyanotic* lesions that prevent proper oxygenation of blood

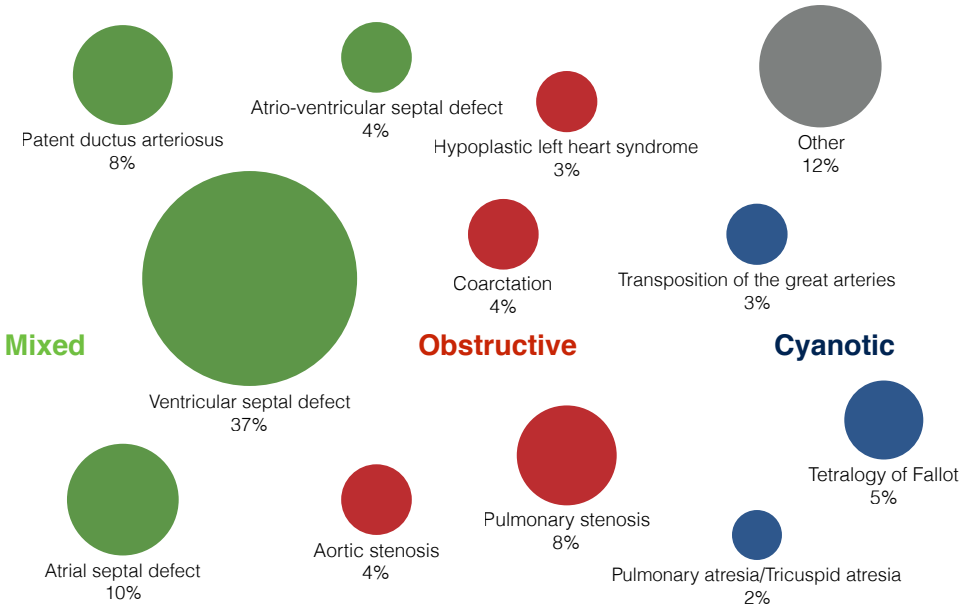

Figure 1: Bubble chart showing the relative incidence of different forms of congenital heart disease. The size of the bubble represents its incidence. The aetiology of lesions can be divided into mixed, obstructive and cyanotic causes. HLHS represents 2 - 3% of all cases of CHD.

1.3.4 Hypoplastic left heart syndrome

HLHS is an example of a single ventricle circulation. In HLHS the left sided heart structures are small and under-developed and unable to support the systemic circulation. (Figure 2). There is a spectrum of severity based on whether the valves on the left side of the heart are small and narrow (stenosis) or unformed (atresia). HLHS accounts for 0.016-0.036% of live births [18] and constitutes 2-3% of all cases of congenital heart disease. [13]

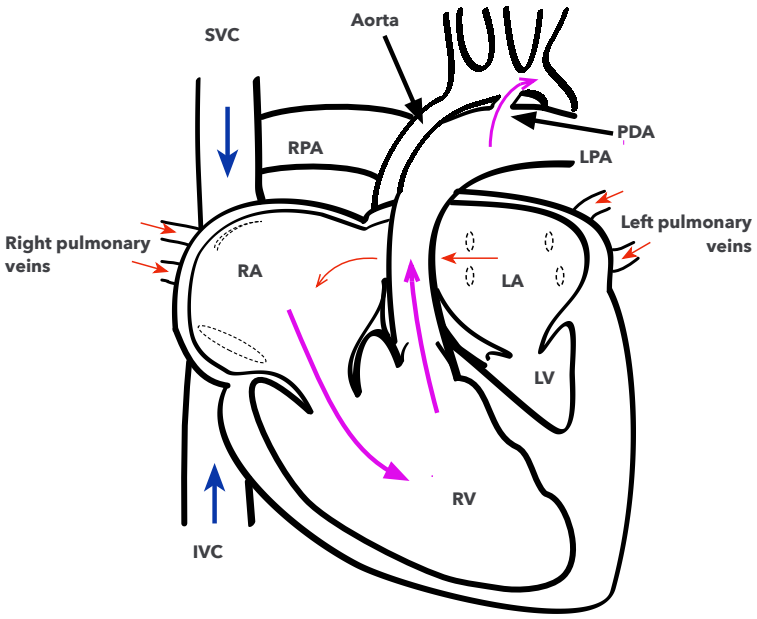

Figure 2: Circulation in HLHS soon after birth. Blue arrows represent deoxygenated blood, red arrows represent oxygenated blood and purple arrows represent blood of mixed origin. The above image demonstrates mitral and aortic stenosis with a hypoplastic LV. The small LV and arch mean systemic perfusion is dependent on mixing of blood across an atrial septal defect and a patent ductus arteriosus. Despite the hypoplastic LV and aortic arch the presence of the foramen ovale and ductus arteriosus permit adequate mixing of blood and systemic perfusion. Once the duct and foramen ovale close in the post-natal period this circulation becomes incompatible with life. Where: SVC -superior vena cava, IVC - inferior vena cava, RA - right atrium, LA - left atrium, RV - right ventricle, LV - left ventricle, RPA - right pulmonary artery, LPA - left pulmonary artery, PDA - patent ductus arteriosus.

Sudden death in the neonatal period can result from coronary and systemic under-perfusion or less commonly from congestion in the pulmonary venous system with hypoxia if there is restrictive inter-atrial communication which prevents blood form leaving the LA. [2] [3] In those with HLHS, where the LV is deemed too small to support a two-ventricle circulation, surgical palliation forms an important role. It typically consists of three staged operations resulting in the right ventricle providing systemic cardiac output. [19] The RV becomes a pressure loaded ventricle.

1.3.5 The pressure loaded right ventricle

Subjecting the RV to raised pressures changes its function. The physiological adaptations are important to understand as those with HLHS have a systemic RV. In patients with a two ventricle (biventricular) healthy circulation but with pulmonary hypertension, the RV must eject against a raised afterload. The ventricle dilates and hypertrophies. This dilatation and increase in wall thickness are in accordance with La Place's law:

$$\sigma \propto \frac{P\ \mathrm{r}}{\mathrm{h}}$$

where: σ = wall stress, P = pressure, r = wall radius, h = wall thickness

As the RV faces increased pressure and becomes more round, wall thickness

increases to maintain wall tension. Maladaptive cardiac growth and contractile dysfunction result from offsetting the increased wall stress. Alterations in myocardial proteins occur with decreased amounts of α-myosin heavy chain protein (MHC) relative to the β-MHC type of protein. The β-MHC protein contains less Adenosine Tri-Phosphate (ATP) than the α-isotope which in turn is associated with reduced systolic and altered energetic function. This, in combination with a decrease in coronary perfusion due to the thicker wall layer, may contribute to ischaemia and eventual heart failure. [20] The RV does not cope well when faced with systemic pressures and a much greater drop in ejection fraction (EF) is noted for every millimetre rise in mercury for the RV compared to the LV. [21]

Pressure-Volume (PV) loops illustrate the simultaneous change in ventricular pressure with volume over the course of the cardiac cycle (See chapter **1.4.5.2 Pressure-volume analysis** for more details). They provide some insight into the changes that occur when the RV is pressure loaded. The first PV loop of the RV was established in 1988 by a group at the Brompton Hospital (Figure 3). *Redington et al* [22, 23] compared healthy LV and RV pressure loops showing ill-defined isovolumetric periods in the RV with ejection continuing despite a pressure decline. This trapezoid shape is efficient when coupled to the low pressure circuit of the pulmonary vasculature.

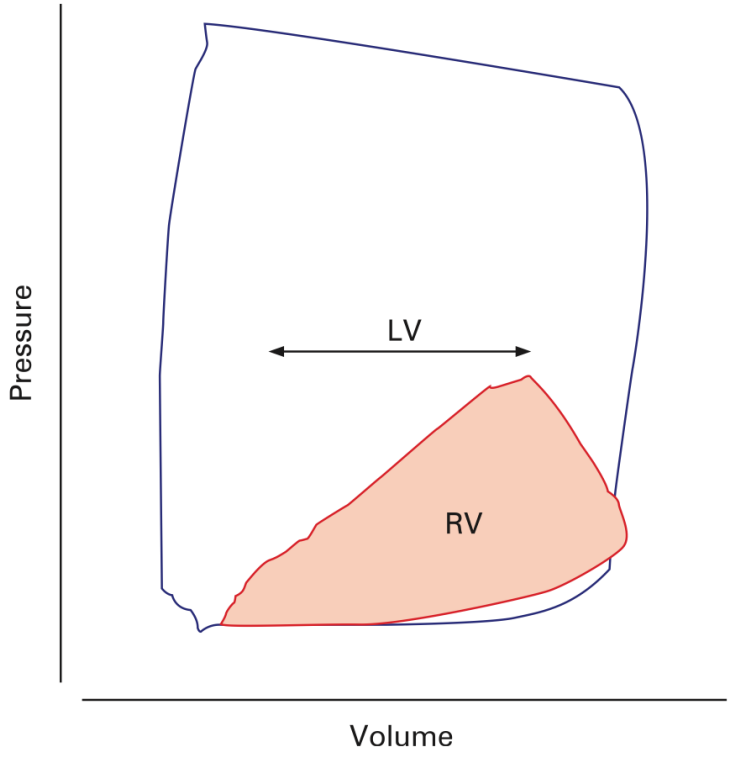

Figure 3: Typical pressure volume loops in the healthy LV and RV. Diagram curtesy of Sheehan, Heart 2008. Compared to the healthy LV the RV displays poorly defined isovolumetric contraction and relaxation intervals

In effect the RV works as a flow pump and experimental results from pig studies with induced pulmonary hypertension suggests it works at maximum efficiency rather than maximum coupling. As afterload increases it switches from a flow pump to a pressure pump with a corresponding fall in stroke volume and ejection fraction. [24] Exposing the RV to a gradual pressure load alters the shape of the PV loop to resemble a LV. Conversely the LV is also able to adapt. When the LV is in the subpulmonary position, such as following Mustard repair

(atrial baffle) for transposition of the great arteries (TGA), the LV PV loop comes to resemble that of the RV. [25]

The RV is highly sensitive to increased afterload. [26] Similar findings have been reported using echocardiographic techniques. [27] In young lambs the addition of a temporary outflow tract obstruction increases RV afterload and leads to a rise in end-systolic pressure and contractility [28] whilst over a longer period of time (application of a pulmonary arterial band) a decrease in cardiac output for the equivalent heart rate is observed. [29]

Congenitally corrected transposition of the great arteries (ccTGA) is an interesting example of a naturally occurring pressure loaded right ventricle within the context of a two ventricular circulation and demonstrates the importance of the ventricular-ventricular interaction. There is atrio-ventricular and ventriculo-arterial discordance of the ventricles. In effect the ventricles have swapped anatomical position. The RV receives oxygenated blood from the left atrium and pumps to the systemic circulation whilst the LV receives systemic venous blood and pumps to the pulmonary circulation. In the absence of any other lesion this condition may go undetected through childhood [30] as there are no outward signs or symptoms. Comparing those born with ccTGA to those having surgical creation of a systemic RV (atrial baffle groups in TGA) demonstrates the systemic RV undergoes a set of adaptive mechanisms that are more complete the closer to birth they occur. [27] However only 25% of those

with ccTGA without any significant associated lesion develop congestive heart failure by the fifth decade, rising to 67% in the presence of an associated lesion. [31] This is an example of the mechanical interdependence of the ventricles. The ventricular-ventricular interaction between the healthy LV and RV augments RV pressure generation and cardiac efficiency. [32] In unison, the RV enhances LV strain and radial motion via the motion of the septal wall. [33] Accordingly two ventricles albeit in a switched position (such as in ccTGA) function better than if there is an absence of one ventricle. [34] This in part explains why those with a single ventricle circulation do worse than those with a two ventricle circulation.

However the presence or absence of a second ventricle in relation to cardiac function is a simplification as this smaller ventricle is of a variable size. HLHS represents a spectrum ranging from a non-existent LV (typically a combination of mitral and/or aortic atresia) to a borderline sized LV (representing mitral and/or aortic stenosis). The shape and size of the remnant LV on RV function has been investigated. *Furck et al*[35] performed a 12 year review of a single centre's experience with the Norwood procedure. Those with mitral stenosis and aortic atresia had the worst outcomes. The large LV remnant in this subtype was proposed as a piggyback ventricle acting as a functional burden on the systemic RV with subsequent deleterious effects such as reduced posterior RV wall motion. [36] *Schlangen et al* [37] studied 57 HLHS patients and found the contractility of the systemic RV is unaffected by the size of the rudimentary LV but those

with the largest LVs have impaired diastolic relaxation as determined by the end diastolic pressure volume relationship. It is clear that the LV remnant plays a role on RV function. In ccTGA the well functioning LV supports the systemic RV, but in HLHS a small dysfunctional LV can be more detrimental than the complete absence of an LV to the systemic RV function. The energetic basis of this is examined in Chapter 4.1.

1.3.6 Stage I: - the Norwood procedure

A number of cardiac operations are performed in those with HLHS. An understanding of the impact of the different surgical procedures is important to help understand and explore the mechanisms that impede systemic RV function and to explain why patients experience a serious burden of comorbidity and premature circulatory failure. [38] The first stage, the Norwood procedure, is performed soon after birth with the aim of reconstructing the native aorta and arch, maintaining pulmonary perfusion via a shunt and promoting mixing of blood with an atrial septectomy. (Figure 4) Three available strategies exist. The hybrid strategy currently performed in a number of centres is not considered in this text as it is not a strategy currently employed at the Evelina Children's hospital and data is not readily available. Two variations of the Norwood procedure are discussed. The use of a Blalock-Taussig shunt was first suggested by *Norwood et al*. [2] The shunt procedure uses a hollow tube made of *polytetrafluoroethylene* (PTFE) to connect the innominate or subclavian artery to one of the branch pulmonary arteries allowing blood to *shunt* from the systemic circula-

tion to the pulmonary circulation. This is now done by a side-to-side anastomosis and is commonly known as a modified Blalock-Taussig (MBT) shunt. Early mortality following the Norwood procedure performed via a MBT shunt was initially 30 - 35%. This was primarily due to infants undergoing a rapid unpredictable fall in pulmonary vascular resistance in the post-operative period. This resulted in reduced systemic and coronary perfusion due to diastolic run-off of blood into the low pressure pulmonary circulation. [38]

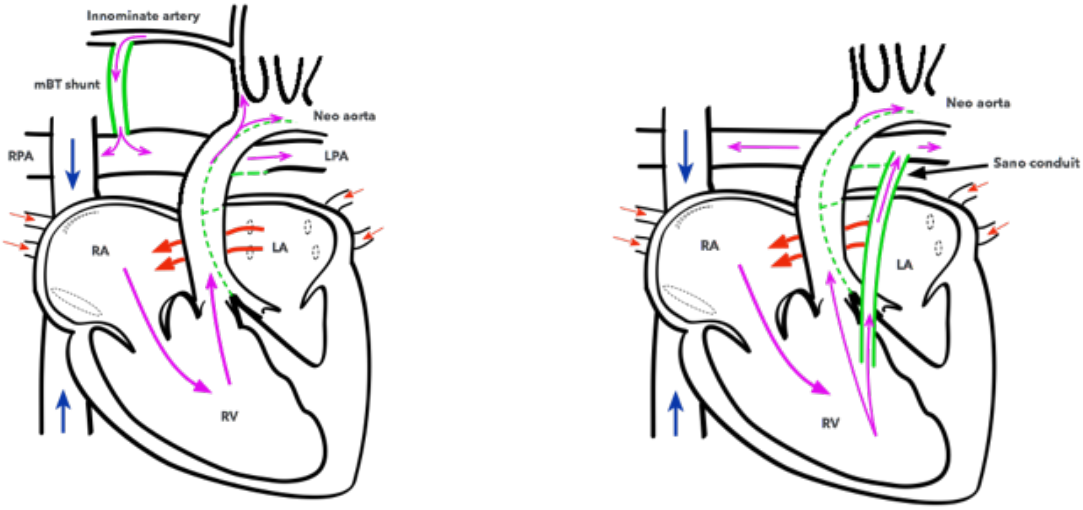

Figure 4: Stage I: Norwood circulation. Mixing of blood is maintained by performing an atrial septectomy. The arch is reconstructed using the main pulmonary artery and pulmonary circulation is maintained by inserting a shunt typically between the innominate artery and the branch pulmonary artery (MBT shunt) (seen on left) or via a right ventricle-to-pulmonary artery conduit (seen on right). The green dashed lines represent the reconstructed aorta. The solid green lines show the MBT shunt and Sano conduit.

In response to the early high mortality rates *Sano et al* [39] developed an alternative method to the MBT shunt consisting of a right ventricle-to-pulmonary artery (RVPA) conduit. A small incision known is a ventriculotomy is made on the superior surface of the RV and a hollow tube is used to act as a conduit to connect the RV to the pulmonary arteries. The initial data reported greater haemodynamic stability with improved short-term survival rates as, although blood could regurgitate into the ventricle through the valve-less conduit, systemic perfusion was maintained as there was no shunting effect that can cause a loss of diastolic blood pressure. As our understanding and experience has improved so has our management of this group of patients. This is reflected by some UK centres reporting a 30 day survival of 85-90%. [40]

1.3.7 Key studies underlying the choice of Norwood procedure

There is much interest over which type of Norwood procedure has the better outcomes for patients and many studies have been limited by small datasets or a lack of randomisation. The Single Ventricle Reconstruction Trial has attempted to answer this question. A large randomized North American study was designed, [41] it found the RVPA conduit was superior to the MBT shunt for the primary endpoint of death or transplant at 12 months however the RVPA conduit had significantly more interventions and complications. At inspection of the most recent data (3 years) there were no differences in transplantation free sur-

vival between the two groups. Echocardiographic measures of function found both RV end-diastolic volume (EDV) and EF superior for the RVPA conduit group up to Stage 2, but this had equalised between groups by 14 months of age. [42]

The trial results were remarkable in that they involved 555 patients across 15 different centres being randomised to either a MBT shunt of RVPA conduit and have represent the largest randomised study to date. However some of the enrolled centres operated only on a small number of patients and there was concern about bias as the smaller centres favouring the RVPA conduits had better results with this technique compared to more balanced results from larger centres. Furthermore there was a significant loss of patients to followup which weakens some of the end-points. Despite the equalisation of function at 14months and survival at 3 years of age, a number of questions remain. Regurgitation through the RVPA conduit in diastole results in ventricular volume loading. This would alter the shape of the ventricle as it has to pump an increased blood volume, but does this differ to the MBT shunt where the volume load is from a combined systemic and pulmonary venous return? The RVPA conduit requires a ventriculotomy to be performed in the systemic RV, after the conduit is removed a fibrous non-contractile scar is left which may have the longer term effects on function that are not yet discernible. Whilst answering the important question of which procedure is best for early and midterm mortality results, the SVR trial is limited by the use of how function is measured. Further-

more the use of ejection fraction to measure function is both a strength in regards to general utility but also a limitation as it is insensitive to early dysfunction. Could other measures be used to determine the impact of the two different operations? This idea was the basis for exploring the effects in functional terms of shape and motion. (See Chapter 5).

1.3.8 Stage II - the bidirectional superior cavo-pulmonary anastomosis

The second surgical stage is typically performed at 3 - 4 months of age as the child begins to outgrow the shunt. A direct anastomosis between the superior vena cava (SVC) and the pulmonary arteries is formed. This is known as a bidirectional superior cavo-pulmonary anastomosis because blood is able to flow from the SVC to either the right or left pulmonary arteries. (Figure 5) The shunt is also taken down resulting in venous return from the head draining directly to the lungs whilst venous return from the lower body still returns to the hert and mixes with oxygenated pulmonary venous flow. Stage 2 surgery reduces the volume overload on the dilated RV leading to improved ejection fraction. [43] It reduces the work of pulmonary blood flow and increases efficiency by directing desaturated venous blood flow to the lungs in comparison to the previous arterial-venous mixture. [38]

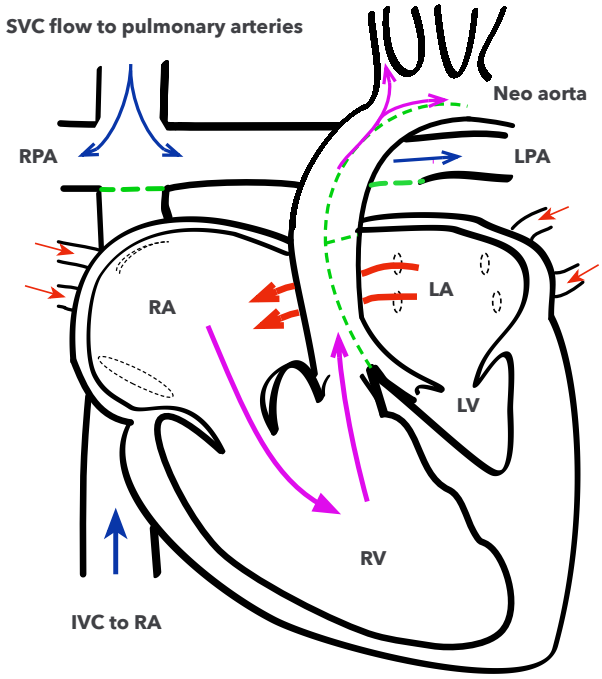

Figure 5: Stage II: Superior cavo-pulmonary anastomosis. At 3 - 4 months of age the shunt/conduit is taken down and a direct anastomosis between the superior vena cava and branch pulmonary arteries is performed to maintain adequate pulmonary flow.

1.3.9 Stage III - total cavo-pulmonary connection

At approximately 3 - 4 years the venous return from the head is diminished as the body grows and saturations dip due to arterial-venous mixing between pulmonary venous return and inferior vena caval flow. Surgical completion of a total cavo-pulmonary connection (TCPC), where the inferior vena cava blood from the lower body is also routed directly to the pulmonary arteries, creates a

Fontan circulation, [8] and results in an improvement in saturations. (Figure 6) The method of TCPC has now tended toward formation of a lateral tunnel (blood is baffled within the atrium) or extracardiac conduit (blood flows through a hollow tube around the outside of the atrium) with comparable outcomes [44, 45] though some studies [46] suggest those with a tunnel are susceptible to developing arrhythmias. In some centres a fenestration is created – in effect a small right to left connection. The addition of a fenestration mitigates early postoperative mortality but with the consequence of a decrease in arterial saturations which worsen during exercise and the increased risk of a paradoxical stroke. The benefits of closing the fenestration at a later date are not fully demonstrated. *Meadows et al* [47] investigated the closure of the fenestration in 20 patients and found improvements in arterial saturations but with decreased cardiac output and no improvement in exercise tolerance. However minute ventilation-CO2 extraction improved during exercise reducing the work of breathing as CO2 extraction was improved by a reduction in ventilation-perfusion mismatching.

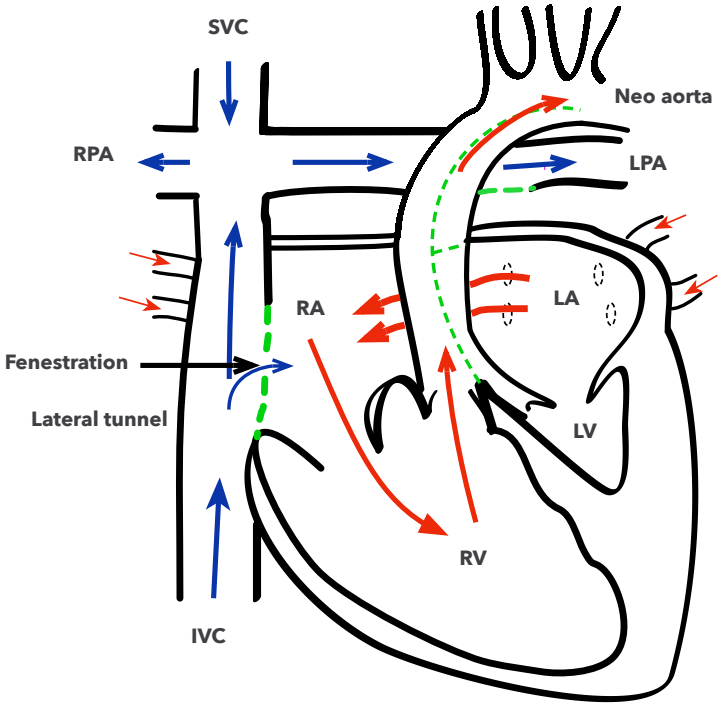

Figure 6: Stage III: Total cavo-pulmonary connection. Diversion of the inferior vena cava either via a lateral tunnel or extra-cardiac conduit at 3 - 4 years of age maintains pulmonary blood flow. A small fenestration is shown. This circulation is also known as a Fontan circulation.

1.3.10 Circulatory failure in the Fontan circulation

In those with HLHS, circulatory failure contributes significantly towards mortality.[48] The Fontan circulation exposes patients to high systemic venous pressures and relative pulmonary hypotension due to the lack of a subpulmonary ventricle. This leaves them exposed to a wide range of complications with

a progressive deterioration in function over time. [49] The long-term morbidity for those with a single ventricle circulation includes reduced exercise tolerance, [2, 6, 18, 47] increasing cyanosis, protein losing enteropathy, [50] plastic bronchitis, arrhythmias and thromboembolic events. [38, 48]

The incidence of exercise intolerance following HLHS-Fontan has been measured at 55-63%. [5] During exercise, patients with a Fontan circulation exhibit diminished peak oxygen consumption (VO2 max), decreased heart rate response and lower stroke volumes leading to reduced cardiac output (CO). [51, 52] The causes of exercise intolerance in this group are multifactorial. The lack of a subpulmonary ventricle, to drive blood through the pulmonary bed alongside abnormalities in cardiac function and systemic vascular resistance have all been suggested as contributing to diminished exercise capacity. [7, 53]

The underlying morphological differences underpinning the functional adaptations of each ventricle are outlined in Chapter 1.3.2 and it appears that those with a single RV (HLHS) are at a higher risk of heart failure than those with a single LV.[4] In a large study, *Anderson et al* [54] found that the systemic RV has worse systolic function compared to the systemic LV with diastolic dysfunction existing in 81% of patients as measured by echocardiography. However the effects of inadequate preload could induce similar effects, making these differences difficult to tease out.

Systemic RV function is dependent on good returning blood volume (preload). The preload on the systemic RV is postulated to be inadequate due to the absence of a subpulmonary ventricle which assists systemic ventricular filling. [7] Other causes of low preload are related to the flow of blood across the lungs which may be damaged from previous operations and scars. A low pulmonary vascular resistance (PVR) and low ventricular filling pressures are essential for augmenting cardiac output especially during exercise. [55] Elevated PVR as a cause of lowered preload has been proposed as a limitation to pulmonary blood flow [56] and may be related to down-regulation of endogenous pulmonary vasodilators, chronic pulmonary microemboli and loss of passive recruitment of capillaries and loss of pulsatile blood flow. [57] The trans-pulmonary gradient should increase in exercise [58] mediating a fall in PVR. The absence of a subpulmonary ventricle means that those with a Fontan circulation are not able to increase pulmonary pressures accordingly. The use of sildenafil, a pulmonary vasodilator, has mixed results depending on age. In children it has been shown to improve ventilatory efficiency during exercise but without improvements in peak VO2 max. [59, 60] Whilst in older groups of patients the administration of sildenafil may result in a fall in PVR. [61]

The shape and architecture of the tricuspid valve also display more variation in HLHS. [62] There is an increased incidence of tricuspid regurgitation (TR) occurring in 25% of patients within 10 years of the Norwood procedure. [63] Severe TR may require surgical repair due to the volume overload placed on the ventricle

by re-circulation of regurgitant blood. Reducing TR and hence altering the volume, shape and amount of work the heart has to perform has been shown to improve cardiac function and outcomes. [64, 65]

Many patients with HLHS report symptoms of decreased cardiac performance. The rising number of patients now surviving beyond infancy underlines the importance of being able to accurately assess cardiac function in this group. However there appears to be a complex interplay between preload, systolic and diastolic dysfunction. Being able to understand this in more detail may be beneficial in understanding the underlying disease pathology.

1.3.11 The challenge of determining function in the single RV

Ejection fraction (EF) is typically used to assess and grade ventricular function. EF measures the change in size of the ventricle between end-systole and end-diastole and expresses this as a percentage relative to its maximal size at end-diastole:

$$EF = \frac{EDV - ESV}{EDV} \times 100\%$$

where EF = ejection fraction, EDV = end-diastolic volume, ESV = end-systolic volume

In adults with acquired heart disease, EF is well studied and used extensively to predict outcomes in those with systolic heart failure. In subjects with HLHS

it has been shown to have a useful prognostic value. [66, 67] However within this group, a number patients have a preserved EF not in keeping with significant symptoms of reduced cardiac performance. [5, 68] This discrepancy is likely due to a number of factors. As in the adult population, diastolic dysfunction may play a role - also known as heart failure with preserved ejection fraction (HF-pEF). [54] However difficulty in assessing the RV may be due to the complex interplay of myocardial architecture and loading conditions. [69] For instance:

- The RV has a very anterior thoracic position, which may limit echocardiographic windows and prevent full assessment of the entire RV structure. [70]
- The systemic RV has a different geometry to a healthy RV and LV and within the spectrum of HLHS there is a wide range depending on the LV morphology. This leads to reduced inter-user reproducibility even on CMR assessment. [71]
- Following surgical shunt/conduit palliation at Stage I, compensated ventricular volume overloading occurs. Thus despite the presence of significant ventricular dilatation, preserved volumetric performance may be present and not necessarily in keeping with clinical signs. [7, 72, 43]

Other markers of cardiac function have been proposed for assessing the RV as part of a biventricular system but the significance of these for the single ventricle remains unclear. Early promising work into abnormal tissue doppler indices [73, 74] has recently been shown to resolve when corrected for higher heart rates which are typical in children or the presence of tricuspid regurgitation which is

common in those with HLHS. [62, 75] The prognostic value of findings such as the presence of prolonged isovolumetric contraction and relaxation times are yet to be fully understood.

1.4 Cardiac magnetic resonance and its applications

Technological developments in CMR offer the potential to develop new biomarkers of function alongside the standard volumetric assessment detailed above to overcome some of the existing limitation in assessing cardiac function in those with HLHS. (See chapter **1.3.11 The challenge of determining function in the single RV**) This section outlines the uses of CMR for the assessment of those with HLHS at each of the different stages of surgery. It describes the benefits of the technique and the potential limitations. There then follows an overview of different CMR sequences that are used for assessing cardiac function and potentially how they might be developed and applied to assessing those with HLHS. This will provide the necessary information to contextualise and appraise the methods and results included in later chapters.

1.4.1 CMR - advantages and disadvantages

The advantages of using CMR for assessment of CHD [76] are acquisitions are not limited by anatomy. Images are resolvable in any 2D plane or in other cases in 3D without the limitation imposed by echocardiographic acoustic windows. This is beneficial in assessment of CHD where complex anatomy can require detailed anatomical reconstruction. Flow, volume, function and shunt

assessments are possible providing detailed haemodynamic data. CMR does not expose the patient to ionising radiation. At present cardiac magnetic resonance imaging (CMR) is the gold standard for assessing right ventricular volume and function. [77–79] It provides detailed non-invasive anatomical and functional data on the cardiovascular system. Most commonly this is used to measure the change in volume of the heart as it contracts to give a measure of the function. Importantly, the technology surrounding magnetic resonance imaging (MRI) is rapidly developing and with it the potential to develop new translational tools for studying the function of the heart. Detailed 3D imaging of the heart allows the study of its shape in space and its motion throughout the cardiac cycle. Advanced flow imaging permits assessment of the whole blood-pool velocity paving the way for measuring ventricular energetics.

However CMR is expensive and time consuming. It requires highly trained operators and clinicians to interpret the data. Patients must be able to to lie supine and still for a prolonged period of time which may necessitate a general anaesthetic in those too young to comply. The data quality is not as highly temporally or spatially resolved as echocardiography. Some implanted metallic objects are not suitable for the magnetic field and MR conditional pacemakers and other metallic implants can cause significant susceptibility artefact which can make interpretation of images more difficult. CMR does not provide invasive pressure measurements unlike catheterisation. Additionally the time for acquisition is much longer than for CT and requires comprehensive post-pro-

cessing for data interpretation.

1.4.2 CMR in the assessment of HLHS

In those with HLHS, CMR assessment of ventricular and valvular function and vascular anatomy is used to plan surgery. [18, 80, 81] It has improved accuracy in measuring RV volumes in HLHS compared to echocardiography. [82] It has become the gold standard for accuracy and reproducibility in assessment of volume, mass, and wall motion. [83] Cardiac MRI has become the mainstay of evaluating function and anatomy in those with HLHS where available. It has been shown to be viable for surgical planning prior to Stage II [80] and Stage III of surgery. It is rarely performed in newborns as the relatively good echocardiographic windows combined with the haemodynamic instability mean performing a MRI under a general anaesthetic is unwarranted.

Pre-Stage II and pre-Stage III scans have well defined protocols for assessment and have recently been defined by the Society of Cardiovascular Magnetic Resonance (SCMR). [84] Pre-Stage II scans should assess the inter-atrial communication, the presence and degree of tricuspid regurgitation, RV function, patency of the Damus-Kaye-Stensel anastomosis, arch patency, shunt patency, size of branch pulmonary arteries and pulmonary vein patency and also the pulmonary to systemic blood flow ratio (Qp:Qs). The presence of any additional collateral vessels should also be noted.

Pre-stage III scans should include all of the above but instead of shunt patency the superior vena cava (SVC) flow needs assessment. The presence of collateral vessels is also assessed using a combination of flow measurements and MRI angiogram techniques.

At the Evelina London Children's Hospital, pre-stage II and III CMR scans are performed in accordance with SCMR guidelines however at present those having undergone completion of a Fontan (post Stage III) do not routinely undergo CMR. Scans are performed on a clinical basis and usually come under the remit of the following referral headings:

1. unstable requiring assessment in the peri-operative period
2. routine before transition to adult care typically at 16 years of age
3. increasing exercise intolerance of an uncertain cause
4. increasing cyanosis of an uncertain cause
5. other symptoms of heart failure such as protein losing enteropathy, enlarged liver or embolism

Scans performed after completion of Fontan can be divided into those requiring CMR for an anatomical assessment and those requiring XMR for a detailed physiological assessment. The important elements for assessment include patency of the Fontan pathway, arch obstruction, ventricular parameters and systemic to pulmonary collaterals.

The extensive use of CMR based assessment in clinical practice offers the opportunity to conduct studies on patients with HLHS undergoing routine clinical imaging. The following section outlines some commonly used sequences and how these could be developed into providing additional functional data based on the concepts of ventricular shape, motion and energetics.

1.4.3 Cine imaging

1.4.3.1 Balanced steady state free precession cine imaging

The motion, size and function of the heart can be captured using cine MR imaging. Cine imaging is used extensively for assessing ventricular function. Gradient echo based sequences have short repetition times most suitable for fast cine imaging. Sequences can be *spoiled* or *balanced*. Following the radiofrequency (rf) pulse residual transverse magnetisation can interfere with the signal during the following repetition time. Spoiled sequences apply a gradient to dephase this signal at the end of each repetition time. The short repetition time and echo time give a T1 weighted image. This is appropriate for cine phase contrast imaging. Balanced imaging utilises an additional gradient pulse to rephase all transverse magnetisation. After a number of repetitions the transverse magnetisation reaches a steady state hence the name *balanced steady state free precession (bSSFP)* cine imaging. Balanced imaging has increased signal, allowing a larger bandwidth to be used and improving imaging efficiency.

Imaging of cardiac function performed using cine bSSFP imaging generates white blood images of the heart. Images are acquired at multiple points after the R wave of the QRS complex over many cardiac cycles. A retrospectively ECG-gated sequence allows imaging of the entire cardiac cycle in a single breath hold. Retrospectively gated sequences acquire data continuously marking the R wave of the QRS complex with a synchronisation pulse. Data is then allocated at the end of the acquisition of k space. In contrast to prospectively ECG gated sequences, the retrospective acquisition allows capture of the whole of the cardiac cycle. This is particularly valuable for assessment of diastolic function or where beat-to-beat variation can alter the R-R wave interval. Prospective ECG gating allows the shortest R-R wave interval to be selected and in some instances under sampling techniques can only be performed if the data is acquired at fixed intervals after the start of the R wave which does not occur in retrospectively gated sequences where the desired number of phases are stretched to fit into the given cardiac cycle (Figure 7).

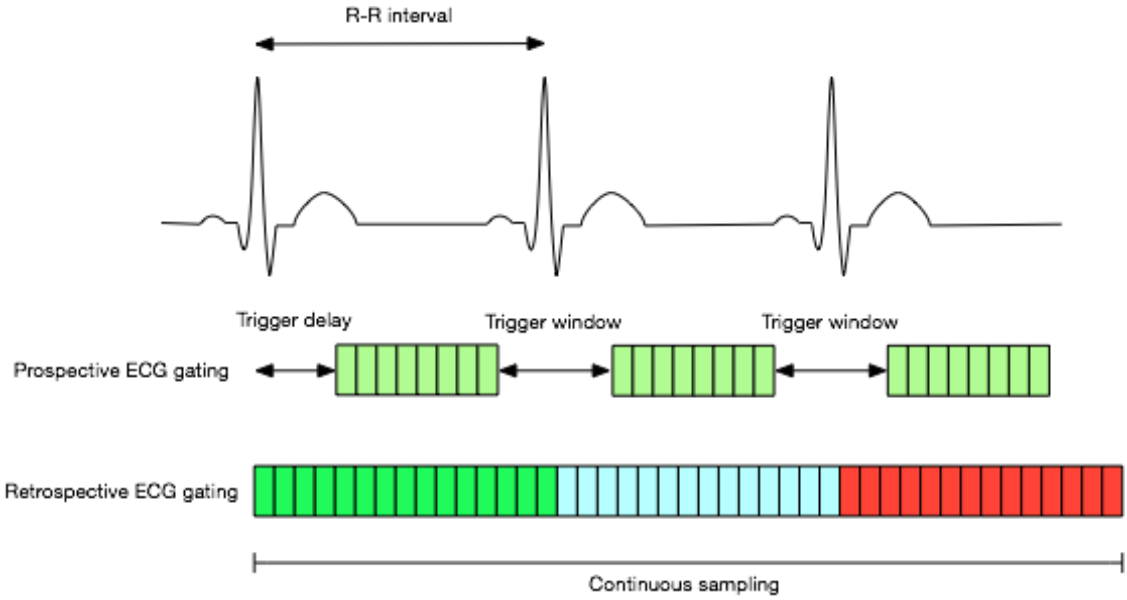

Figure 7: Prospective vs. retrospective ECG gating. Normal variability within the R-R interval of the ECG means a trigger window needs to be employed in prospectively ECG-gated sequences so as to await the next R wave. A small portion of the beginning and end of the R-R interval is missed. Retrospectively ECG-gated sequences acquire continuously and re-arrange the data into phases after detecting the next R wave. This can lead to small differences in the timing of acquired phases between different cycles.

CMR permits the heart to be imaged in any 2D plane determined by the operator. Long axis imaging provides functional data on the longitudinal function of the heart whilst a stack of cine image slices orientated in the short axis plane allows assessment of end diastolic volume (EDV), stroke volume (SV) and calculation of ejection fraction (EF) and wall mass. Cine stack imaging can be used to determine ventricle size throughout the cardiac cycle. Cine data can may be used to look for jets of turbulence caused by stenosis, to look for re-

gurgitation through incompetent valves or assess wall motion abnormalities. [84]

Calculation of ventricular parameters involves segmentation of the ventricular cavity. Manual tracing of the endocardial contour for each slice from apex to base at end-systole and end-diastole allows calculation of the blood volume via the modified disc summation method and also an accurate measure of ejection fraction (See chapter **1.3.11 The challenge of determining function in the single RV**). The position of the atrio-ventricular valve can be confirmed by linking the short-axis stack to the four-chamber view of the ventricle. In addition an epicardial contour at each slice in end diastole only allows calculation of the myocardial wall mass. An axial stack of slices offers less variability for the RV but not necessarily greater accuracy. [85] Consistency between inclusion or exclusion of papillary muscles and trabeculations is important to ensure low inter-operator variability. [84]

1.4.3.2 Motion Assessment: Strain and deformation

Cine imaging permits assessment of the motion of the ventricle in different short or long axis planes. Motion can be quantified using strain to assess both systolic and diastolic function. This section reviews the possibility of utilising strain as a measure of function in those with HLHS.

Strain analysis is a measure of the change in length of the heart relative to the original length. It is unitless and expressed as a percentage.

$$\varepsilon = \frac{L_1 - L_0}{L_0}$$

where ε = strain, L_1 = length after deformation, L_0 = original length

A shortening is represented by a negative value whilst a lengthening has a positive value. There are two forms of strain and whilst Langrangian strain, a measure of strain relative to a fixed length, is usually quoted in clinical practice it has been suggested that Natural strain, strain measured relative to a reference value which can change with deformation, may be more suitable for cardiac practice. Strain rate can be derived from this and is a measure of the rate of change in length and measured in s^{-1}.

Strain has been seen to be useful for detecting early cardiac dysfunction in adults with cardiomyopathy. It is more sensitive than ejection fraction [86] as the ventricular hypertrophy that is frequently seen as a response to dilatation leaves ejection fraction preserved or even supranormal. [87] Strain could be applied as a useful potential early biomarker in those with HLHS -they also demonstrate ventricular hypertrophy and dilatation as a consequence of volume loading shunt/conduit surgery leaving EF relatively insensitive to dysfunction. (See chapter **1.3.9 Stage III - total cavo-pulmonary connection**) However strain data is reliant on the quality of the acquired cine imaging and is

therefore prone error if there is wrapping artefact or poor breath-holds which can distort data. Additionally as cine data is an average of multiple heart beats so too is strain - it is a measure of the *average* motion of the heart so reliant on a regular heart rhythm

1.4.3.3 Key studies in strain imaging in HLHS

The gold standard for MR strain analysis is tagging. [88, 89] There are a number of studies and reviews assessing strain rates in the healthy heart. [90–92] Consistency between different studies is greatest for longitudinal and circumferential strain values. [93]

Fogel et al [34] assessed the motion of the systemic RV in 7 patients with HLHS and compared this to 11 patients with ccTGA using 2D MR tagging techniques to compare the inter-ventricular effects on wall motion. Strain was altered depending on the presence or absence of a LV. The presence of a LV augmented strain values and decreased heterogeneity. In comparison to the healthy LV the systemic RV in HLHS has abnormal clockwise twist apparent in the inferior wall and altered radial shortening. It is unsure whether these changes are due to incomplete remodelling, altered electrical activation pathways, ischaemia or an idealistic energy state for the given situation. A further study by the same group found strain in the single RV altered across operative stages. Those having completed Stage II surgery had the lowest strain values. This was postulated due to any one of volume unloading, baffle placement or even the

results of surgical scar formation. These studies were interesting in that they were able to compare a range of single ventricle types albeit in a small number of patients. However the age range between patients was not comparable due to the small number enrolled in the study making broader inferences difficult. The major limitation of this type of MR tagging technique is that they require complex post-processing which is not readily available.

Echocardiographic measures of strain are commonplace and speckle tracking based methods have been pioneered for angle independency. Studies performed in those with HLHS show significant mechanical dyssynchrony of the systemic RV [94] in the presence of a normal ECG. Application of echo strain imaging specifically to those having undergone a RVPA conduit as part of the Stage I Norwood procedure localises abnormal regional strain to the right ventricular outflow tract [95] corresponding to the position of the ventriculotomy scar. [96] These measures have the advantage of bedside assessment but they are limited by acoustic windows, RV geometry, [70] and the quality of the image. There is also a large standard deviation on regional strain data of this type which may reflect a degree of inaccuracy or inter-user variability.

Feature tracking (Diogenes MRI, Tomtec, Germany) analysis utilises MRI steady-state free precession cine imaging of the heart to provide strain data. Conventional short axis and long axis SSFP cine images are used. The endocardial borders of the RV are manually defined in one time-frame and then

automatically propagated using the analysis tool. The software propagates the endocardial contour through all time frames tracking the endocardial-blood border and adjacent features to provide strain data based on voxel motion tracking. This data can be regional or global to give a measure of systolic or diastolic function. The primary benefit of feature tracking is that it rapidly extracts measures of strain from conventional MR imaging techniques. [97] This allows the analysis of large amounts of data retrospectively from the acquisition of data from routine clinical scanning. It is not limited by acoustic windows.

Global assessment of circumferential strain using feature tracking correlates highly with tagged imaging in children with heart failure, [98] although only a mid-ventricular slice was used in this study. It also correlates in adult patients with myocardial scar in comparison to echocardiographic measures of function . [97] Strain has been shown to be strongly linked to outcomes in those with LV dysfunction using echocardiographic speckle tracking which has the disadvantage of being angle dependent. [99] Those with altered global circumferential strain display the strongest likelihood of an adverse event. It is possible to track altered myocardial motion during dobutamine stress imaging. [100]

The major advantage of feature tracking is that the technique can be applied retrospectively to existing datasets. However feature tracking derived strain values are susceptible to high inter-user variability particularly for longitudinal and radial *regional* segmental assessments [98, 101, 102] with better reproducibility

for global rather than segmental analysis. [101, 102]

Utilising MR based strain analysis could be suitable for assessing the RV provided the limitations surrounding its interpretation are understood. Feature tracking is easy to use and can be applied to cine data which is readily collected. However the use of feature tracking does not have the same level of inter-user reproducibility as 3D tagging. Additionally the current methods of deriving and analysing regional strain are not validated and must therefore be viewed cautiously.

1.4.3.4 Computational assessment: Shape and function

A stack of cine images can be used to determine the shape and size of the ventricle at any point during the cardiac cycle. Computational tools have been used to generate 3D atlases of cardiac geometry using cine imaging of the ventricle to compare differences in ventricle shapes in 3D space. [103, 104] Rather than being limited to volume, wall mass and ejection fraction these techniques allowed a comprehensive three dimensional assessment of shape, orientation and topology without pre-supposing any particular shape or aspect. They were successful in showing differences in LV shape in babies born prematurely compared to at term. [105] However these techniques are time consuming and require technological expertise and vast amounts of post-processing of data. The results are also difficult to interpret without referencing traditional measures of size. Applying this technique to those with HLHS where the right

ventricle is exposed to a selection of surgical procedures would allow the creation of a map of 3D geometry and to determine the impact of the procedures on the ventricular shape. This may permit subtle differences in shape to be detected before they are apparent to the naked eye or through global measures of size such as EDV alone. [43]

Computational modeling has an role in helping to understand and analyse haemodynamics in those with HLHS. It has been used to assess systemic RV filling. [9] A ventricle with effective energy conservation imparts just enough kinetic energy to the blood to achieve sufficient cavity expansion with minimal energy loss. A toroidal ring forms beneath the TV during early inflow growing in size and moving apically followed by atrial contraction and the creation of a second ring. If atrial contraction happens early (fused EA waves) then the new blood adds to the existing toroidal ring causing energy losses through viscous dissipation. Lower cavity aspect ratios (dilated shaped hearts) displayed the greatest viscous energy dissipation. These hearts impeded the normal movement of toroidal flow of blood towards the apex of the heart instead causing it to spread out and leading to energy loss. These models of inflow haemodynamics are theoretical and based on a number of modelling parameters. Other work has concentrated on modelling blood flow through the Fontan circuit [106–109] demonstrating that shape can significantly alter haemodynamics and energy losses. Whilst a potential powerful tool in simulating blood flow and the effects on the heart, computational models are only as powerful as the data that is fed

into the algorithm and errors can be multiplied if the given assumptions are not well understood. Implementing these techniques and trying to correlate them to function may be the first step towards us gaining a better understanding of heart physiology and function and as models receive greater data inputs the results will be more refined. The use of computational shape modelling is used to assess the impact of the different Norwood operations on the shape of the RV. (Chapter 2.12).

1.4.4 Phase contrast flow imaging

1.4.4.1 2D phase contrast imaging

Flow MRI is used extensively for assessing shunts, stenosis, regurgitation, differential pulmonary arterial flow and significance of collateral vessels in those with HLHS. The velocity and flow of blood can be determined by utilising velocity encoded cine (VENC) spoiled gradient echo sequences. Placing the body in a homogenous magnetic field causes an equal phase shift of all magnetic spins irrespective of whether static tissue or moving blood is assessed. Applying a gradient across this field causes spins to precess at a frequency according to their relative field exposure (Figure 8). In addition blood moving though the field gains a different phase. The spins within static tissue can be re-phased by applying an equal but opposite gradient echo resulting in the spins of blood flowing into the slice ending with a different phase. This is proportional to the velocity of the blood. Phase discrepancy can also occur through motion along more than one direction and from magnetic field inhomo-

geneities. A second acquisition with a different flow sensitivity minimises velocity changes only to the flow encoded direction. [110] Resultant images are displayed on a greyscale with white indicating flow towards and black indicating flow away from the flow encoded direction.

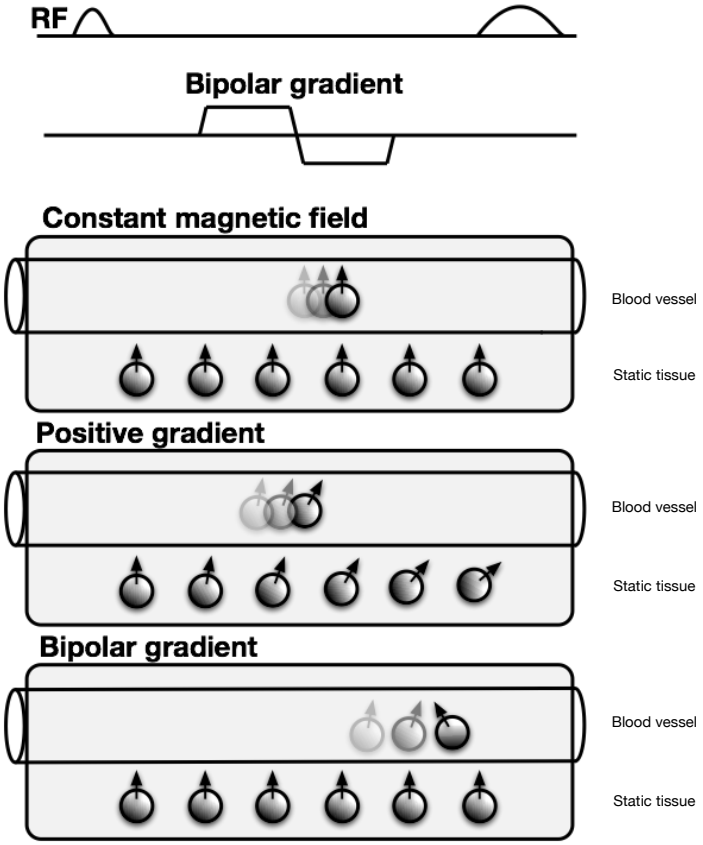

Figure 8: Blood and static tissue in a magnetic field. The application of a bipolar gradient causes static tissue to become rephased whilst moving blood gains a phase proportional to its velocity.

1.4.4.2 4D phase contrast imaging

Developments in flow analysis now permit the acquisition of time resolved three dimensional velocity mapping also known as four dimensional (4D) flow MRI. [111] Visualisation of blood flow in a 3D volume over time permits both qualitative and quantitative analysis of motion patterns and retrospective analysis of flow in any desired plane.[112] The potential applications include flow volumes, pulse wave velocities, [113] pressure gradients, [114] wall shear stress [115] and turbulent kinetic energy, [116] alongside providing important new insights into flow characteristics and pathological adaptations such as in those with a bicuspid aortic valve. [117]

4D flow MRI provides a detailed overview of the velocity of blood in three directions helping to capture the intricacies of blood flow within the heart. Echocardiography is reliant on flow being directed towards or away from the insonation point. Velocities may be underestimated when using 2D echocardiography. Applying 3D techniques allows assessment of the peak velocity within the voxel irrespective of the vector direction. Three-dimensional CMR acquisitions provide a detailed overview of the velocity of blood in three directions helping to capture the intricacies of flow within the whole heart. This is important, as filling of the LV cavity does not occur solely from base to apex. Vortices form below the mitral ring and move apically during healthy diastolic filling. [11] 2D PC MRI or echocardiography may miss these subtleties, or require larger study populations before differences become detectable. Additionally

the mitral valve is elliptical and moves throughout the cardiac cycle. [118] It becomes distorted in cardiac disease such as DCM making accurate plane orientation for 2D PC flow techniques more technically challenging. Three-dimensional flow echocardiography is currently a tool under development but this too is limited by the patient's habitus. [119] This detail is not adequately captured by two-dimensional (2D) doppler echocardiography or 2D PC flow MRI which are limited to a single imaging plane and measure velocities in only one direction.

Initial 4D flow sequences performed a flow encoded and flow compensated measurement per direction known as a six-point technique. This was extremely time consuming. Current sequences make only four measurements, a reference scan and velocity scan in each direction, and are known as four-point techniques. This has improved scanning time. [120] However 4D flow still remains limited by the acquisition time. Multiple acquisitions for determining velocity direction are required. Flow measurements must be respiratory gated to avoid movement artefact and triggered according to the cardiac cycle. Conventional sequences require 20minutes, not including navigator efficiency, and thus may be 30 - 40 minutes in principle. [121] Furthermore 4D flow is highly sensitive to eddy current effects, [122] Maxwell terms, gradient field distortions [123] and velocity aliasing. [124] Early work suggests higher Tesla scanners may provide greater signal-to-noise ratios but are yet to be used clinically. [125] Following the acquisition post-processing techniques must be performed to remove these inaccuracies before the dataset is suitable for analysis.

Advances in acceleration techniques [126] have brought down nominal scanning times to the region of 5 - 7 minutes for high resolution whole heart acquisitions. Prospective ECG gating allows advanced data encoding methods and acceleration techniques offer increases in acquisition time by a factor of 8 over fully sampled acquisitions. However due to the need to ECG-trigger from a R wave the cardiac cycle is incompletely sampled (Figure 7). The effects of this need to be evaluated. Furthermore the accuracy of accelerated reconstructions particularly in relation to temporal and spatial blurring requires evaluation before routine introduction into clinical practice.

Despite long acquistion times 4D flow MR technqiues are beginning to be employed as a diagnostic tool particularly for CHD where complex anatomy and flow patterns can be difficult to interpret when limited to two dimensions (Figure 9). Amongst other uses they have been used to describe flow patterns in those with bicuspid aortic valves, [117] describe pulmonary arterio-venous malformations, [127] to assess haemodynamics in single ventricle circulations [128, 129] and to quantify blood flow in patients with complex shunts. [130]

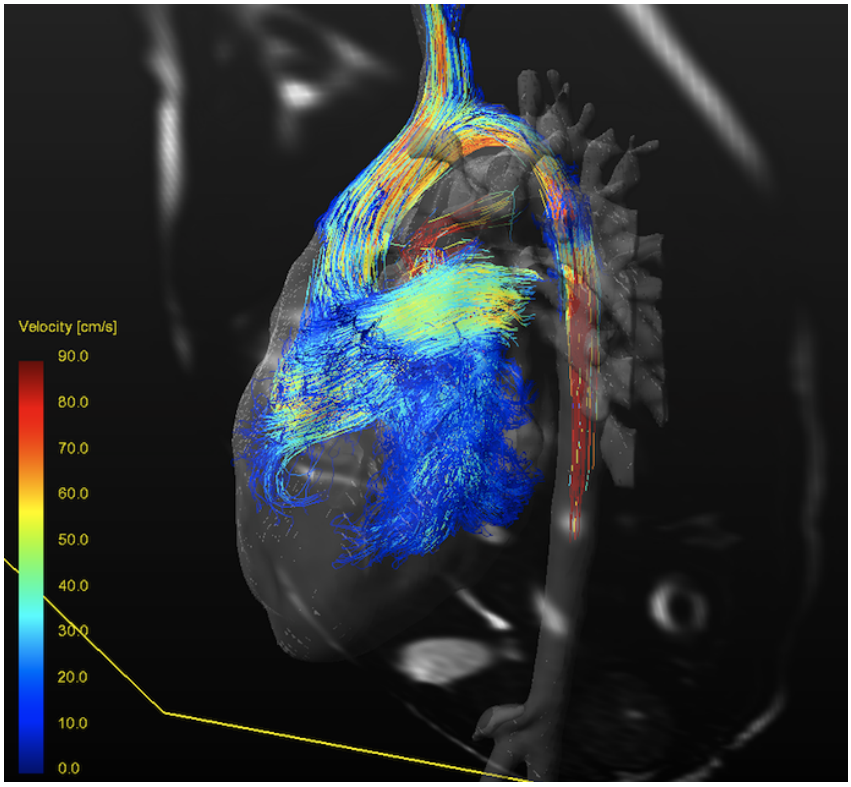

Figure 9: Pathlines in a criss cross heart. The colour of the pathlines are velocity encoded with the fastest velocities displayed in red and the slowest velocities in blue. In this congenital heart condition the inflow of blood into each ventricle can be seen to cross at the atrial level. 4D flow imaging helps us to understand complex anatomy in 3D.

Clinical interpretation of 4D flow data is usually in the form of either traditional quantitative measurements of flow through segmented blood vessels or qualitative descriptions of streamline or pathline data. Streamline data represents the instantaneous velocity vector of a particle and changes with each phase of the cardiac cycle. Pathline data averages the path that a particle takes through the cardiac cycle to form pathlines. Proprietary software such as GTFlow (GT-

Flow, Gyrotools, Zurich) or EnSight (CEI, Research Triangle Park, NC) are used to both visually assess the data and extract flow measurements. Despite the potential of 4D flow CMR particularly in CHD, the current limitations to mass clinical introduction remain acquisition time, resolution and accuracy, alongside a suitable workflow for timely post-processing.

Proprietary software is used to analyse the images. The vessel of interest is identified and a region of interest drawn around it. The contour is propagated across all time points. Adjustments are made to the contour to account for vessel motion during the cardiac cycle. Values for forward flow, backward flow, peak velocity and cardiac output amongst others can then be determined.

1.4.4.3 Errors in flow imaging

An understanding of sources of error in PC flow acquisition is important as an appreciation and suitable allowance for these effects must be made in the interests of accuracy. Phase contrast (PC) images are susceptible to phase correction errors. [131] Phase correction errors represent the apparent presence of flow in static tissue. The error accumulates into areas of true flow leading to a 1 - 2% error. This cumulative error can result in stroke volumes much greater than expected. Phase offset errors, eddy currents and concomitant field gradients are caused by the steep magnetic field gradients alongside the paramagnetic affect of tissue. Post-processing can correct for this by creating a region of interest (ROI) within static tissue where there is no apparent flow and

deducting this from flow within vessels or else by defining static tissue across the whole image and calculating a correction slope which can be subtracted from the whole image to improve accuracy. Measuring the flow of blood through a 2D slice requires a plane orthogonal to the vessel to be determined. Selection of an off-angle slice leads to underestimation of the true velocity of blood. [132] A true representation of a wave requires sampling at a rate of twice the frequency (Nyquist limit). Correct selection of the VENC by the MRI operator determines the sampling rate. Values lower than the real velocity result in aliasing within the image and values above the velocity lead to decreased sensitivity to low velocities. Selection of the correct temporal and spatial resolution by the operator is important to minimise operator error and record accurate flow measurements.

1.4.4.4 Kinetic work

There has been recent interest in the use of four-dimensional (4D) phase contrast (PC) flow magnetic resonance imaging (MRI) to non-invasively measure intra-cardiac kinetic energy (KE). [10, 118] Kinetic energy (KE) is the amount of energy required move blood due to its inertia. [133] Although a small proportion of the overall energy that the heart consumes per beat; alongside stroke work it is part of the work performed to eject blood and therefore a marker of the *useful* work of the heart. [134]

The total energy expenditure of the heart per beat is composed of the internal

and external work. Internal work represents a large proportion of the work of the heart with the energy used to rearrange cytoskeletal structures; stretch elastic and viscous elements in the myosin cross bridges and maintain cell membrane potentials. Much of the internal energy consumption is released as heat energy contributing to the heart's inefficiency. [135] External work is referred to as the *useful* work of the heart and is composed of stroke work and kinetic work. Stroke work constitutes the greater part and is the energy used to overcome the systemic blood pressure. The remainder of the external work is imparted as kinetic energy onto the blood volume. Importantly kinetic work can now be derived non-invasively offering the opportunity to study it in detail without the risks of an invasive catheter intervention. (See chapter **1.4.5.2 Pressure-volume analysis**) Whilst metrics such as ejection fraction give a measure of the change in shape of the ventricle it provides no idea of its energetic cost. Measuring kinetic energy would give a measure of part of the useful work performed by the heart in pumping blood. This has led to a growing interest into its applicability.

Investigating KE parameters in those with HLHS would offer an opportunity to study the energetic changes that occur in the systemic RV. The dilated hypertrophic RV often has normal values not in keeping with patients perceived symptoms. Assessing how the useful work of the heart is altered might provide insights into its efficiency. The heart beats over 100000 times per day and small inefficiencies would accumulate up over time. Therefore small inefficien-

cies could become significant over months or years. There is however currently no literature on measuring KE in those with single ventricle circulations and the majority of work has focused on determining the intra-cardiac KE of blood to ascertain normal indices in health.

Prec et al [136] were one of the first to try and determine the role of KE as a proportion of the total work performed by the heart. Limited by the angiographic techniques of the time they found that the KE of the right heart represented 2.4 - 12.5% of total external work and the KE of the left heart represented 0.25 - 2.0% of total external work. The differences were thought to be due to the higher systemic vascular pressures compared to pulmonary artery pressures that the respective ventricles had to work against. This work formed the first study into KE. It was limited by the methods available at the time with values derived by making assumptions on fixed vessel sizes and mean pressure values.

The methods of calculating the kinetic energy from 4D flow differ slightly between research groups but follow the same principles. Firstly a 4D flow sequence is used to measure velocities in a whole-heart volume. Balanced SSFP images are acquired and used to segment the blood pool. Kinetic energy is then calculated using the formula:

$$\text{Kinetic energy} = \tfrac{1}{2}\ \text{mass} \times \text{velocity}^2$$

Carlsson et al [118] took the sum of the kinetic energy of each particle within the ventricular cavity at an instantaneous time point. The KE value was then plotted for each time point through the cardiac cycle. Both the right and left ventricles were found to have three peaks of KE during the cardiac cycle coinciding with systole, early diastole and atrial contraction. The RV had a higher systolic peak (7.5 ± 0.8mJ) than the LV systolic peak (4.9 ± 0.4mJ) due to better conservation of energy and the different outflow tract geometries. In both ventricles the early diastolic peaks were larger than the late diastolic peaks. The LV early diastolic peak was higher than the RV early diastolic peak. This was postulated to be due to a suction effect from elastic recoil of LV muscle and the different movement of the tricuspid valve plane which acted like a hinge sliding over static blood rather than imparting energy onto it. Mean values over the cardiac cycle for both ventricles were very similar (RV 2.3 ± 0.3mJ; LV 2.1 ± 0.2mJ). During exercise the proportion of kinetic energy imparted to blood is thought to rise. Computational modelling predicted a 57-times increase in KE at peak exercise (rising from 0.3% to 2.9% of total work) in contrast to potential energy, which increased only 7-times. [118] This was more pronounced in the RV where KE increased from 2.8% to 24% of the total work of the heart. Conditions with outflow tract obstruction displayed higher KE proportions relative to external work as the smaller cross-sectional area for flow meant that where cardiac output was preserved the blood velocity and consequently the KE had to increase. [133] This study used only a small number of healthy volunteers with

a narrow age range to determine normal intra-cardiac parameters. The method of determining KE was computationally intensive. They were not able to exercise their patients and relied on a computational model to describe these effects.

Fredriksson et al [10] assessed the pathway of different flow components of blood. Particles were seeded at end systole and pathline analysis used to determine different components of flow. Flow was divided into:

1. particles entering and leaving the heart in one cycle;
2. particles entering but not leaving;
3. particles starting in the heart and leaving and;
4. particles that remain in the heart for more than two cycles.

The peak velocity achieved at each timepoint for each flow component was summated, before being divided by the flow component volume to form an energy density. Direct flow in the RV followed a curving route that did not extend into the apex. Furthermore it comprised the largest volume of blood in the ventricle at end diastole and possessed the highest pre-systolic energy (0.4 ± 0.3 mJ/particle) of all the flow components. Assessment of the inflow patterns demonstrated that they follow the motion of the atrio-ventricular valve plane. The right atrio-ventricular valve plane is hinged and accordingly the tricuspid valve inflow sweeps around the infundibulum. The movement of the left atrio-ventricular valve is in the long axis direction of the ventricle. Mitral valve inflow

is towards the apex and changes direction in the mid-portion of left ventricle. This correlated with computational models of ventricular inflow. [12] This study used a differing method of determining KE but the magnitude of the values were comparable to other studies indicating the validity of the differing techniques. However the determined parameters of KE were only in health with no description of disease.

Most recently *Arvidsson* [134] assessed atrial kinetic energy using a similar intracavity time summation method. Three peaks were found during the cardiac cycle coinciding with ventricular systole, early diastole and atrial contraction. The left atrial peak KE was greater than the right atrial peak KE in early diastole and correlated directly with the ventricle wall mass indicating that LV wall recoil is essential for LV filling in early diastole whereas the RV fills by conserved helical flow and AV plane motion. Reassuringly KE values from each of the three studies studies have all been within the same magnitude despite differing techniques for deriving the values. Atrial values of KE are extremely small and whilst physiologically interesting the clinical impact is yet to be understood.

Early work considering the effect of heart failure on intra-ventricular kinetic energy has begun. [137] The presence of disease is seen to change kinergetics. *Eriksson* [137] used the same method as *Fredriksson* [10] to calculate KE for different blood flow components. Patients with LV dysfunction had a smaller proportion of direct flow compared to the healthy adults but with a similar energy

density. The retained flow (>2 cycles) contained a much higher energy density. This indicated that ventricular dysfunction changes the energetics within the heart with less efficient flow mechanisms occurring as demonstrated by a reduced direct flow component (loss of energetic momentum) and higher end diastolic volumes with higher energy density of the large residual component. Interestingly they were able to show that KE indices are altered in the small number of dysfunctional ventricles that they studied. This was not correlated with any clinical outcomes. However it does show the potential for this to be utilised in those with HLHS as a potential marker of dysfunction. See Chapter 4.

1.4.5 XMR - Combined catheter and MRI imaging

1.4.5.1 XMR - Applications, advantages and disadvantages

Combined cardiac catheter and MRI guided imaging (XMR) involves the simultaneous placement of a vascular catheter whilst undergoing a MR scan to provide detailed insights into circulatory physiology. It provides simultaneous catheter derived pressure and MRI derived volume data which is more accurate and reproducible than values derived solely by either catheter techniques or MRI techniques. [138] This is in contrast to utilising only one modality which introduces assumptions which can skew the data. For instance:

- using only a catheter technique requires extrapolating the area from a ventriculogram into a volume
- CMR alone provides volumetric data but no indication of pressure data

- echocardiography is simple to perform as a bedside investigation but it does not provide pressure data and also requires area to be converted into a volume which is not as robust for the RV as it is for a normal shaped LV due to its differing shape.

Despite the advantages of XMR, catheter derived measures of resistance and shunt quantification are still in common use in many centres. The uptake of XMR is limited by the high level of expertise, equipment, time and post-processing required. XMR has the disadvantages of all of the risks expected of a catheter based procedure including, but not limited to, bleeding, infection, valve and vessel damage and thromboembolism. [139–143] Furthermore conductance catheters are not suitable for the MR environment necessitating the need for MR safe equipment. [144] Fluid filled catheters are therefore used and are more susceptible to dampening of pressure traces. However where available it offers the potential for accurate, reproducible data that can be used to guide clinical management.

The current clinical practice for patients at the Evelina hospital with HLHS and exhibiting signs of heart failure is for them to undergo XMR for assessment of their PVR, and additionally ventricular pressures and presence of collateral vessels. This procedure has been well described [145] and is frequently performed in conjunction with a pharmacological stress study to assess the response of PVR to higher heart rates (see Chapter 1.4.5.4.). At present only

vessel flow and ventricular volumes are recorded but the use of XMR allows for a much richer dataset to be analysed. The combination of pressure, volume and flow data allows for an in depth study of ventricular haemodynamics. In particular both systolic and diastolic function as well as preload and afterload can be derived. In Chapter 1.3.11 the difficulties in accurately assessing RV function were described. XMR provides valuable pressure data in addition to flow and volume data allowing functional indices to be characterised under the particular loading condition at that time. Studying the energetics of the systemic RV using XMR techniques to express the performance of the systemic RV in terms of work and energy could provide useful insight in to the function of the ventricle. [146, 147] The literature covering energetics in those with HLHS is sparse. Studies generally involve small sample sizes or data is collected during separate procedures which may not be physiologically accurate. The main studies and their outcomes are discussed below and despite the small amount published it opens the opportunities for some interesting work to be done in the area.

Tanoue et al [148] used an estimation method to assess the mechanical efficiency of a 3 staged or 2 staged surgical palliation in those with HLHS. They showed Stage II interim surgery is beneficial for high risk patients as it removes the volume loading on the single ventricle allowing contractility and mechanical coupling to improve in comparison to those proceeding directly from Stage I to Stage III. These results are in keeping with the results noted by clinicians where

better outcomes occur with a staged technique. *Senzaki et al* [149] used pressure-area analysis to show Fontan patients have lower cardiac index due to higher afterload and abnormal contractile response to inotropic agents. It should be noted that many of *Senzaki's* studies were later withdrawn by the publisher due to improper ethical consent. *Schmitt et al*, [150] applied XMR to assess load independent markers of function. The technique was first verified in animal studies [151] and then pressure-volume loops were created in a heterogenous group of subjects with single ventricle circulations. [150] Aorto-pulmonary flow was found to augment pulmonary blood flow with increasing pharmacological stress. Importantly they demonstrated the feasibility of using XMR to derive some measures of energy and also load-independent measures of function using pressure-volume loops.

1.4.5.2 Pressure-volume analysis

Pressure volume-analysis provides an interesting assessment of ventricular work in particular the use of load independent assessment of function. Many markers of ventricular function are load *dependent*. They vary according to the patient's current physiology and can change depending on whether they have drunk well or are dehydrated. Load *independent* markers reflect the intrinsic property of the heart and do not vary in this fashion. This is important as loading conditions vary tremendously between operative stages in patients with HLHS. Patients frequently demonstrate preserved compensatory ejection fraction values. This is one of the reasons for ejection fraction being relatively in-

sensitive towards detecting early cardiac dysfunction. (See chapter **1.3.11 The challenge of determining function in the single RV**) If the pressure-volume analysis could be applied to those with HLHS then additional meaningful data could be used to understand the ventricle's properties. XMR is available and already utilised safely in other forms of congenital heart disease. at the Evelina hospital. The challenge is to generate pressure-volume loops for analysis. This following section provides a brief overview of pressure-volume loop physiology as a background for developing this into a study of ventricular function in those with HLHS.

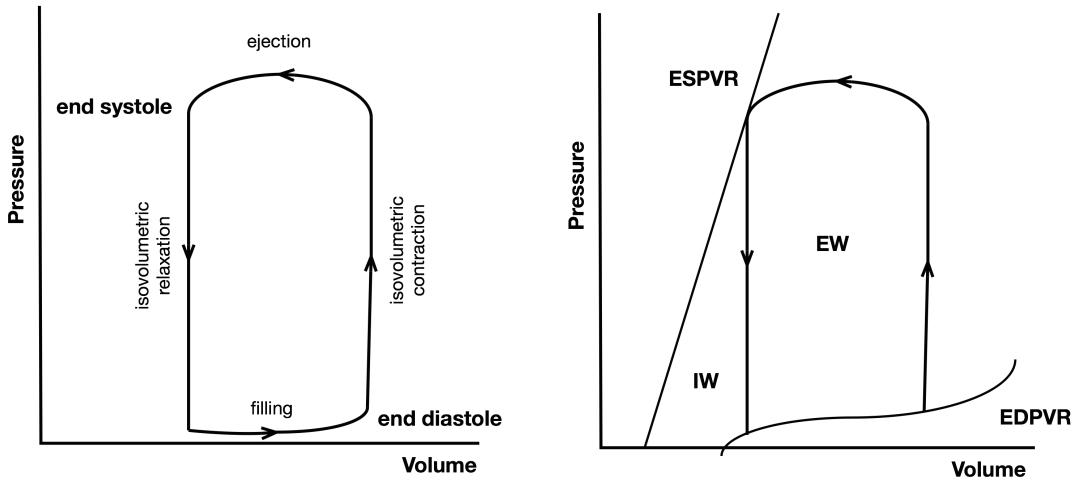

Figure 10: Typical pressure volume loops seen in the healthy LV. A counter-clockwise rotation of the curve occurs through the cardiac cycle. Starting at the lower right point which coincides with end-diastole, the heart first contracts with no change in volume, the isovolumetric contraction time. As the aortic valve opens blood is ejected and the volume falls. At end-systole the aortic valve closes and pressure falls with no change in volume, the isovolumetric relaxation time. The opening of the atrio-ventricular valve causes filling of the heart and return to the starting point.

The PV loop shows the simultaneous ventricular pressure against ventrciular volume over the cardiac cycle as the heart ejects and fills during systole and diastole respectively. The stroke work performed by the heart can be derived from the area represented by the ventricular pressure-volume (PV) loop (Figure 10). [135, 152] A cardiac catheter is placed within the ventricle whilst the change in ventricular volume is measured.

Varying preload whilst maintaining a fixed arterial resistance and stable contractile conditions allows the generation of a series of pressure volume loops (Figure 11a).

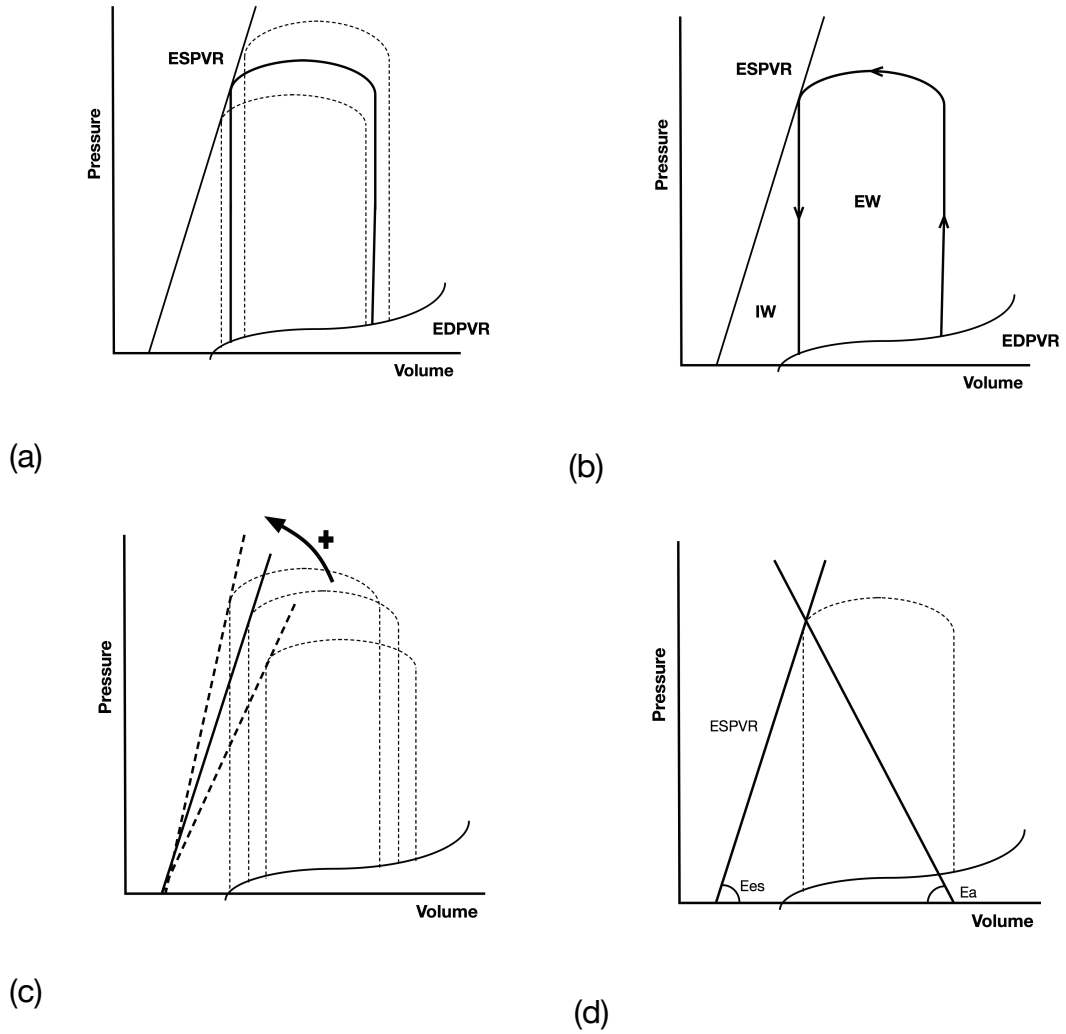

Figure 11: ESPVR and Ventriculo-arterial coupling ratio. (a) Varying preload allows the construction of multiple PV loops. The ESPVR follows a broadly linear trend whilst the EDPVR is non-linear. (b) The internal and external work of the heart can be measured by the area encompassing the PV loop and the ESPVR and EDPVR. (c) Inotropic agents increase myocardial contractility resulting in a increase in the slope of the ESPVR (Ees). (d) Afterload is the gradient of a line drawn between the end diastolic volume and the end systolic pressure (Ea). The relationship between contracility and afterload is known as the ventriculo-arterial coupling ratio (Ees:Ea) and is a measure of hydraulic coupling between ventricle and vessel.

The end-systolic pressure points of each loop have a broadly linear relationship within physiological ranges known as the end-systolic pressure volume relationship (ESPVR). [153] In expressing the heart as a time varying elastance model the slope of the ESPVR is a measure of the contractility (Ees) or elastance of the ventricle under that given condition. This is the pressure required to elicit a change in volume or its resistance to expand. A similar line can be drawn between the end-diastolic points of each loop and is referred to as the end diastolic pressure volume relationship (EDPVR). The slope of the EDPVR represents the relaxation properties of the heart. The area encompassed by the EDPVR, ESPVR and isovolumetric contraction lines represent the total work the heart performs (Figure 11b). [152] Increasing contractility increases the slope of the ESPVR (Figure 11c). ESPVR and EDPVR are load independent parameters as they do not vary based on preload or afterload. They provide an important measure of the intrinsic properties of the heart.

The relationship of end-diastolic volume (EDV) to the end systolic pressure gives the afterload that the heart pumps against. It is a measure of the elastance of the artery (Ea). (Figure 11d) Afterload is a better marker of end systolic ventricular stress compared to systemic vascular resistance which is more reflective of peripheral vasomotor tone. [154] The ratio of Ees:Ea is known as the ventriculo-arterial coupling ratio. [155] It is a measure of the ability of the arterial system to match the hydraulic load imparted onto it by the ventricle contracting and ejecting blood. The greatest mechanical efficiency occurs when after-

load is less than Ees.

Maximal stroke work occurs when Ees equals Ea, [155, 156] corresponding to a ratio of SV to effective EDV of 50%. In other words ejection fraction is also 50%. However EF is not usually less than 50% in healthy individuals and *in vivo* energetic efficiency occurs at higher ratios [155] with a typical ratio of Ees:Ea usually 1.5:1.0. [147, 157] The heart is able to maintain work and efficiency at 90% of optimal values between a large range corresponding to ejection fractions between 40-80%. As a healthy person ages the arterial vessels become more stiff and this is represented by a fall in Ees:Ea. [158, 159]

Deriving PV loops from a XMR approach requires a number of considerations to the methodology to ensure useful physiological data is being collected. Traditionally, deriving ESPVR involved occluding the systemic veins to alter the preload on the heart. The subsequent pressure and volume change over multiple beats were averaged and used to plot the ESPVR. (See chapter **1.4.5.2 Pressure-volume analysis**) However CMR based ventricular volumetric cine assessments are acquired over a number of minutes making the effects of a temporary occlusion obsolete before the end of the acquisition. Therefore deriving ESPVR by this method would be inaccurate. The single-beat estimation method appeared to be a promising alternative. It was initially described in the LV, [160] and has since been validated for the RV [161] and more recently in single

ventricle physiology.[150, 151] Making the assumption that for the physiological range the ESPVR is broadly linear, *Brimioulle et al* [161] described a method by which the maximal pressure generated by the heart is estimated at each state based on the intersection of two lines representing maximal rise in pressure in systole (dP/dt_{max}) and the maximal fall in pressure in diastole ($-dP/dT_{min}$). This pressure value is plotted against the volume of the ventricle at end diastole. A line linking this point to the end systolic pressure point of the PV loop provides a reliable estimate of the ESPVR. Most recently applying combined cardiac catheter and MRI techniques to assess pressure volume loops and ESPVR has been validated for the single ventricle physiology. [151, 162] However the single-beat estimation method technique is not applicable for estimating EDPVR which follows a non-linear relationship. In place of EDPVR, Tau (τ), the early relaxation constant, has been shown to be a reliable substitute as it is relatively load independent.[149, 150] It is calculated from the reciprocal of the natural logarithm of the early maximal fall in ventricular pressure during diastole.

Studying the energetics of the systemic RV using XMR techniques to express the performance of the systemic RV in terms of work and energy could provide useful insight in to the function of the ventricle. [146, 147] It appears feasible albeit with a modified approach to deriving parameters of contractility and relaxation. Patients would require an anaesthetic, (the effects of this are considered in chapters 3.2.6) and patients would still be exposed to the same risk of any catheter based techniques. Applying PV loop based analyses in those with

HLHS would require consideration and minimisation of these risks. [162] However load independent measures of function and an energetic assessment would be useful in providing a deeper insight into single ventricle performance; particularly *if* the data was collected on a more homogenous group of young symptomatic patients then this might provide additional insights into the mechanisms of circulatory failure.

1.4.5.3 Stress imaging

Assessment of ventricular work only under resting conditions provides a limited understanding of the pathological processes underpinning symptoms of exercise intolerance that are experienced by subjects at higher heart rates. However as XMR is performed under a general anaesthetic this precludes the use of a treadmill or exercise bike to stress the circulation. Instead pharmacological stimulation using dobumtaine has previously been proposed and used to simulate the effects of exercise. [163] Dobutamine (DL-3-4dihydroxy-N-(3-(4-hydroxyphenyl)-1-methyl-n-propyl)-phenylethylamine) is an analogue of isoproterenol. It acts on the adrenergic receptors of the heart and also on peripheral receptors. At low levels it has mainly inotropic effects on the myocardium with increasing chronotropic effects at higher levels. At high levels it also reduces peripheral afterload. Dobutamine stress has been shown to be safe and reliable at low levels (7.5mcg/kg/min). [149, 164, 165] at levels of 20mcg/kg/min [166] and even high dose at 40mcg/kg/min. [167] Dobutamine has a logarithmic relationship to the dose response curve. Once the early dose response is achieved a doubling

of the dose will lead to a doubling of the haemodynamic effect.

Oosterhoff et al [163] examined the accuracy and reliability of pharmacological stress in lieu of exercise on cardiac physiology. In healthy adults low dose dobutamine resulted in a stable end-diastolic volume (EDV) with stroke volume (SV) and ejection fraction (EF) increasing via a fall in end systolic volume (ESV) and a rise in heart rate. It compared favourably to exercise (Figure 12).

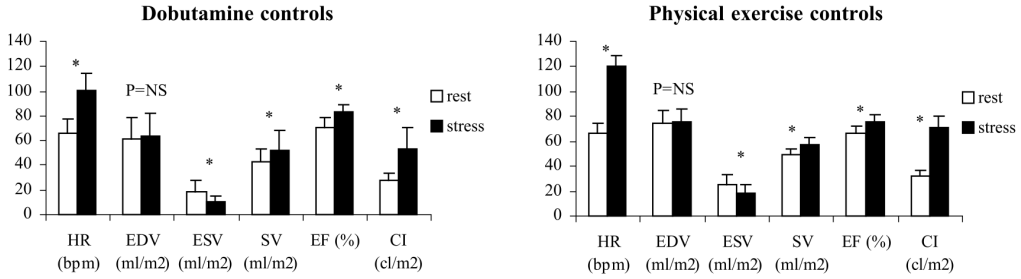

Figure 12: Effect of dobutamine compared to exercise on healthy controls. Taken from Oosterhoff, JCMR 2005. End diastolic volume remains stable and a fall in end systolic volume drives a rise in stroke volume and ejection fraction. This in combination with a rise in heart rate in both groups contributes towards an overall increase in cardiac output.

Four existing studies compare how patients with a Fontan circulation respond to dobutamine. These have employed a range of modalities for assessing the contractile and energetic response of the ventricle. *Senzaki* [149] and *Schlangen* [37] used catheter data, *Robbers-Visser* [165] used CMR alone and *Schmitt* [150] used XMR (Table 2). All studies show a fall in EDV with a variable fall in ESV resulting

in a mixed response to SV. However there is a consistent increase in heart rate driving cardiac output. The cardiac output at higher heart rates is limited yet markers of contractility are normal. The fall in EDV at higher heart rates is suggestive of a restriction to preload but this is only inferred from the available data. This differs markedly to healthy individuals. Similar responses have been reported in ccTGA where a baffle repair restricts flow through the atria. [168] In interpreting the available data, the differing methodologies and the heterogenous morphology and ages of the single ventricle populations in each of the studies mean direct comparison of results must be viewed carefully.

	Robbers-	Senzaki	Schmitt	Schlangen
Group	HLHS	HLHS	Mixed	HLHS
Age	Children	Children	Mixed	Children
Dobutamine	7.5	5	10	10
Method	MRI	Catheter	XMR	Catheter
EDV	↓	↓	↓	↓
ESV	↓	↓	↓	↔
SV	↔	↑	↔	↓
EF	↑	↑	↑	↔
HR	↑	↑	↑	↑
C.O.	↑	↑	↑	↑
Contractility (Ees)	↑	↑	↔	↑
Relaxation (Tau)		Normal and falls	Normal and falls	Normal and falls
Stiffness		↓	↑ (non sig)	↔
Afterload (Ea)	↓	High at baseline, no change	↔	
VA coupling		↑	↔	

Table 2: Summary of evidence from stress MRI studies involving children.

The use of dobutamine in HLHS in lieu of exercise also appears to offer consistent results. Supine CPET demonstrates a fall in EDV and a rise in HR are simi-

larly responsible for augmentation of cardiac output. [61] This point is important to establish as during XMR, muscle relaxants are used and the lack of muscle contraction is counter to normal Fontan physiology. [169]

Applying pharmacological stress under XMR conditions offers a useful surrogate to exercise, albeit with limitations. End diastolic volume falls and cardiac output is maintained via a rise in heart rate but the cause for why cardiac output is limited is less certain. Investigating cardiac function in terms of ventricular mechanics and work and applying it to a homogenous group of young symptomatic patients with HLHS may provide further details on why they experience symptoms of reduced exercise capacity.

1.5 Conclusions

Assessing the systemic RV is challenging. Developments in CMR technology offer the opportunity to characterise the function of the systemic RV in terms of energy, shape and motion. Many of the techniques described in this chapter have been employed only in adults thus far, and translating the application of these techniques to children with systemic RV physiology will require a number of adaptations and assumptions to be made. These have been detailed within each section above. However two important features stand out from the background assessment and literature review:

The first is CMR studies require patients to be supine or anaesthetised which is

counter to normal Fontan physiology. The available literature suggests the derived data should still be reflective of the underlying cardiovascular physiology but it is clear any results will need to be interpreted carefully in this respect.

The second is rare conditions such as HLHS mean single centre studies frequently suffer from small sample sizes. Collaborative projects between different institutions can be beneficial in this respect. In the Evelina London Children's Hospital, there are approximately 250 patients with HLHS under the care of the medical team with an additional 20 patients born each year. Whilst this represents a relatively large cohort of patients a joint project was initiated with a second centre to study this condition in greater depth. Building links and collaborations in this way is an important step towards improving our understanding of rare conditions.

There is a great richness of information to be gathered through multi-modality imaging, computational modelling and collaboration. These areas represent a highly technical field which comes at a cost in terms of expertise, training, equipment and good-will. Ultimately, in exploring new methods of characterising the systemic RV in HLHS this thesis hopes to provide further insight into the functional limitations faced by this group of patients.

To explore the interaction between cardiac function and shape, motion and energy in HLHS a stepwise approach is used:

1. Firstly a study to understand ventricular work and function in HLHS during a range of conditions using MRI catheterisation (XMR) techniques combined with pressure-volume analysis. (Chapter 1.4.5) We hypothesised that In those with HLHS, load-independent measures would provide us with insight into ventricular dysfunction.
2. Continuing with the theme of energetics; translation of a non-invasive MRI sequence into a tool to assess cardiac function based on indices of kinetic energy (KE). (Chapter 1.4.4) Subjects with a systemic RV undergo early circulatory failure and those with the largest, stiffest LV remnants have poorer outcomes. We hypothesised that an analysis of the intra-cardiac systemic RV kinetic energy would reveal that subjects with the largest LV remnants would have the most diminished diastolic KE values. Furthermore we hoped that that markers of function based around ventricular energetics should be better than markers based around ventricular volumetrics.
3. Finally employing computational post-processing tools to build upon our understanding of the shape and motion of the ventricle in relation to cardiac function. (Chapter 1.4.3) We hypothesised that strain would be reduced in those with a RVPA conduit .

2. Methods

2.1 Ethics

In all studies involving adults the local research ethics committee approved the design and volunteers and patients gave written consent (10/H0802/65). In studies involving children the local research and ethics committee approved that any child undergoing a clinically indicated MRI scan (anaesthetized or unanaesthetized) could undergo an additional 15minutes of scanning for research purposes (09/HO802/78). Those undergoing clinical XMR were permitted to have their data used for research purposes (Ethical approval 09/H0804/62). The attending medical professional was used to identify children who were felt suitable for inclusion into the studies. The family was provided with verbal and written information about the study and was allowed to consider whether they wished to participate and to seek further information if necessary. A signed consent form was completed for all studies. Assent was taken from younger children where they wished and was sought in all children who were deemed competent.

CMR scans of patients who underwent RVPA conduit were provided by Boston Children's Hospital, USA (ethical approval IRB-P00012488). CMR scans of patients who underwent MBT shunt were provided by Evelina London Children's Hospital, UK (ethical approval 08/H0810/058).

2.2 Study designs

The XMR data was acquired as a separate study involving prospective data collected from ten consecutive studies in patients with HLHS undergoing clinical XMR. Patients were referred by their clinician for assessment of exercise intolerance. Modified NYHA criteria were used by the referring clinician to qualify their level of exercise intolerance. All had undergone completion of a total cavopulmonary anastomosis at our institution and were scanned under general anaesthesia using low-dose inhaled sevofluorane with remifentanyl whilst maintaining normocarbia as per institutional preference. All subjects underwent cardiac MRI on a 1.5 Tesla scanner (Achieva; Philips Healthcare, Best The Netherlands) using a two-channel coil. Importantly all patients were too short in stature to undergo a cardiopulmonary exercise test. XMR assessments last approximately three hours and the young age of the patients meant that a general anaesthetic was required. The use of supine anaesthesia is further discussed in chapter 3.2.6. However the major disadvantages were: (1) lying supine is counter to normal Fontan physiology where systemic venous return partially relies on the action of the muscles to pump blood through the peripheral circulation; (2) anaesthesia involves the administration of medication which can potentially change the vascular resistance and; (3) positive pressure ventilation is counter to the normal mechanics of inspiration. To counter this only a light anaesthetic was utilised, patients were ventilated on minimal pressures and in a fractionated oxygen content close to room air. Response to this is consid-

ered on page 136.

A second study collecting 4D flow data was performed prospectively on 41 consecutive adults and children with single ventricle physiology (31 systemic right ventricle, 10 systemic left ventricle), 43 healthy volunteers (35 adults and 8 children) who acted as the negative control and 14 patients with left ventricle (LV) dysfunction (11 dilated cardiomyopathy, 3 ischaemic cardiomyopathy) who acted as the positive control. The aim being to compare health with single LV and single RV if enough volunteers were recruited.

Patients with a single ventricle circulation were recruited only at pre-Fontan and post-Fontan stages of their surgical palliation. Patients with a systemic-pulmonary shunt (the earliest palliative stage in the first few weeks of life) were excluded from the study due to their volume loaded physiology. All healthy volunteers were without cardiovascular disease, in sinus rhythm, with normal ECG and normal blood pressure. All patients under the age of 10 years were scanned under general anaesthesia using low-dose inhaled sevofluorane with remifentanyl whilst maintaining normocarbia as per institutional preference. Single LV datasets were collected to act as a control group for the Fontan group. Only a limited number of single ventricle subjects (n =5) had undergone cardio-pulmonary exercise testing (CPET) as most were of young age and short stature. As such an estimated assessment corresponding to the New

York Heart Association (NYHA) functional classification of heart failure symptoms was performed.

The collaboration between Boston and Evelina involved the most recent scans from both institutions from 2004-2014 of any patient with HLHS who underwent a Norwood procedure as the primary palliation were included and analysis occurred in a core laboratory (Kings' College London). Datasets consisted of balanced steady state free precession (bSSFP) cine imaging in 4 chamber and short axis orientations acquired on a Phillips Achieva MRI scanner according to recent guidelines.[84] At Evelina London Children's Hospital all children with HLHS undergo routine pre-operative CMR to help with surgical planning for Stage II and Stage III. Subjects only undergo cardiac catheterisation if additional information is needed for planning or optimising clinical status prior to surgery. At Boston Children's Hospital CMR is performed on those considered lowest risk (ie no echocardiographic evidence of ventricular dysfunction, severe AV valve regurgitation, atrial restriction or arch obstruction), with most still also undergoing additional cardiac catheterisation. Exclusion criteria for the study were subjects with other diagnoses such as unbalanced atrioventricular canal defect, or subjects that received an initial procedure other than a Norwood. There were differences in MRI selection criteria between the two institutions that were inherent in the design of the study. These are noted more in chapter 5.1.5.

2.3 Cardiac catheter - Stress MRI protocol

The research protocol is outlined in Figure 13. The preference would have been to use a pressure wire as it provides higher fidelity data than fluid filled catheters which are are susceptible to dampening. However due to the magnetic field of the MRI scanner they were not safe to use. Fluid filled Magnetic Resonance (MR) compatible catheters were used instead. Care was taken to minimise excess tubing to reduce damping. A catheter was placed in the systemic RV under X-ray guidance. A second MR compatible catheter was placed in one of the branch pulmonary arteries.

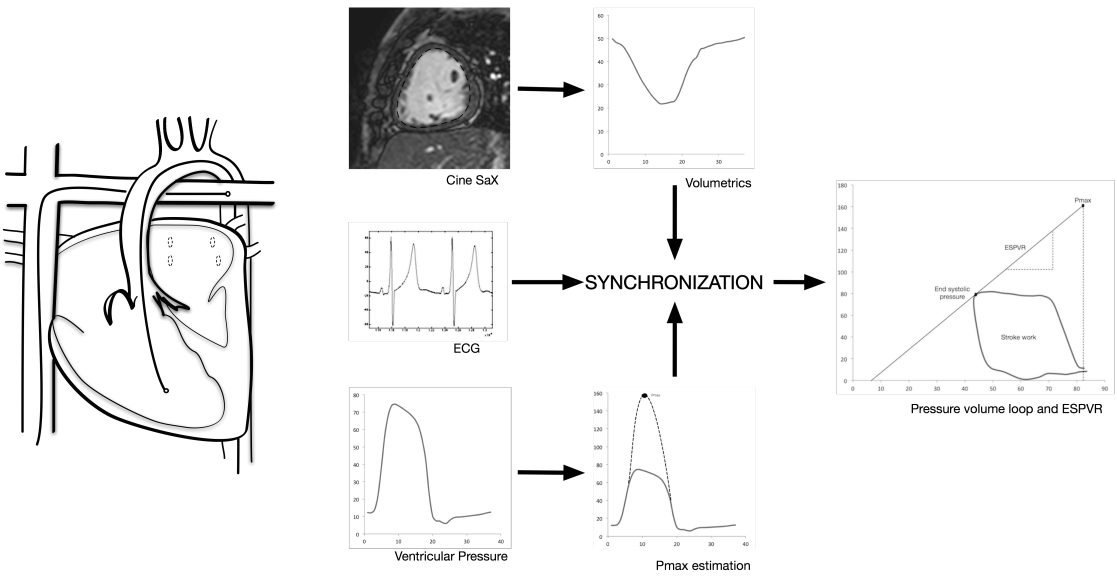

Figure 13: Workflow for composing pressure volume loops using cine MRI and invasive ventricular pressure measurements.

A mean pulmonary artery and mean pulmonary capillary wedge pressure were recorded and the difference used to calculate the trans-pulmonary gradient. Pressures were recorded on a haemodynamic tracer system (TechnoMed Medical Solutions, UK). Patients received a standard heparin bolus for anti-coagulation, which was monitored using activated clotting time to reduce the risk of thrombus. Once the catheters were in-place, the patient was transferred to the MR scanner to undergo simultaneous pressure and volume measurements.[145]

Invasive ventricular pressures, pulmonary and pulmonary capillary wedge pressures were recorded at rest and then repeated with infusion of dobutamine first at 10mcg/kg/min and then at 20mcg/kg/min to assess the incremental response to different levels of stress. Simultaneous cine short axis stacks of the ventricle with aorta, left pulmonary artery (LPA) and right pulmonary artery (RPA) 2D PC flow were performed during each condition. See chapter **1.4.4.1 2D phase contrast imaging** The protocol was terminated if the patient became haemodynamically unstable (a supra-physiological rise in blood pressure or heart rate). All patients tolerated the stress imaging.

2.4 Cine MR imaging

A retrospectively ECG-gated balanced-SSFP (bSSFP) cine short axis stack planned parallel to the atrio-ventricular valve plane of the systemic ventricle

was performed to assess volumes, wall mass and function. See chapter

1.4.3.1 Balanced steady state free precession cine imaging Images were acquired during end expiratory breath holds covering apex to base. Typical imaging parameters: TR = 3.0 - 3.6 ms; TE = 1.5 - 1.8 ms; parallel imaging (SENSE) factor 2; flip angle 60°; field of view 200 to 400 mm, slice thickness 6 to 8 mm depending on patient size, in-plane resolution 1.3 to 2.0 mm; acquired temporal resolution 30 to 40 phases, breath-hold duration 5-7 seconds per slice, 10-14 slices to cover the heart. The initial imaging demonstrated that inconsistencies in breath holds affected the accuracy of the ventricular segmentation. A 15mm respiratory gating window was required on awake patients to ensure breath holds were consistent between slices to reduce spatial misalignment. This occasionally meant the breath hold had to be repeated. The cross-sectional area of the outflow tract was measured on these images in two planes on the bSSFP images.

2.5 Two dimensional phase contrast flow MRI

A free-breathing retrospectively ECG triggered two-dimensional (2D) phase contrast (PC) flow was acquired orthogonal to the ascending aorta at the level of the right pulmonary artery (RPA) and additionally orthogonal to the superior and inferior vena cavae (SVC and IVC) with NSA 3, spatial resolution 1.5 x 1.5 x 6mm, acquired temporal resolution 30 phases. This was used to determine aorto-pulmonary collateral (APC) flow. The peak velocity of flow in the aorta

was used to target the velocity encoding (VENC) range of the 4D flow PC scan.

2.6 Four-dimensional phase contrast flow MRI

Preliminary work on this subject required validating a 4D flow sequence for clinical use. This work was led by a colleague and I was involved in recruiting subjects, performing the acquisition, analysing the data and preparing the manuscript. An edited version of this paper is reproduced to demonstrate the technical developments undertaken to validate 8-fold acceleration of 4D flow MRI technology prior to its use later in this chapter to derive kinetic energy.

Towards Highly accelerated Cartesian time-resolved 3D flow cardiovascular magnetic resonance in the clinical setting

Giese et al, *Journal of Cardiovascular Magnetic Resonance* 2014, **16**:42

The fidelity of k-t PCA (principal component analysis) was first investigated on fully sampled datasets with under-sampling applied retrospectively. A range of different acceleration factors were used to compare the data quality. Subsequently, k-t PCA with 8-fold nominal undersampling was applied on 10 healthy volunteers and 5 patients with different congenital heart diseases (CHD). Scan parameters are listed in *Table 3.* Quantitative flow validation was performed in vessels of interest and compared to 2D through-plane flow acquisitions. Particle trace analysis was used to qualitatively visualise flow patterns in patients.

Vessels of interest and phase contrast acquisition parameters

#	CHD	2D flow	3D flow					Age	GA
		Vessels of Interest (v_{enc} [cm/s])	Spatial res. [mm^3]	# Phases (Δt [ms])	FoV [mm^3]	v_{enc} [cm/s]	Scan time [min]		
0	Volunteers	AAo (200), MPA (200), RPA (200), LPA (200), SVC (100)	2.5x2.5x2.5	24	320x320x140	200	5.6	29y	no
1	HLHS (I)	AAo (200), LPA (150), RPA (200)	2.5x2.5x1.75	32 (17)	140x70x200	400	3.6	11m	yes
2	ToF	AAo (200), MPA (150)	1.78x1.61x2.5	24 (33)	200x280x100	200	5.2	21y	no
3	HLHS (II)	AAo (250), DAo (150), LPA (70), RPA (70), SVC (70)	1.26x1.61x1.79	24 (21)	141x180x79	200	5.2	2y	yes
4	HLHS (III)	AAo (200), LPA (80), RPA (80), SVC (80), IVC (80)	2x1.4x2	24 (37)	208x320x130	150	7.1	11y	yes
5	DILV	AAo (200), LPA (80), RPA (80), SVC (80), IVC (80), Fen (150)	1.18x1.71x1.72	24 (24)	151x220x95	150	6.8	3y	yes

Table 1: Scan parameters. HLHS (I-III): Hypoplastic Left Heart Syndrome after step I, II or III of the Fontan procedure, ToF: Tetralogy of Fallot, DILV: Double Inlet Left Ventricle. Nominal scan times excluding navigator efficiency are given. GA: general anaesthesia.

Table 3: 4D flow validation study: scan parameters

Accelerated 4D flow data was successfully acquired in all subjects with 8-fold nominal scan acceleration thereby outperforming previously validated under-sampling techniques for Cartesian 4D flow imaging. Nominal scan times excluding navigator efficiency were in the order of 6 min and 7 min in patients and volunteers. Figure 14a shows flow curves retrospectively undersampled with a *k-t* acceleration factor of R = 4, 8 and 10 along with the reference flow curve (R=1). Datasets were reconstructed using *k-t* SENSE (top row) and *k-t* PCA (bottom row). The accumulated flow error for both reconstructions as a function of the acceleration factor is shown in Figure 14b. Flow error increased significantly with acceleration factors above 8. *K-t* PCA outperformed *k-t*

SENSE above this threshold.

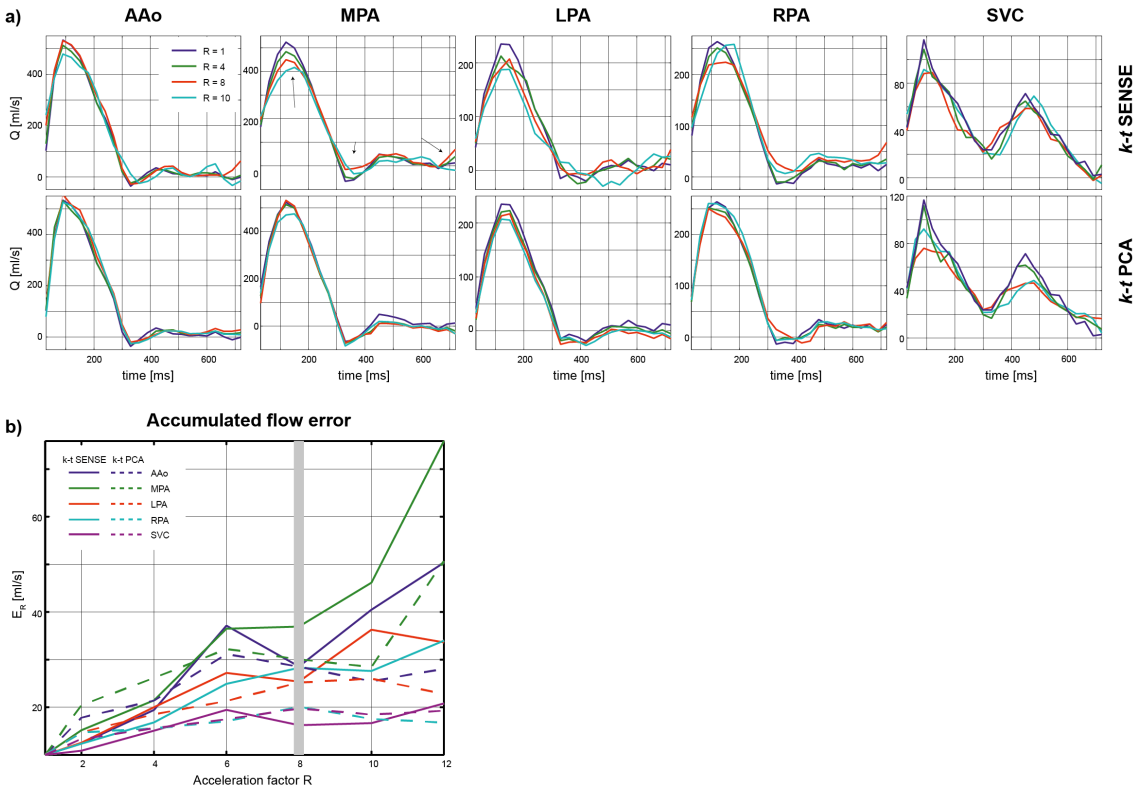

Figure 14: Retrospective undersampling with different kt acceleration factors

A correlation and Bland-Altman analysis of all stroke volumes derived from 2D flow acquisitions and undersampled 4D flow data reconstructed using *k-t* PCA is shown in Figure 15. Linear regression resulted in a correlation coefficient of $R^2 = 0.93$ and the Bland-Altman analysis revealed a mean deviation of 2.5 ml and a standard deviation of 8.4 ml corresponding to 5.6 ± 14.9% with respect to the stroke volumes derived from the 2D flow datasets. Mean differences in stroke volume in selected vessels of interest were 2.5 ± 8.4 ml and 1.7 ± 4.7 ml

in volunteers and patients, respectively.

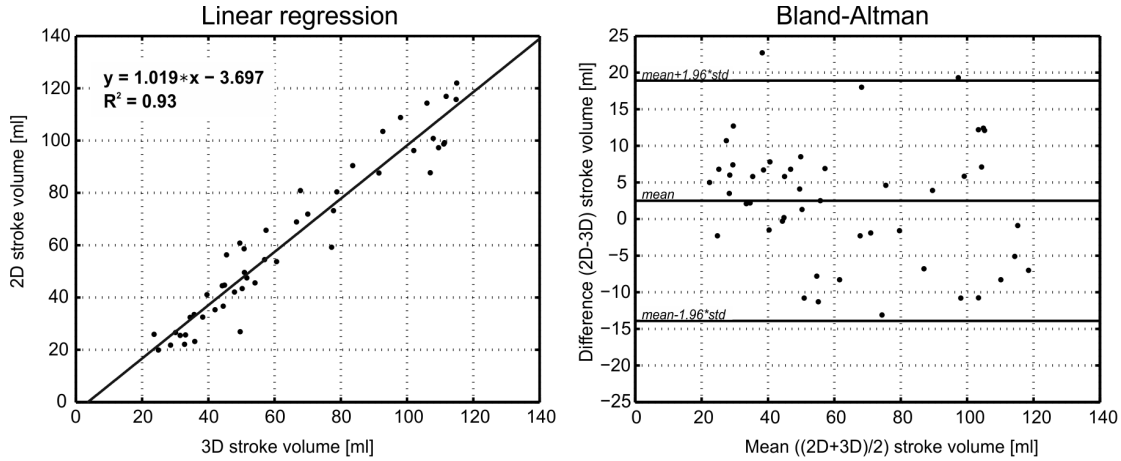

Figure 15: Liner regression and Bland Altman plots of 2D vs. 4D flow measurements

Qualitative flow pattern analysis in the time-resolved 3D dataset revealed valuable insights into hemodynamics including circular and helical patterns as well as flow distributions and origin in the Fontan circulation.

In conclusion, highly accelerated 4D flow using k-t PCA with a factor of 8 was demonstrated to be clinically feasible. Nominal scan times of 6 minutes were well tolerated and allowed for quantitative flow assessment in all great vessels.

Following this validation a free-breathing prospectively ECG triggered 4D flow whole heart MRI sequence was acquired using a targeted VENC based on 2D PC aortic peak velocity. The mean field of view was 300x70x150mm, with a spatial resolution specific to the size of the patient: small children (<20kg) 2.0mm isotropic voxels, large children and adults (20-90Kg) 2.5mm isotropic voxels, large adults (>90Kg) 3mm isotropic voxels. The number of phases was adjusted to between 24-32 phases to acquire a temporal resolution of <35ms. These factors also helped ensure that the scan acquisition was within 15minutes as stipulated in the research ethics. Other imaging parameters included: TR= 3.8ms; TE=2.4ms; Flip angle 5; acceleration kt+= 8; bandwidth 500Hz. Respiratory gating for motion correction was applied giving a nominal scan time of 5-7minutes. [126, 170] Data was reconstructed using in-house implemented kt-PCA method [171, 172] and subsequently corrected for background errors. The analysis of flow data was performed using proprietary software (GTFlow, GyroTools LLC, Zurich, Switzerland). Balanced cine SSFP images were used to help segment the motion of the mitral valve annulus throughout the cardiac cycle on the 4D PC imaging. This allowed us to measure peak through-plane inflow velocities into the left ventricle (the mitral E wave) and compare them to changes in diastolic KE.

2.7 Flow and volume analysis

Analysis of MRI volumetric and flow data was performed using a Viewforum workstation (Viewforum EWS, release 2.0, Philips Healthcare, Best, Netherlands). RV volumes and wall mass were measured using a Viewforum workstation (Viewforum, release 2.0, Philips Healthcare, Netherlands). End-diastolic (EDV) and end-systolic (ESV) volumes were manually contoured from a cine short-axis stack corresponding to the ventricle cavity. Trabeculations were excluded from the blood volume. The difference between EDV and ESV was the stroke volume (SV). Ejection fraction (EF) was calculated from: (EDV-ESV)/EDV x 100. Tricuspid regurgitation was recorded from the original MRI report. (Mild <15%, moderate 15-25%, moderate-severe 25-45% and severe >45%).

Cine short and long axis imaging was used to categorise the LV remnant. The function of the systemic RV is affected more by the shape and size of the LV remnant rather than the presence or absence of forward flow across the mitral/aortic valve. LV morphology was therefore described in terms of (1) shape: slit-like or globular and; (2) size: based on the median volume of the LV. Slit-like LVs tended to represent those with mitral atresia/aortic atresia (MA/AA) whilst those with globular LVs tended to represent those with mitral stenosis/aortic atresia (MS/AA) and mitral stenosis/aortic stenosis (MS/AS).

APC flow was calculated as follows:

$$Q_{APC} = Q_{Ao} - (Q_{SVC} + Q_{IVC})$$

where: Q = flow, Ao = ascending aorta, SVC = superior vena cava, IVC = inferior vena cava

2.8 Pressure-Volume loops

Pressure-volume loops were constructed for each condition. The end-systolic pressure-volume relationship (ESPVR) was derived at each state from a validated maximal pressure (P_{max}) estimation method using the average of multiple pressures. [161] The slope of the ESPVR represents the elastance of the ventricle (E_{es}). The slope of the relationship of end diastolic volume (EDV) to end systolic pressure (ESP) defines the elastance of the artery (Ea). Ventriculo-arterial coupling is represented by the ratio of E_{es} to E_a. The area within the pressure volume loop was used to establish ventricular stroke work and multiplied by heart rate to calculate power. Tau (τ), the early relaxation constant, was calculated from the reciprocal of the natural logarithm of the early maximal fall in ventricular pressure during diastole.

The LV is a prolate ellipsoid and RV geometry differs markedly from this. When calculating RV preload different assumptions must be made. Therefore preload values were taken from multiple averaged measurements and calculated using a modified *La Place* formula: [173]

$$\sigma = \frac{Pr}{h(2 + \frac{h}{r})}$$

where:

σ = mean end diastolic wall stress

P = RV pressure (dynes/cm^2)

r = endocardial radius of curvature (cm)

h = wall thickness (cm)

The branch pulmonary artery flows and trans-pulmonary gradient were used to calculate pulmonary vascular resistance. [138]

2.9 Calculation of Kinetic Energy

Initially the endocardial border of the left ventricle was manually segmented in the first time frame from the short axis cine stack bSSFP images using CardioViz3D software. [174] This allowed the generation of endocardial surfaces and a separately labelled mask image. LV motion, as seen in the cine data, was tracked by an image registration based method [175, 176] using the "Image Registration Toolkit" (IRTK, IXICO Limited) to create displacement fields. The displacement fields were used to morph the systemic ventricular myocardial mask creating a 4D ventricular mask.

Particles from the 4D flow sequence were seeded within the mask at a density

equivalent to the voxel size of the 4D flow images for each time frame and the phase contrast 4D data used to measure the velocity.

KE was calculated by taking the instantaneous velocity magnitude of a particle and applying the following formula:

$$Kinetic\ energy = ½\ mass \times velocity^2$$

The mass of blood was derived from multiplying the mean density of blood ($1060 g/mm^3$) by the voxel volume represented by each particle.

To allow comparison between hearts of different sizes the KE values were indexed and expressed as a *kinetic energy density* also described as an *indexed kinetic energy* based on the instantaneous volume blood present in the ventricle at that phase of the cardiac cycle. The resultant parameter was expressed in the form of energy per millilitre of blood (mJ/ml). KE values were expressed as a fraction of the R-R interval. KE was measured throughout the cardiac cycle. KE in different parts of the cardiac cycle is demonstrated in Figure 16 for a healthy LV.

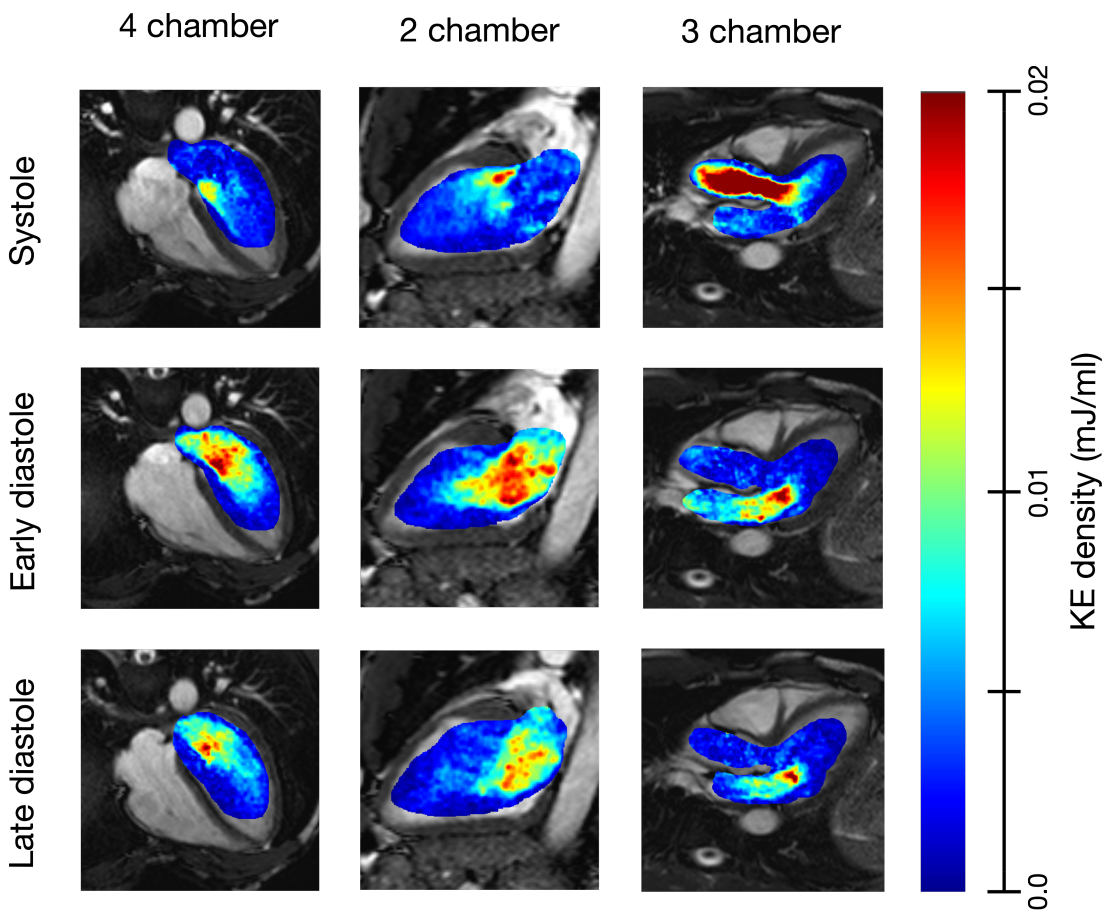

Figure 16: Illustrative example of 2, 3 and 4 chamber views of a healthy heart demonstrating the KE density during different portions of the cardiac cycle.

2.10 Calculation of Kinetic and Particle Energy

A new systolic metric of function was developed around the work used to perform useful ejection of blood compared to the total kinetic work performed in systole. The blood particles were divided into ejected and residual compo-

nents. Ejected blood was defined as blood that started in the ventricle at end-diastole and was ejected through the aortic valve during the systolic phase and represents the useful work imparted onto blood. Residual blood was defined as blood that started in the ventricle at end-diastole and remained in the ventricle at end-systole (see Figure 17) this represented the less energetically efficient processes. The peak of the total kinetic energy achieved by each component of blood was chosen to reflect the maximum systolic energy exerted by the heart on the blood (see Figure 18). We expected to see that most KE would be imparted to ejected blood and any energy imparted to the residual blood would be small in healthy hearts.

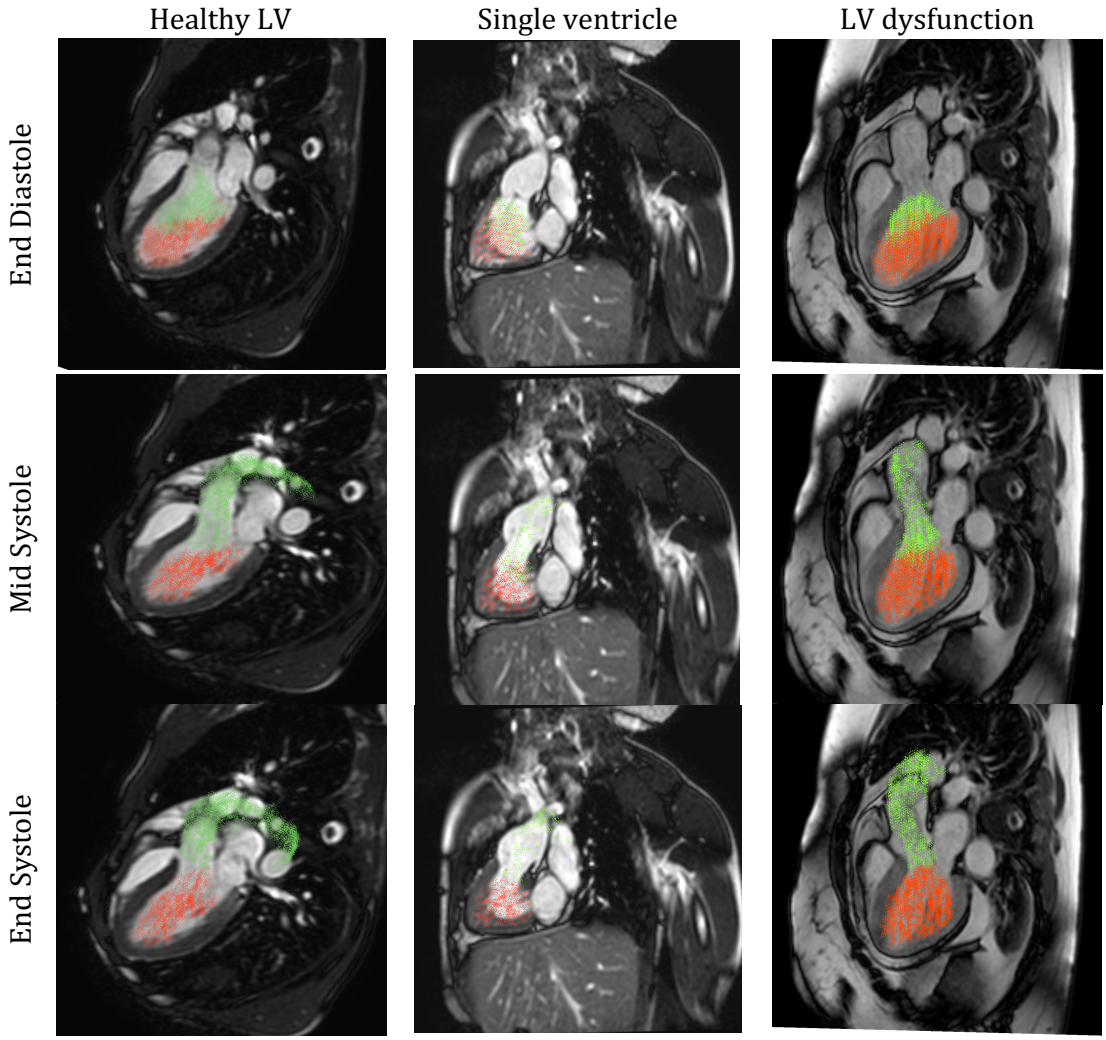

Figure 17: Three chamber views showing examples of ejected and residual particles from each of the three groups. Particles are seeded throughout the ventricle cavity in end diastole and based on streamline velocity vectors tracked through systole. Red particles represent retained particles and green particles show ejected particles.

Two energetic metrics were derived. In the first method, the peak instantaneous kinetic energy achieved by each component of blood was chosen to reflect the maximum systolic energy exerted by the heart on each blood component (see Figure 18). This is comparable to other published methods. In the second method, a novel approach was used. An advantage of 4D flow MRI is the ability to study the motion of individual particles of blood. The individual peak energy value achieved by each particle was summated for each blood component to provide a measure of particle energy (PE). Assessing the motion of blood on a particle-by-particle basis represents a Lagrangian approach to assessing fluid dynamics. Our aim was to see if either metric offered useful insights into ventricular function.

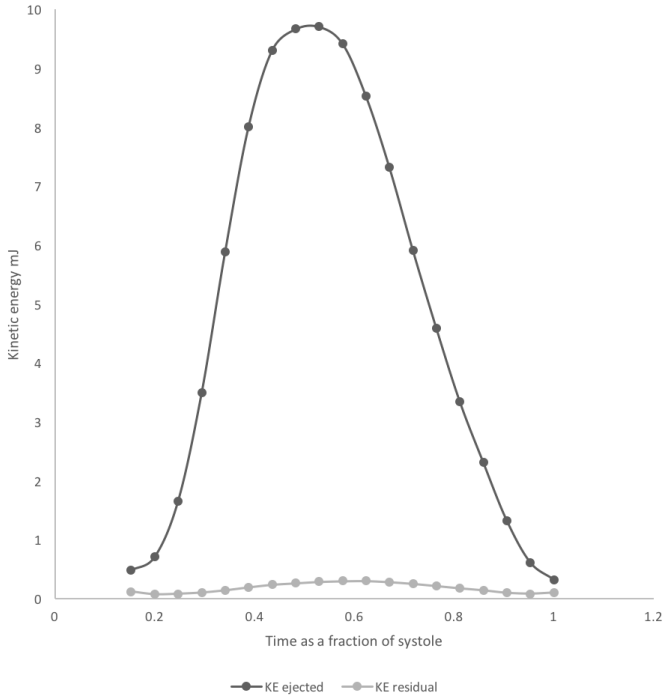

Figure 18: Typical kinetic energy curves for the ejected and residual blood components in a healthy volunteer. To allow for different heart rates the time is indexed as a fraction of total length of systole.

To compare hearts of different sizes the KE and PE values were indexed. Indexing to body surface area was considered but since the heart grows allometrically and also can vary in size dependent on physiology and pathology it was felt to be more accurate to index it based on the blood volume and express it as an energy density based on the volume of the ejected and residual blood components. Ejected energy was divided by stroke volume (SV)

and residual energy was divided by end-systolic volume (ESV). The resultant parameters were respectively known as iKE_{ej} or iPE_{ej}, and iKE_{res} or PE_{res}. They were expressed in the form of *energy per millilitre* of blood (mcgJ/ml). [137]

As a smaller outflow tract could cause acceleration of blood and act as a confounder in any analysis we compared the relationship between the size of the outflow tract and peak energy values. In addition, the time and location at which each particle reached peak velocity was assessed. For the ejected blood streamline data showed this invariably occurred in the aorta.

2.11 Energy ejection fraction

The *kinetic energy ejection fraction* (KE EF) index was calculated corresponding to the following formula:

$$KE\ ejection\ fraction = \frac{KE_{ejected}}{KE_{ejected} + KE_{residual}} \text{ x } 100$$

Where:

$KE_{ejected}$ = peak total KE value of the ejected blood component during a single cardiac cycle,

$KE_{residual}$ = peak total KE of the residual blood component during a single cardiac cycle.

The *particle energy ejection fraction* (PE EF) was calculated corresponding to

the following formula:

$$\text{PE } ejection\ fraction\ = \frac{PE_{ejected}}{PE_{ejected} + PE_{residual}} \text{ x } 100\%$$

Where:

$PE_{ejected}$ = total individual peak PE value of the ejected blood component during a single cardiac cycle,

$PE_{residual}$ = total individual peak PE of the residual blood component during a single cardiac cycle.

These relationships determined the proportion of useful energetic work done in ejecting blood compared to the overall energetic work during systole. KE EF reflecting the instantaneous kinetic energy, PE EF representing a particle-based approach to particle energetics. These values were compared to VV EF for each patient group to determine their impact.

2.12 Creation of a Cardiac Atlas

The RV myocardium of all short-axis cine stacks was manually contoured at end-diastole, using ITK-SNAP (2.4.0). [177] The septal wall was included as part of the RV whereas the LV free wall was excluded from the segmentation as only the RV shape was of interest. Trabeculations were also excluded from the segmentation. [84] The position of the LV was marked on the most basal slice, as illustrated in Figure 32, to correctly align each segmentation and allow comparison of cases.

A 3D geometrical model was then built from each RV segmentation using previously described methods. [104] The 3D geometrical model is described by a detailed set of 3456 variables that govern the geometry and orientation of the model in 3D space. They include traditional 2D geometric indices of thickness, length, and diameter which were automatically extracted from these computational models.

Finally, a computational atlas was built from the collection of 93 RVs which described the change of shape from an average anatomy. To more easily permit comparison between the MBT and RVPA groups, the cardiac atlases which contained the largest variability in shape were detected using a principal component analysis (PCA). As a result the description of each shape was reduced from 3456 variables to 10 variables. The variables which represent the largest variability in shape have previously been described in the literature as *anatomical modes.*

2.13 Strain analysis

Longitudinal and short-axis cine images were used to compare systolic and diastolic strain in the two HLHS populations using CMR feature tracking software (Diogenes MRI, Tomtec, Germany). The endocardial borders of the RV were manually defined in 1 time frame then automatically propagated

through all time frames, tracking the endocardial-blood border and adjacent features to provide strain data. The 4-chamber view was used to measure RV longitudinal function. The short-axis images were used to assess RV circumferential and radial function at basal, mid-ventricle, and apical levels. Short axis stacks were linked to the position in the 4 chamber view to choose the appropriate slice. Global strain was recorded as the mean of the segmental strain values for systolic strain, systolic strain rate, and diastolic strain rates. Strain measures the change in length of the myocardium relative to its original length. Positive strain values indicate a lengthening of the ventricle (as seen in radial motion) and negative values indicate a shortening of the ventricle (as seen in longitudinal and circumferential motion). Values of a greater magnitude, irrespective of the vector, reflect improved motion. Regional strain particularly in the area of the ventriculotomy would be useful to determine if the scar caused dyskinesia. However in view of the high variability of regional strain only global strain value were recorded.

2.14 Statistical analysis

Statistical analysis was performed using SPSS version 23 or Stata 13.1 (for KEEF).

Analysis of categorical variables comprised of Chi-squared tests (eg tricuspid regurgitation and LV morphology). Continuous variables were expressed as

mean ± SD. Unpaired t-tests were used for inter-group comparisons in cohorts containing only two subgroups. Paired t-tests were used for comparison in age and sex matched subjects. For cohorts with three or more subgroups, one-way analysis of variance (ANOVA) with Bonferroni-adjusted, post hoc t-tests were used for the majority of variables, provided the assumptions for ANOVA were met (normal distribution, equality of variance). However, this did not apply for ejection fractions (VV EF, KE EF, PE EF) which were bounded by 0% and 100%, do not exhibit equal variance, and, in the case of KE EF and PE EF, were highly left skewed. Ejection fractions were thus analyzed using a generalized linear model (GLM), assuming a binomial distribution for the dependent variable and utilizing a logit link function and robust standard errors. [178] Quantile-quantile (Q-Q) plots and the Shapiro-Wilk method was used to assess for normality. Throughout a p value < 0.05 was considered significant.

Multiple linear regression analysis was performed using early diastolic KE as the dependent variable and iEDV, iESV, iSV, indexed wall mass and indexed LV remnant volume as the independent variables.

Inter-user variability of the single ventricular volume segmentations and aortic flow measurements was quantified using an intra-class correlation coefficient 2-way model with absolute agreement. Measurements were sampled for 10 subjects from the systemic RV group by two authors (JW, KP).

Values of kinetic energy were indexed to the volume of blood within the ventricle at each recorded time-point and expressed as a proportion of the R-R ECG interval to allow comparison between subjects of differing sizes, heart rates and function. The Haycock method of calculating body surface area (BSA) was used as an index to compare differently sized children. This method is used in chapters 3 and 4. However several studies have shown there exists a non-linear relationship between cardiovascular dimensions and BSA within the paediatric population. The heart grows at a different rate to the body. Allometric cardiac growth occurs with age so linear indexing to body surface area is permissible only between fully-grown adults of different sizes. [179] [180] This allometric growth of the heart means comparisons between individuals of different ages is best performed by indexing volumes to BSA raised to the power of 1.3 ($ml/BSA^{1.3}$) and indexing measures of length to the square root of BSA ($mm/\sqrt{m^2}$). [181, 182] Indexing in this way has been shown to have a bearing on prognosis. [183] This technique was adapted for the later paper in Chapter 5 along with conventional indexing of values to allow for a comparison.

3. Characterising ventricular function: XMR

The XMR study provided data for two publications. The first focusing on the response of PVR during pharmacological stress and the second assessing ventricular energetics during stress. An edited version of the first manuscript is reproduced below outlining the effects of nitric oxide on pulmonary vascular resistance. It forms the preliminary work to pressure-volume loop assessment of the systemic right ventricle using XMR. My involvement was patient selection, data collection, data analysis and editing the final manuscript.

3.1 Magnetic Resonance Imaging catheter stress hemodynamics post Fontan in hypoplastic left heart syndrome.

Pushparajah *et al*, Eur Heart J Cardiovasc Imaging. 2016 Jun;17(6):644-51.

Given our knowledge of the exercise limitations in those with HLHS we sought to quantify their response to pharmacological stress compared to a healthy cohort of adults and additionally assess the impact of a pulmonary vasodilator on cardiac output. The major findings in this study were that healthy adults are able to sustain a 61% rise in cardiac output with administration of dobutamine at 10mcg/kg/min followed by a 19% rise in cardiac index with administration of dobutamine at 20mcg/kg/min. In comparison, in subjects with HLHS the equivalent response to incremental dobutamine are a 40% rise followed by a plateau

in cardiac index. The addition of inhaled nitric oxide, a selective pulmonary vasodilator, did not cause any change in the measured pulmonary vascular resistance (baseline mean pulmonary vascular resistance was 1.51 ± 0.59 WU.m^2) or improvements in cardiac output. These results suggest that the blunted increase in cardiac index that occurs during dobutamine stress is not due to a limitation in pulmonary vascular resistance. Investigation of the function of the ventricle might help distinguish whether abnormal ventricular function, afterload or preload are responsible for these effects.

3.2 Pressure-volume loop derived cardiac indices during Dobutamine stress; a step towards understanding limitations in cardiac output in children with hypoplastic left heart syndrome

International Journal of Cardiology. 2017 Mar; 230:439-446

3.2.1 Background

In this section a group of children with HLHS exhibiting symptoms of diminished exercise capacity were studied. The focus was on assessing ventricular energetics and function whilst applying incremental dobutamine stress to study the changes in physiology through a range of heart rates and to help unravel the cause of the blunted cardiac output shown in the preliminary study. Evidence suggests impaired systolic and diastolic function may contribute towards reduced cardiac output [54, 184] but the load dependency of many of the

measures of function in this group of patients give inconsistent results. [69–71] Using load independent measures of function as described in Chapter 1.4.5.2 would allow a detailed understanding of the limitations of cardiac function. We hoped that stepwise increments of dobutamine might unmask ventricular dysfunction only seen at the highest heart rates (Chapter 1.4.5.3) and explain why these patients have to a limited ability to increase cardiac index (CI). [51, 52]

3.2.2 Results

Ten consecutive studies were performed with all patients having undergone staged palliation for HLHS. All were prospectively recruited and all tolerated the full dobutamine protocol. Table 4 shows the demographics. Mean age 8.6years (range 3.5 - 11.6yrs), mean weight 25.8Kg (range 16 - 46Kg), mean time since Fontan completion 5.5 years (range 0.5 - 9 years). No significant tricuspid regurgitation in any patient. All subjects recruited into the study were referred for assessment of reduced exercise capacity. All patients were NYHA 2 as described by their clinician.

ID & morphology	Age (Y)	Weight (kg)	Time since Fontan (Y)	Saturations (%)	TR
1. HLHS	9.2	26.5	5.7	98	Mild
2. HLHS	11.6	45.9	8.9	95	None
3. HLHS	9.2	20	6.7	92	None
4. HLHS	5.9	21.5	3.5	95	None
5. HLHS	5.8	16	3.5	93	Mild
6. HLHS	9.1	14.1	6.5	98	Mild
7. HLHS	5.5	16	0.5	93	Mild
8. HLHS	7.6	30	4.2	92	None
9. HLHS	10.1	34.4	8	93	Mild
10. HLHS	12.2	34.6	6.5	96	None
Mean ± SD	8.6 ± 2.3	25.8 ± 10.2	5.5 ±2.6	95 ±2	

Table 4: XMR study: patient demographics. TR is tricuspid regurgitation

MRI derived indices of Cardiac function

Tables 5 and 6 show haemodynamic response and MRI derived parameters. Ejection fraction (54.0 ± 6.7%) was in the normal range but baseline CI was low (2.7 ± 0.6 L/min/m^2) compared to published values for healthy children which is usually in the range of 3.3-5.1L/min/m^2. [179, 180] During administration of 10mcg/kg/min dobutamine there was an expected rise in CI (p =0.01). This was driven solely by a rise in HR (p = 0.0001). SV remained the same as although ESV fell

(p = 0.001) there was a similar fall in EDV (p = 0.0001). At maximum stress with 20mcg/kg/min dobutamine there was no further increase in CI, HR rose (p = 0.002), however SV fell (p = 0.045) as the fall in EDV was greater than the fall in ESV.

ID	Heart rate (bpm)			iCO (l/min/m^2)			EF %			Mean BP (mmHg)		
	Rest	Dob10	Dob20	Rest	Dob10	Dob20	Rest	Dob10	Dob20	Rest	Dob10	Dob20
1	53	113	127	2.2	5.0	4.7	49	66	63	46	66	60
2	69	107	142	2.3	3.9	4.3	49	65	67	71	122	120
3	59	95	140	2.1	4.1	4.1	57	81	73	59	110	153
4	76	115	138	2.4	3.9	4.3	46	55	60	59	104	99
5	60	128	141	3.0	4.9	5.3	56	58	66	46	60	73
6	68	95	105	3.3	4.1	4.4	61	70	71	44	56	57
7	65	120	132	3.9	4.4	4.6	67	69	76	41	43	48
8	62	113	141	2.9	4.4	3.4	49	65	55	51	91	81
9	68	141	149	2.5	4.1	4.4	49	68	64	55	71	66
10	69	122	132	2.3	3.1	3.0	57	62	66	42	80	81
Mean	65	115*	135 *	2.7	4.2 *	4.2 *	54.0	65.9 *	66.1 *	51	80 †	84 †
±SD	±7	±14	±12	±0.6	±0.4	±0.6	±6.7	±7.1	±6.2	±10	±26	±32
ANOVA P value		**0.0001**			**0.0001**			**0.001**			**0.012**	
Post-hoc compared to rest				* denotes p < 0.01			† denotes p < 0.05					

Table 5: XMR study: haemodynamic response. Where bpm indicates beats per minute, iCO indexed cardiac output, EF ejection fraction, BP blood pressure, Dob dobutamine

ID	iRVEDV (ml/m^2)			iRVESV (ml/m^2)			iSV (ml/m^2)			APC as % of CO
	Rest	Dob10	Dob20	Rest	Dob10	Dob20	Rest	Dob10	Dob20	Rest
1	80	65	58	38	20	21	41	45	37	14.5
2	65	53	42	31	17	13	33	35	30	10.8
3	63	53	40	26	10	10	36	43	29	27.8
4	69	60	50	36	26	19	33	34	31	22.4
5	80	63	49	30	24	18	49	39	37	12.5
6	81	61	54	31	17	18	51	43	42	0.0
7	72	56	44	12	19	9	61	39	35	7.2
8	97	60	44	49	21	20	48	39	24	21.4
9	74	45	46	37	13	17	37	29	29	6.6
10	58	40	35	25	15	12	33	25	23	6.1
Mean	74	56 *	46 *	32	19 *	16 *	42	37	32 †	12.9
±SD	±11	±8	±7	±10	±4	±4	±10	±6	±6	±8.6
ANOVA P value		**0.0001**			**0.0001**			**0.019**		
Post-hoc compared to rest				* denotes $p < 0.01$			† denotes $p < 0.05$			

Table 6: XMR study: MRI derived volumetric indices. Where iRVEDV indicates indexed right ventricular end diastolic volume, iRVESV indexed right ventricular systolic volume, iSV indexed stroke volume, APC aorto-pulmonary collateral flow, CO cardiac output

Contractility and Coupling

In expressing the heart as a time varying elastance model (a pressure-volume loop) the slope of the ESPVR is a measure of the elastance of the ventricle under that given condition. This is the pressure required to elicit a change in volume of the ventricle and measures ventricular contractility (Ees). The elastance

of the aorta is the relationship of the LV end systolic pressure to the stoke volume. It measures the load on the arterial system (see Chapter 2.8 for further details). Figure 19 shows the MRI-catheterization derived indices of contractility and coupling. Contractility (as measured by end-systolic elastance, Ees) increased 67% during the low dose dobutamine stress (10mcg/kg/min) (p = 0.045) with no further increase with dobutamine 20mcg/kg/min. This was accompanied by a stepwise increase in afterload (as measured by arterial elastance, Ea), which reached significance at dobutamine 20mcg/kg/min (p = 0.012). The ventriculo-arterial coupling ratio (Ees:Ea) was calculated. This is a ratio of elastances of the aorta and ventricle. The heart has the greatest mechanical efficiency when elastances are matched. [155, 156] However physiologically the heart works with a typical ratio of 1.5:1.0. [147, 157] (See also Chapter 1.4.5 for further details). The ventriculo-arterial coupling ratio (Ees:Ea) was 1.45 ± 0.2 at rest. It remained adequately coupled during administration of incremental doses of dobutamine due to increases in both contractility and afterload. The wide standard distribution may explain why although increases in contractility and afterload were seen between some conditions of dobutamine these were non-significant.

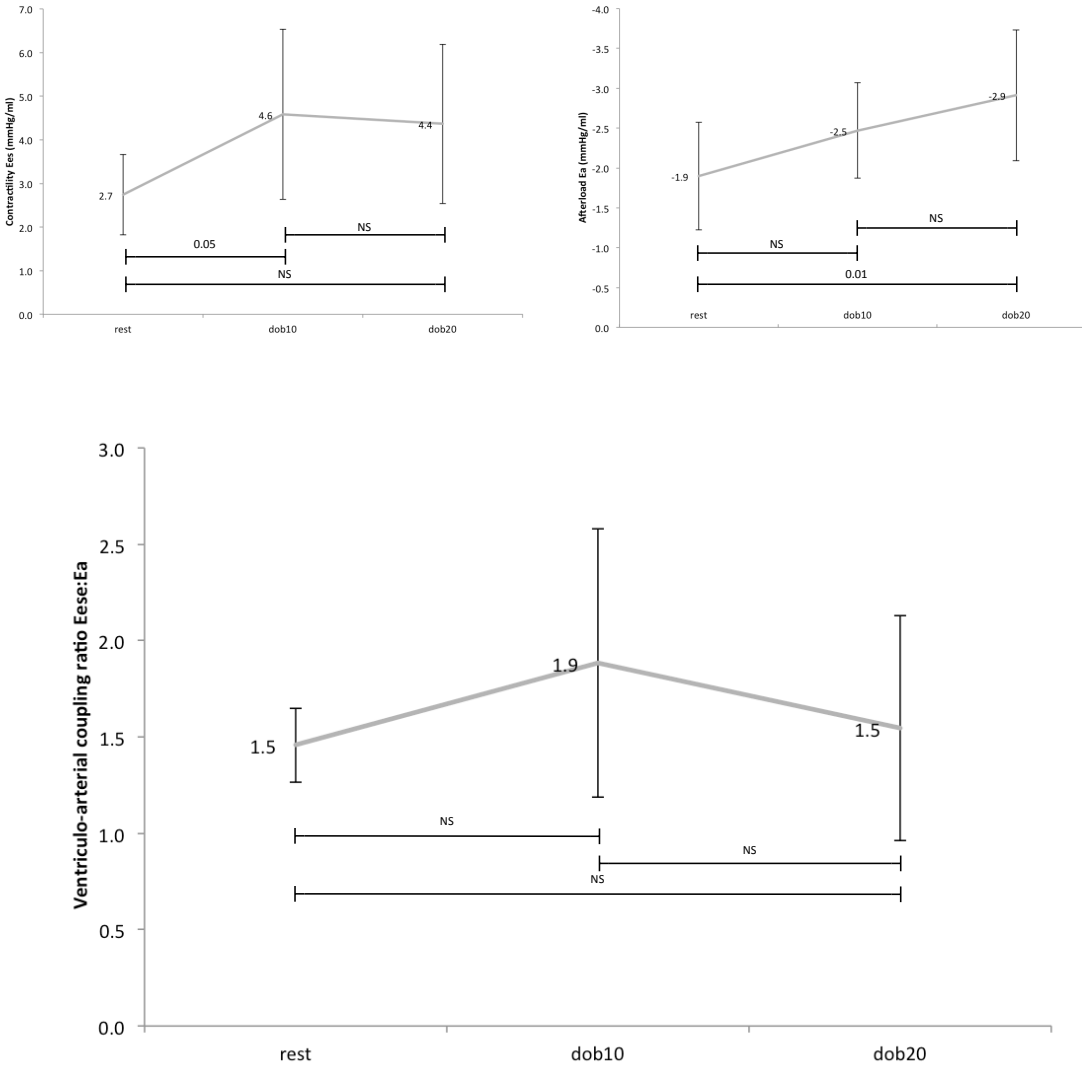

Figure 19: Effect of dobutamine on ventriculo-arterial coupling. Mean effects of dobutamine stress on contractility (top left), afterload (top right) and ventriculo-arterial coupling ratio (lower)

Ventricular work

Figure 20 (top panel) shows PV loops for each condition of dobutamine. During dobutamine stress although there was a change in the shape of the PV loop,

stroke work did not alter from resting conditions however large corresponding increases in HR meant cardiac power increased significantly (114%) with dobutamine 10mcg/kg/min (p = 0.001) but plateaued with dobutamine 20mcg/kg/min as the late fall in SV offset any further incremental rise in power (lower panel).

Myocardial Relaxation

Parameters of diastolic function were normal at rest (Table 7) with an end diastolic pressure (EDP) and early relaxation constant (Tau) that compared to the literature. EDP remained low throughout the study, which is not in keeping with the rise that usually occurs during stress in healthy subjects. When indexing EDP to the RVEDV (mmHg/ml) to give an indexed filling pressure, there was no significant change with application of stress (p =0.99). There was an overall stepwise improvement in myocardial relaxation as demonstrated by the fall in Tau, which reached significance at dobutamine at 20mcg/kg/min (p = 0.038).

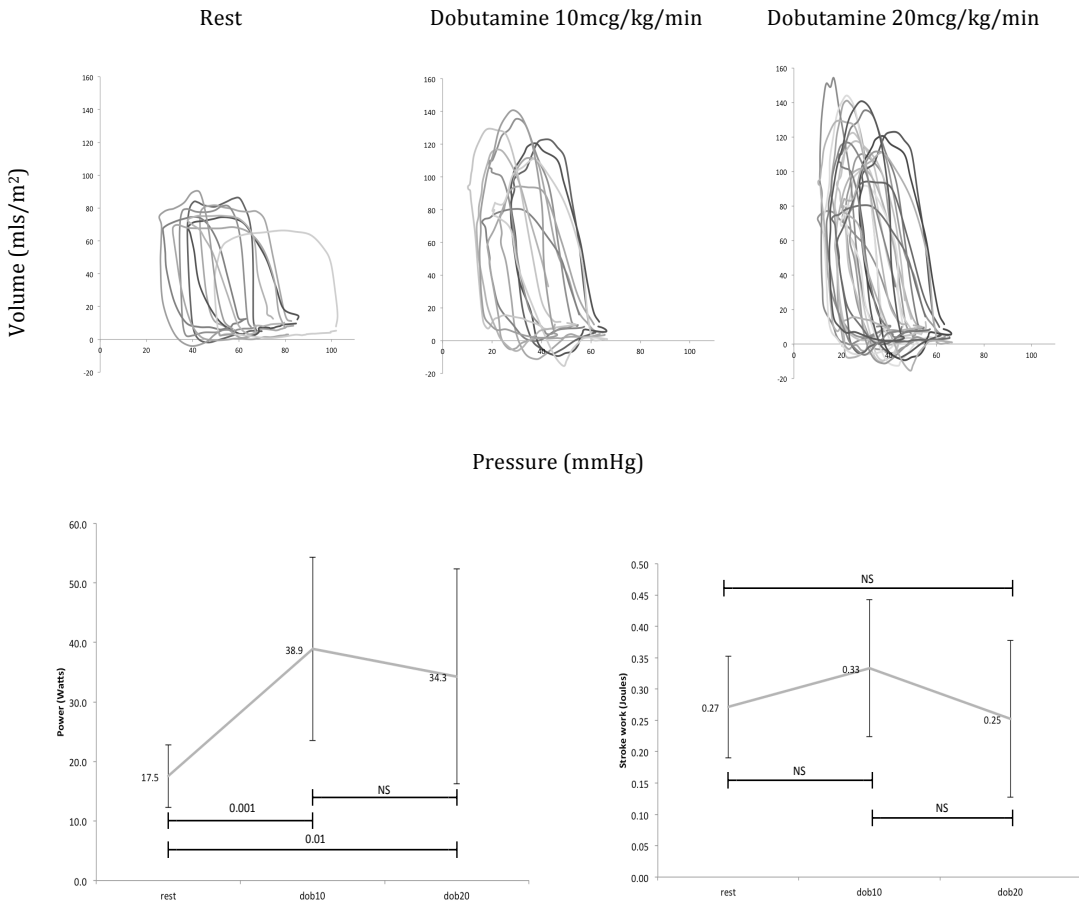

Figure 20: Pressure-volume loops and energetic effects of dobutamine. Top panel shows pressure volume loops for all ten subjects at rest, with dobutamine at 10mcg/kg/min and with dobutamine at 20mcg/kg/min (right panel). Volumes are indexed to body surface area to allow comparison of loops. Lower panel shows the response of power (left) and stroke work (right) to dobutamine.

ID	EDP (mmHg)			Tau			Preload x10^3 dynes/cm^2			PVR ($WU.m^2$)		
	Rest	Dob10	Dob20	Rest	Dob10	Dob20	Rest	Dob10	Dob20	Rest	Dob10	Dob20
1	8.0	4.8	7.0	28.9	22.8	17.7	80	33	28	0.9	1.7	1.7
2	7.5	9.5	6.0	12.5	6.4	4.3	68	61	27	0.9	0.42	2.0
3	12.5	11.5	10.5	45.7	22.0	18.5	77	53	28	0.8	1.5	1.6
4	4.5	4.5	4.0	28.7	27.0	8.8	37	27	25	2.1	2.5	2.1
5	12.0	9.0	10.7	28.6	12.4	4.6	81	41	36	1.0	0.5	0.5
6	3.5	4.0	6.0	18.0	13.0	6.3	19	18	16	0.9	0.8	0.8
7	10.7	9.5	11.0	62.5	18.8	27.0	89	70	46	0.95	0.9	1.1
8	5.0	2.0	2.0	18.4	18.8	14.2	36	46	36	1.5	1.8	1.7
9	10.0	10.0	7.0	28.8	23.4	19.8	42	31	22	1.9	1.8	1.5
10	6.5	6.3	3.8	22.6	30.7	21.6	32	16	19	4.4	3.7	3.4
Mean	8.1	7.4	7.1	30.1	19.3	13.8 *	52	36	26 †	1.7	1.7	1.8
±SD	±3.1	±2.8	±2.7	±14.3	±7.4	±8.0	±30	±19	±10	±1.2	±1.1	±0.8
ANOVA P value		0.72			**0.005**			**0.037**			0.97	
Post-hoc compared to rest				* denotes $p < 0.01$			† denotes $p < 0.05$					

Table 7: Cardiac diastolic function. Where EDP indicates end diastolic pressure, Tau is the early relaxation constant, PVR is pulmonary vascular resistance

Preload and PVR

There was a stepwise fall in preload of 30% between rest and dobutamine 10mcg/kg/min and of 50% from rest to dobutamine 20mcg/kg/min. This reached significance with dobutamine at 20mcg/kg/min (p = 0.008). The relationship of preload to SV is shown in Figure 21. The change in preload was not related to PVR, which was in the normal range (1.7 ± 1.2$WU.m^2$) and remained unchanged throughout (Table 7). APC flow contributed 12.9% of cardiac output

at rest (Table 6).

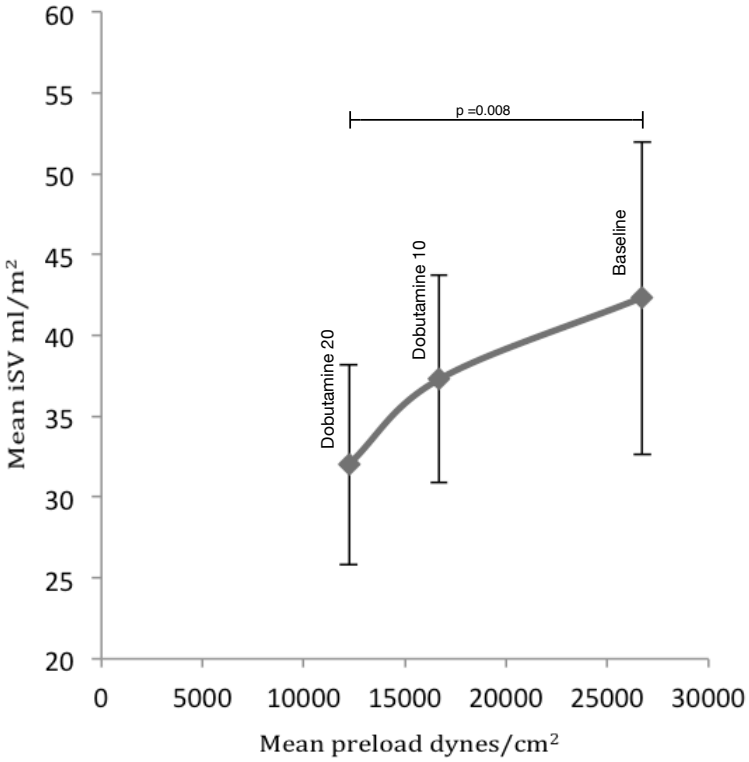

Figure 21: Relationship of mean preload to mean indexed stroke volume. Standard deviation bars are shown.

Reproducibility of ventricular volumes and aortic flow

Intra-class coefficient (95th confidence interval) was 0.97 (0.86 - 0.99) for aortic SV, 0.97 (0.80 - 0.99) for EDV, 0.95 (0.82 - 0.980) for ESV, 0.95 (0.82 - 0.98) for SV and 0.89 (0.58 - 0.97) for EF.

3.2.3 Discussion

In this study XMR was used to gain further insights into the causes of reduced functional status in patients with HLHS post-Fontan. The hypothesis was load independent measures of function would allow for a detailed analysis of whether abnormalities in systolic or diastolic indices of the systemic right ventricle might become apparent with application of stepwise increments of dobutamine stress and explain the abnormal CI and blunted response to stress previously demonstrated in the literature. [185] However, in this study using pressure-volume loop derived indices of function, there were no abnormalities in systolic or diastolic ventricular function. In fact, this symptomatic group of patients had normal functional indices and the major factor limiting SV and CI was a fall in preload with a corresponding plateau in indexed EDP.

Relevance to previous studies

Previous studies have shown [185] that CI is low at rest with a blunted response to dobutamine stress compared to normal left ventricles. The rise in CI with dobutamine 10mcg/kg/min is driven by an increase in HR, and there is no further rise in CI at peak stress. [165] This is because SV does not rise with dobutamine 10mcg/kg/min and in fact falls with dobutamine 20mcg/kg/min. This inability to increase SV is driven by an incremental fall in EDV, and is unrelated to PVR. The use of XMR allowed us to gain additional insights into the physiology of the blunted CI response in these HLHS post-Fontan patients during dobuta-

mine stress. In healthy adults dobutamine increases SV whilst EDV remains stable. These are similar to the volumetric changes seen during exercise. [163] Studies assessing ventricular function in response to dobutamine [150, 165, 149] and exercise [61] have shown similar findings in patients post-Fontan: a low base line CI and with moderate stress a HR driven rise in CI with no change in SV. These studies involved older patients with mixed systemic ventricular morphology. None had looked at high dose dobutamine, although recently *Van De Bruaene et al* [61] showed a similar finding of no additional rise in CI between moderate and peak exercise. The possible causes for the observed fall in SV with peak stress may be (1) inadequate preload; (2) abnormal systolic or diastolic myocardial properties; (3) altered afterload or uncoupling of the heart; or (4) or combination of all of these.

Preload and PVR

In Fontan circulation the absence of a subpulmonary ventricle might be expected to reduce the preload of the ventricle. [55] This could lead to an inability to respond to the higher systemic venous return needed during stress. [186, 187] In this study the observed resting preload values for the systemic RV were of a similar magnitude to the healthy LV (32 x 103 ± 4 x 103 dynes/cm^2). [188] However during dobutamine stress changes in preload mirrored SV with an unexpected fall at peak stress. We were able to unmask a limitation in the filling of the ventricle that was not evident at resting conditions.

Elevated PVR has been proposed as a factor for low preload. However baseline PVR was normal in this group of young patients and remained low throughout the procedure. In older Fontan patients PVR was found to be elevated at rest and values subsequently fell to normal during administration of dobutamine. [150] The difference in PVR values between this study and ours, is reflected in the difference in ages between the two study groups. Completion of the Fontan results in an absence of pulsatile blood flow this has the effect of reducing endothelin and increasing the risk of pulmonary emboli. Older subjects have had a longer cumulative exposure increasing their likelihood of raised pulmonary tone. This may explain the increased benefits seen with administration of sildenafil in older Fontan patients [61] compared to children during exercise. [188] Interventions to improve the trans-pulmonary gradient are currently focusing on minimising power loss within the Fontan circuit [189] and new techniques to improve the duration of forward flow through the systemic veins may offer therapeutic benefits.

Systolic function

Previous studies using load-dependent markers of function have suggested systolic function as measured by EF is reduced in those with single systemic RV circulations compared to those with single systemic LV circulations. [184] Our data for EF falls into a similar range as that published in the literature. Interest-

ingly, through the construction of pressure-volume loops, we were able to look at load independent measures of systolic ventricular function and found contractility increased 67% in response to dobutamine 10mcg/kg/min whilst power output increased by 114%. The systemic RV demonstrated good load independent systolic function albeit at a high energetic cost. The disparity in energetic cost is related to the raising of CI through HR rather than a SV response. Most of the external work performed by the heart is consumed in overcoming systemic afterload. Increased CI mediated by HR causes a disproportionate increase in this work. The increase in HR seen between moderate and peak dobutamine stress was without an increase in CI and so further reduced energy efficiency.

Diastolic function

Findings from echocardiographic-based studies suggest diastolic abnormalities exist in 67-72% of patients undergoing Fontan [54, 184] However our patient cohort had normal EDP and Tau at rest. These findings are in accordance with studies assessing function using a catheterisation technique. [149, 150] Abnormal diastolic myocardial properties are difficult to distinguish from abnormal preload when using load dependent echocardiographic indices [7] and this may explain the differences in findings. We assessed if diastolic dysfunction was unmasked during stress. Interestingly throughout dobutamine administration EDP remained abnormally low. However Tau, a measure of active early diastolic

relaxation, fell indicating improving, rather than abnormal, ventricular relaxation. Those with HLHS often have a dilated ventricle as a consequence of the previous volume loading effects of a shunt dependent circulation. To account for this, we indexed EDP to the RVEDV to provide a measure of filling pressure per millilitre of blood -there were no significant changes. This lends further support to restricted preload rather than diastolic dysfunction as a cause for reduced cardiac output in this group of patients.

Afterload and Coupling

The pressure-volume loops for the systemic RV displayed a similar pattern to that described in the literature for those with pressure loaded RVs. [25] During administration of dobutamine, a gradual increase in the afterload was observed. However the systemic RV matched the increased hydraulic load by increasing Ees. Under resting conditions, the systemic RV has a ventriculo-arterial coupling ratio that compares favourably to the healthy LV [190] and this remained well matched throughout the application of pharmacological stress indicating good energetic efficiency. [147, 157] The systemic RV displayed good contractile reserve and effective coupling during stress may explain the limited benefit found from administering afterload reducing agents to this group of patients during exercise. [191]

A useful comparison would be to contrast Fontan patients with single right

ventricles to Fontan patients with single left ventricles. Both patient groups lack a subpulmonary ventricle so the focus would be on the role that ventricular morphology has on cardiac energetics. Single LV Fontan patients usually have a good sized native aorta and do not need this reconstructed during the first Norwood procedure, unlike those with HLHS. They often require only a shunt and atrial septectomy rather than arch reconstruction with prosthetic material. This would also allow a study of the effects of this arch reconstruction on ventriculo-arterial coupling.

Aorto-Pulmonary Collaterals

Schmitt and colleagues [150] demonstrated the contribution of mean APC flow on cardiac output doubles during stress. We quantified APC contribution only during resting conditions due to the length of the study. Our baseline values were of similar magnitude and we would expect them to increase in the same way. APC flow has the benefit of contributing to preload but leads to diversion of blood from systemic perfusion. Despite this contribution it was unable to offset a fall in preload and EDP under peak stress conditions.

3.2.4 Limitations

In those with a Fontan circulation peripheral muscle contractions and respiratory effort play a prominent role in driving blood through the systemic veins. [169] Care must be taken interpreting data from anaesthetised patients performing

breath-holds. However the results of this study correspond to those observed by subjects undergoing CPET, namely a limited CI and fall in SV. [5, 51, 192, 193] In a recent study assessing the effects of supine cycling on CI in adults with single ventricle circulations,[61] SV was also found to decline with the highest levels of exertion corresponding to the highest level of Dobutamine administered in this study. Pharmacological stress mimics many of the physiological changes the heart is subjected to during exertion and is particularly useful in those too young or small to ride an exercise bike.

The patients in this study were anaesthetised using sevofluorane and remifentanil. We tried to manage the patients with the lowest doses of these drugs to maintain effective anaesthesia. The effects of sevofluorane on loading conditions and contractility has been extensively studied in animals. [194] It demonstrates a dose dependent effect including decreases in systolic arterial pressure, heart rate, cardiac index, left ventricular minute work index, maximum rate of rise of left ventricular pressure (LV dP/dt), and systemic vascular resistance. There were no effects on stroke volume and left ventricular end-diastolic pressure. High-dose remifentanil has been shown to reduce indexed stroke volume, heart rate, and mean arterial blood pressure. [195] However, the synergistic effects of these two anaesthetic agents appear to alter the loading conditions and contractility on the heart in different ways to their individual actions. A study performed in 2005 by *Chanavaz* [196] used echocardiography in a

group of children undergoing anaesthesia to assess ventricular function at baseline with sevofluorane and then reassess the following the addition of remifentanil. The addition of remifentanil was found to reduce heart rate, blood pressure and cardiac index. However, it led to increased systemic vascular resistance with a fall in contractility which is not in keeping with the actions of either drug alone. The effects of these anaesthetic drugs are dose dependent. As we maintained effective anaesthesia with the lowest dose as possible these haemodynamic effects would have been minimised. Indeed, in an earlier study carried out by our group [185] we compared cardiac function in subjects with HLHS-Fontan to a control group of awake healthy adult subjects. There were no significant differences in indexed end diastolic volume, indexed end systolic function and indexed stroke volume. This indicates that through the use of low dose anaesthetic agents and careful management of physiological parameters we may have been able to alleviate some of the published haemodynamic effects of higher dose general anaesthesia during our study protocol.

The systemic RV is not a true prolate ellipsoid. Therefore the formula that are applied to calculate LV wall stress are not applicable to the RV as they over-estimate the values. Although other formulas specific to the RV exist, in HLHS the septal wall is thought of belonging to the systemic RV so a modified formula such as that used by Janz [197] or Quaife [198] for idiopathic hypertension is also not applicable. Stress represents a mean value across the entire RV wall, with

the potential to underestimate stress on the endocardial layer and in regional areas where the myocardium may be thicker (commonly the septal wall in those with a residual LV). Stress may be over-estimated when compared to finite element methods [173] but as a comparative estimation between states it broadly serves its purpose.

The single beat estimation method was originally conceived for the LV and has been validated in the RV. Early work on the systemic RV has been performed [150, 151] and our results are in keeping with these findings. Altering preload would have offered a load independent measure of diastolic function, the end-diastolic-pressure-volume- relationship. However acquiring MRI volumetric data within a suitable timeframe isnot yet feasible. Tau was used instead although it primarily assesses early diastolic relaxation.

3.2.5 Conclusions

Children with HLHS-Fontan and symptoms of mild exercise intolerance display a blunted response in CI and a fall in SV at peak stress due to a failure to adequately preload the heart. The heart rate driven response makes this is an energetically costly process. PVR remains low. Surprisingly the systolic and diastolic function tends to be normal which is not as expected. Once load
ing conditions are removed the ventricle can be seen to be functioning well under that set of conditions.The ventricle is well coupled to the hydraulic load. In

young patients introducing measures that focus on improving the preload of the heart may offer the most benefits.

3.2.6 Summary

Background: Patients with a systemic right ventricle frequently experience reduced exercise capacity. This is related to a limited ability to increase cardiac index. Elucidating the cause of this would help with optimising treatment strategies.

Methods and Results: Prospective data from ten consecutive studies on patients with HLHS undergoing clinical cardiac magnetic resonance with catheterisation (XMR) were analysed. Mean age 8.6 years (range 3.5 - 11.6yrs), mean time since Fontan completion 5.5years. All New York Heart Association (NYHA) class II or greater. Fluid filled MR compatible catheters were placed in the systemic RV and branch pulmonary arteries to record pressures at rest (condition 1), with dobutamine infusion at 10mcg/kg/min (condition 2) and at 20mcg/kg/min (condition 3). Cine short axis stacks of the ventricle were performed at each condition and used to construct pressure-volume loops.

Compared to rest, cardiac index increased with condition 2 ($p < 0.01$) with no further rise at peak stress despite a further, albeit, blunted rise in heart rate ($p = 0.002$). An overall fall in stroke volume occurred ($p = 0.014$) despite good con-

tractility (74% increase, p =0.045) and a well-coupled ventriculo-arterial ratio. End diastolic pressure and early active relaxation, markers of diastolic function, remained normal. Preload fell at peak stress (p <0.008) whilst pulmonary vascular resistance (PVR) was low throughout.

Conclusions: In symptomatic patients with HLHS a fall in stroke volume occurs at peak stress due to a decrease in preload. There is a failure to adequately fill the ventricle implying a ceiling of maximal flow through the Fontan circuit despite a low PVR. Conventional markers of systolic and diastolic function are normal. In children therapies to improve preload may be the most beneficial.

4. Characterising ventricular function: Kinetic Energy

In the previous chapter the energetics of the ventricle were studied using invasive methods. The pressure-volume loops for the single systemic RV resembled that of a healthy LV during resting conditions. Stroke work was assessed and found to increase disproportionately at higher heart rates. Stroke work forms part of the useful work the heart performs in ejecting blood. The other part is kinetic work, the energy given to the blood as momentum. Kinetic work is now quantifiable using non-invasive methods based on 4D flow CMR. This chapter established the kinetic work in those with HLHS and explores how it might be used as a new marker of systolic function.

4.1 Intra-ventricular kinetic energy in HLHS

4.1.1 Background

Using 4D flow MRI to study the KE profile in the systemic RV could provide some insight to the extent of its adaptation as a systemic ventricle. HLHS is characterised by a LV that is too small to support the systemic circulation. [1, 199] There is a spectrum of severity with the size and shape of the LV dependent on the anatomy of the mitral and aortic valves. Furthermore the size and shape of the LV remnant has an impact upon clinical outcomes. Subjects with the largest LV remnant have the stiffest RV function[37] and the worst post-operative outcomes. [35] Existing KE studies have demonstrated distinct energetic differences are present between the healthy LV and RV during the cardiac cycle. [118]

KE declines with ageing [200] and is detrimentally affected in those with LV dysfunction. [137, 201] KE values are also affected by cardiac conditioning. In athletes an increased LV myocardial mass correlated with improved diastolic KE whilst RV diastolic KE improved with a larger end-diastolic volume. [202] KE appears to be a sensitive marker of cardiac physiology.

The aims of this study were to assess the intra-cardiac KE profile in the systemic RV specifically comparing it to other healthy left and right ventricles to understand the degree of adaptation. Additionally the impact that the nonfunctional LV remnant has on the kinetic energy profile of the systemic RV was examined. Those with the largest remnants should cause the greatest adverse effect on diastolic KE.

4.1.2 Results

Eight healthy children (mean age 7.3 years, range 1.5–15 years) were recruited. The reasons for the MRI referrals in children were as follows: exclusion of vascular ring (n =3), assess for tortuosity of head and neck vessels (n =2), assess for arrhythmogenic right ventricular cardiomyopathy (ARVC) (n =2), exclusion of partial anomalous venous drainage (n =1). All children included in the study were confirmed to have structurally and functionally normal hearts by a cardiologist experienced in reporting CMR. Thirty children with HLHS (mean age 6.3 years, range 0.8 years – 16years) were recruited. One was excluded as they moved significantly during the 4D flow acquisition leading to severe artefact. Demographic data is shown in Table 8 All children with HLHS were taking as-

pirin and captopril as per institutional protocol. Patients with HLHS had lower heart rates than healthy children 79 ± 16bpm vs. 104 ±23bpm (P = 0.001) which may be a reflection of the use of general anaesthesia.

Parameter		Healthy	HLHS	P value
Gender	Male:Female	4:4	21:9	
Mean age ± SD	(years)	7.3 (± 6.3)	6.3 (±4.5)	0.54
Mean BSA (range)	(m^2)	0.97 (±0.51)	0.85 (±0.41)	0.48
HF			0.56 (±0.10)	
Fontan			1.03 (±0.43)	
Mean BP systolic ± SD	(mmHg)	115 (±6)	99 (±21)	0.16
Mean BP diastolic ± SD	(mmHg)	71 (±14)	53 (±12)	0.021
Heart rate	bpm	104 (±23)	79 (±16)	0.001
Tricuspid regurgitation	None	8	20	
	Mild	0	10	
	Moderate	0	0	
	Severe	0	0	
Medication	ACE-I	0	30	
	Diuretic	0	0	
	Aspirin	0	30	

Table 8: HLHS KE study: demographic data

The healthy cohort had normal cardiac function (LV EF, RV EF). With no significant differences between the LV and RV for EDV, ESV or SV. As expected LV wall mass was significantly greater than RV wall mass (p <0.05). Those with HLHS had significantly more dilated hearts compared to the healthy

population (iRVEDV $p = 0.015$) with an increased stroke volume (iSV $p = 0.014$) leading to preserved cardiac function. Indexed systemic RV wall mass was significantly increased compared to the healthy LV and RV ($p = 0.0001$). The degree of tricuspid regurgitation was at most mild. There were no difference in ventricular volume or function between those having undergone HemiFontan or Fontan surgery although there was a trend towards less ventricular dilatation following Fontan but this did not achieve significance. The MS/AS group tended to have a globular LV remnant whilst those with MA/AA had either a slit-like or no LV remnant. The morphologically globular shaped LV group were composed of 18 patients and the morphologically slit-like LV group composed of 11 patients. The median LV volume was 2.4mls. There were no differences in RV size or function between those with globular or slit-like LV remnants or between those with the largest or smallest LV remnants. (See Table 9)

	Number	iEDV (ml/m^2)	iSV (ml/m^2)	EF (%)	Indexed Wall mass (g/m^2)
Healthy LV	8	69.2 (±9.6)	28.1 (±2.3)	59.0 (±3.3)	47.0 (±5.8)
Healthy RV	8	68.4 (±9.2)	39.1 (±6.6)	57.6 (±10.6)	23.2 (±3.0) ₸
All HLHS	29	93.7 (±24.5) ₸	53.8 (±11.6) ₸	58.7 (±8.4)	76.5 (±23.7) **
ANOVA p value		**0.02**	**0.001**	0.92	**0.0001**
HemiFontan	14	100.4 (±29.8)	57.9 (±10.9)	60.2 (±10.0)	77.3 (±23.2)
Fontan	15	88.1 (±19.1)	50.1 (±12.1)	57.4 (±7.2)	78.9 (±24.6)
p value		0.19	0.08	0.39	0.86
Globular LV group	18	91.4 (±27.8)	52.1 (±10.7)	58.8 (9.6)	72.9 (±21.3)
Slit-like LV group	11	98.3 (±20.7)	56.9 (±13.9	58.6 (±7.3	88.4 (±25)
p value		0.48	0.30	0.94	0.10
LV > 2.4mls group	15	94.4 (±25.2)	54.4 (± 11.4)	59.9 (± 10.3)	75.2 (±22.6)
LV < 2.4mls group	14	93.7 (±20.3)	53.4 (±13.0)	57.5 (± 6.5)	81.7 (± 25.0)
p value		0.94	0.82	0.46	0.48

P value compared healthy LV

** p <0.001

* p <0.01

₸ p <0.05

Table 9: HLHS KE study: MRI derived ventricular parameters. iEDV indicates indexed end diastolic volume, iSV is indexed stroke volume, EF is ejection fraction, LV is left ventricle, RV is right ventricle

The KE profile of the healthy LV and RV are shown in Figure 22. They were composed of two peaks corresponding with systole and diastole. The diastolic peak was a fused monotonic peak. Systolic KE peak in the RV was greater than the LV but this did not reach significance. There was a larger diastolic KE peak in the LV compared to RV (p =0.05).

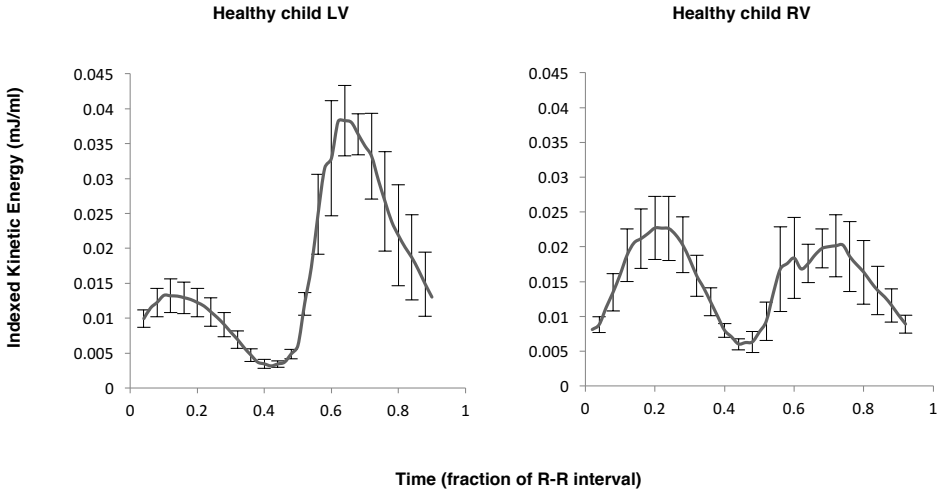

Figure 22: Mean intra-ventricular kinetic energy values for 8 heathy children over the cardiac cycle in the LV and RV

In comparison the systemic RV also displayed two peaks of KE (see Figure 23). The systolic KE peak was of a similar magnitude to the healthy LV and RV. However, the monotonic diastolic KE peak was significantly lower than the healthy systemic LV (p = 0.023) (see Table 10) and more in keeping with a healthy RV.

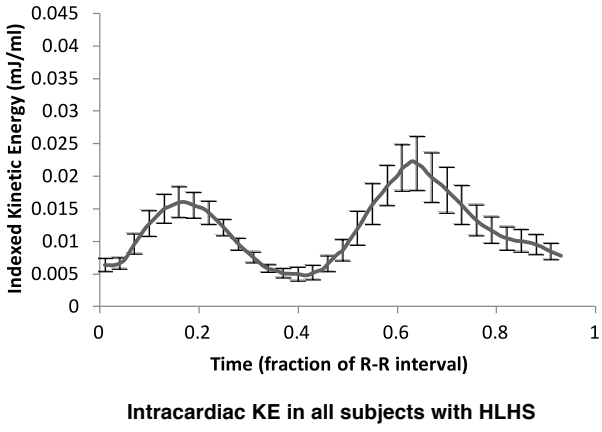

Figure 23: Mean intra-ventricular kinetic energy values during the cardiac cycle for all subjects with HLHS

	Systolic KE (mcJ/ml)	End- systolic KE (mcJ/ml)	Early diastolic KE (mcJ/ml)
Healthy child LV (n=8)	14.2 (±6.6)	3.2 (±2.0)	53.8 (±9.2)
Healthy child RV (n=8)	25.5 (±11.9)	5.0 (±2.9)	28.9 (±12.1) Ŧ
Single RV (n=29)	17.2 (±12.7)	2.7 (±1.8)	31.3 (±23.4) Ŧ
ANOVA p value	0.131	**0.027**	**0.019**

P value compared to healthy child LV

** p <0.001

* p <0.01

Ŧ p <0.05

Table 10: HLHS KE study: comparison of intra-cardiac kinetic energy (KE) based on ventricular morphology

Figure 24 shows the KE curves for those with HLHS. There were no differences in any of the intra-cardiac KE parameters between the HemiFontan and Fontan circulations. Those with globular LVs had significantly lower diastolic KE than those with slit-like LVs 21.3 ± 7.8mcJ/ml vs 45.0 ± 31.1mcJ/ml; p =0.024. Similarly those with a larger LV remnant (n = 15) had lower diastolic KE than those with a smaller LV remnant (n =14) 20.5 ± 6.0mcJ/ml vs. 41.0 ± 29.0mcJ/ml; p = 0.016. (See Table 11 and Figure 25)

a

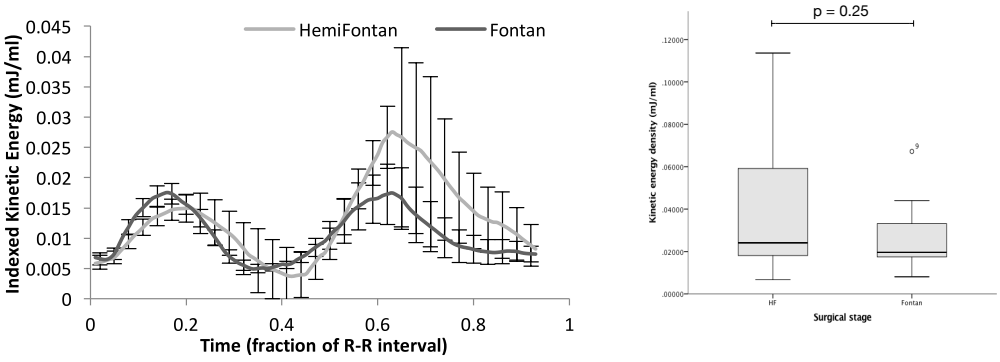

Comparison of intracardiac KE in HLHS for subjects with hemifontan or Fontan physiology

b

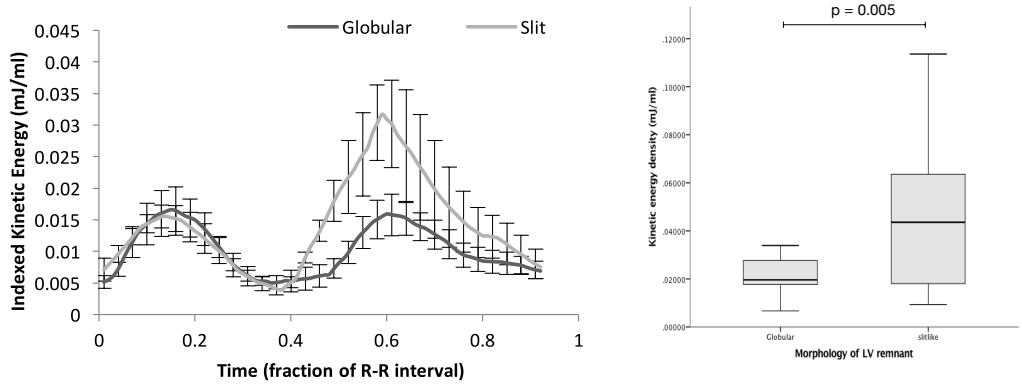

Comparison of intracardiac KE in HLHS for subjects with a globular or slit-like LV remnant

Figure 24: Intra-cardiac KE values over the cardiac cycle for those with HLHS. The top panel shows subjects divided according to surgical stage, the bottom panel shows subjects divided according to the morphology of the LV remnant. On the right are Box and Whisker plots of the mean early diastolic KE values for each corresponding KE curve.

	Systolic KE (mcJ/ml)	End- systolic KE (mcJ/ml)	Early diastolic KE (mcJ/ml)
Fontan (n =15)	18.4 (±16.1)	2.5 (±0.9)	26.5 (±15.8)
HemiFontan (n =14)	15.9 (±8.0)	3.0 (±2.4)	36.5 (±29.2)
p value	0.6	0.39	0.25
Slit-like LV (n=12)	17.1 (±7.6)	3.5 (±2.6)	45.0 (±31.1)
Globular LV (n=17)	17.3 (±15.6)	2.2 (±0.7)	21.3 (±7.8)
p value	0.97	**0.044**	**0.005**
LV < 2.4mls group (n =15)	17.5 (±9.0)	3.5 (±2.2)	41.0 (±29.0)
LV > 2.4mls group (n =14)	16.9 (±16.3)	2.0 (± 0.05)	20.5 (± 6.0)
p value	0.89	**0.026**	**0.016**

Table 11: Intra-cardiac KE values in those with HLHS based on surgical stage and the size and morphology of the LV remnant

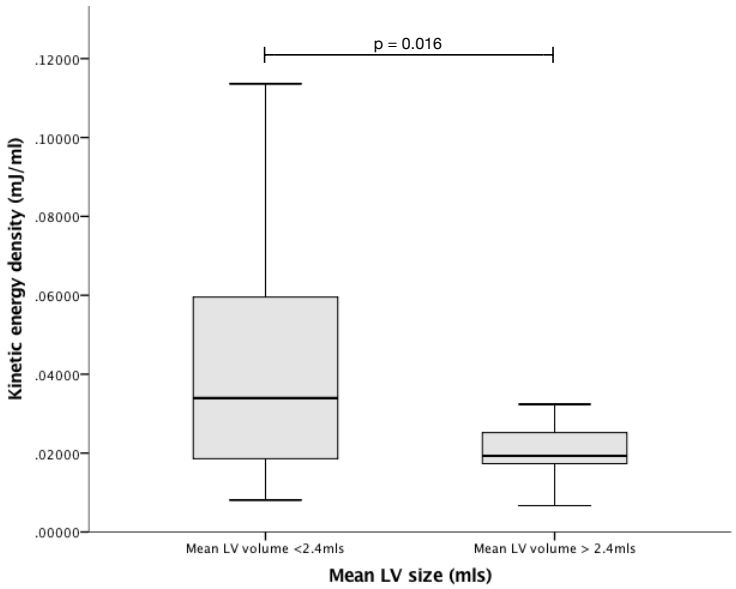

Figure 25: Boxplot demonstrating the diastolic kinetic energy for those with the largest and smallest LV remnants

There were no strong correlations between the early diastolic KE in those with HLHS and parameters of iEDV, iESV, iSV, wall mass or size of LV remnant (see Table 12)

	R^2	P
iEDV	0.041	0.29
iESV	0.123	0.063
iSV	0.006	0.684
iMass	0.077	0.162
iLVmass	0.121	0.064

Table 12: Multiple linear regression analysis of early diastolic kinetic energy in the systemic RV

4.1.3 Discussion

The focus of this study was to assess KE in the systemic RV of those with HLHS and contrast this with healthy ventricles. The derived values of kinetic energy were of similar magnitude to previously published data despite using a different methodology. *Carhäll et al* [203]chose a single timepoint (isovolumetric contraction) and then tracked particles forward and backward through the cardiac cycle to calculate KE. In contrast we calculated instantaneous KE from the velocity data based on cine segmentations of the ventricle. This was similar

to *Carlsson et al* [118] differing only in the level of manual segmentation. Both techniques produce values of KE that are very similar and appear equally valid. The major findings of the study were: (1) interestingly the KE profile closely resembled the healthy RV rather than showing any significant adaptations; (2) the shape and size of the morphological LV remnant was observed to have an important impact on diastolic KE values as hypothesised.

The initial part of the study required determination of normal KE values in children. Briefly, children frequently exhibit a single fused diastolic monotonic peak compared to the two diastolic peaks seen in adulthood due to the higher heart rates common in children. In children the diastolic kinetic energy peak in the LV was observed to be greater than that of the RV. Furthermore the RV had a greater systolic peak due to outflow tract geometry. However, unlike in adults, this did not quite reach significance. It is likely that with a larger cohort of children any differences in RV systolic KE would have reached significance. Reassuringly these findings were in keeping with the existing literature. [10, 118, 134, 137, 204]

The characteristic diastolic KE profile of the LV is due to the greater recoil of the LV myocardial mass. A suction like-effect is created drawing blood into the ventricle. This effect is less prominent in the healthy RV due to a lower myocardial mass. *Carlsson et al* [118] postulate that the differing motions of the tricuspid valve and mitral valve are responsible for generating more diastolic KE in the

LV. They hypothesise that the hinge-like motion of the tricuspid valve tends to sweep over and around the blood without imparting much additional KE whilst the mitral valve draws in blood from the atria. We are skeptical of this theory. Although there are differences in shape between the mitral valve annulus and tricuspid annulus with the mitral valve displaying a reduced antero-posterior direction making it more saddle shaped, both have the same area and circumference so blood flow and velocities will be equivalent. {Makaryus et al., 2017, #80358} Valve opening is a consequence of pressure gradients from active ventricular diastolic relaxation with no discernible active process from the leaflets themselves.

In those with HLHS the diastolic KE profile continued to closely resemble that of a healthy RV. This was unexpected. In Chapter 3.2 the pressure-volume loops for the systemic RV were altered to resemble a healthy LV pressure-volume loops. Despite the single RV being in the systemic position there were no alterations in diastolic KE. The intrinsic architecture of the RV is responsible limiting the production of diastolic KE. However the systemic RV undergoes changes in volume and mass which do not appear to alter the diastolic KE. As a consequence of the first and then second stages of surgical palliation the RV undergoes extreme changes first in volume loading and then volume reduction. [43] Overall it remains dilated and hypertrophied. In well trained athletes, right ventricular dilatation and left ventricular hypertrophy are associated with increased diastolic KE values. [202] In contrast this association was not seen in

those with HLHS -neither myocardial mass or ventricular volume altered the KE. The observed findings are in keeping with *Gewillig's* hypothesis [7] that the systemic RV, following Stage 2 of the palliation, is *an overgrown and under-filled ventricle*. Whilst remaining well-coupled to the systemic circulation [200] it is unable to generate the same levels of diastolic KE as seen in the healthy LV. The observed changes in mass and volume are a compensatory response to reduce wall tension and persist with no added kinetic energy advantages. Interventions and measures to reduce the extent of early volume loading, such as earlier timing of Stage II surgery might therefore be postulated to improve energetic function.

In assessing other factors which alter the kinetic energy of the RV we looked at the size and shape of the LV remnant. In those with HLHS the presence of a larger LV remnant has a bearing on the stiffness of the systemic ventricle and also on outcome following surgery. Those with the largest LVs have been demonstrated to have the stiffest ventricles and the poorest outcomes. [35, 37] In this study we observed that the presence of a morphologically globular LV remnant leads to a reduced diastolic KE. Additionally those with the largest LV remnant similarly had the lowest diastolic KE values. These findings were in keeping with other literature but importantly we were able to demonstrate this non-invasively and also show that parameters of KE which reflect the useful work and energy of the heart are altered offering this metric as a potential new marker of diastolic dysfunction. The presence of a non-functioning piggy-back

ventricle adversely affected the development of diastolic KE by decreasing ventricular compliance and the greater the size the more the impact on energetic momentum. A larger dysfunctional LV has a greater negative ventricular-ventricular interaction on the RV. This in turn may well lead to altered conservation of momentum and higher viscous energy losses. [9] Interestingly these results were not detected by using measures of ejection fraction. Lower diastolic KE values have also been demonstrated to occur with ageing and in those with LV dysfunction. This raises the question as to whether the group with the largest LV remnants may be predisposed to developing symptoms of heart failure at an earlier stage.

The accuracy of the 4D flow data, particularly velocity is important in measuring KE. Previous work performed by our group [126, 170, 205] shows the validity of using accelerated 4D flow sequences to acquire highly temporally undersampled data. Mean bias was only -0.06m/s with no systematic bias seen on Bland-Altman plots. The 4D flow data used in this study was meticulously collected. The velocity encoding (VENC) value was determined using a 2D phase contrast sequence prior to the 4D flow scan to ensure peak velocities were not underestimated. Three-dimensional CMR acquisitions provide a detailed overview of the velocity of blood in three directions helping to capture the intricacies of flow within the whole heart. This is important, as filling of the LV cavity does not occur solely from base to apex. Vortices form below the mitral ring and move apically during healthy diastolic filling. [11] 2D PC MRI or echocardiography may miss these subtleties, or require larger study

populations before differences become detectable. Additionally the mitral valve is elliptical and moves throughout the cardiac cycle. [118] It becomes distorted in cardiac disease such as DCM making accurate plane orientation for 2D PC flow techniques more technically challenging. Three-dimensional flow echocardiography is currently a tool under development but this too is limited by the patient's habitus. [119] This detail is not adequately captured by two-dimensional (2D) doppler echocardiography or 2D PC flow MRI which are limited to a single imaging plane and measure velocities in only one direction.

4.1.4 Limitations

The number of CMR scans from those with HLHS was limited. Whilst interesting conclusions were able to be drawn, a larger case series might continue to provide more detail particularly as the children age.

The 4D flow MRI sequences used prospective ECG triggering which acquired 90% of the cardiac missing some of late diastole. This meant that atrial peaks were not evident in all subjects. However given the majority of changes seem to occur in systole and early diastole we were still able to draw interesting conclusions from the data. Only CMR data was acquired. The addition of invasive catheter data to assess the compliance of the ventricles particularly in those with HLHS would have been useful albeit with the risks of an invasive procedure.

Almost all scans were acquired with the subject under general anaesthesia.

This represents a reversal of normal Fontan physiology. [206, 207] The effects and influence of general anaesthesia agents have been discussed in detail in the limitations section of Chapter 4.2.7. Ethical considerations and institutional practice did not allow awake scans to be performed. As increasing patients survive into adulthood and tolerate awake scans the acquisition more faithful physiologically representative should become available.

4.1.5 Conclusions

The systemic RV demonstrates incomplete adaptation as a pressure loaded ventricle. Its kinetic energy profile remains inherently limited by its architecture as it continues to resemble a RV rather than a LV. Diastolic KE values are most adversely affected by the presence of a non-functioning larger LV remnant. This is in keeping with the literature demonstrating that this group have the worst post-operative outcomes.

4.1.6 Summary

Background: In HLHS the RV performs as a systemic ventricle, however the adaptation is incomplete. Patients experience early circulatory failure and those with the largest LV remnants have poorer outcomes. Intra-cardiac KE differs between the healthy LV and RV and is sensitive to changes in systolic and diastolic function. We compared intra-cardiac KE in healthy children to those with HLHS to study the energetic limits imposed on the systemic RV and how residual LV size affects the KE profile.

Methods and Results: 4D flow MRI was acquired in 8 healthy children (1-16 years) and 30 children with HLHS (1-16 years) undergoing clinical MRI (15 HemiFontan, 15 Fontan). Intraventricular KE was measured throughout the cardiac cycle and indexed to ventricular volume. LV remnant was grouped into shape (slit-like or globular) and size (median volume =2.4mls).

Two intra-cardiac KE peaks were present reflecting systole, and the fused inflow of early diastole. The healthy LV displayed a larger diastolic peak compared to the healthy RV (p <0.05). Compared to the healthy RV those with HLHS had a similar diastolic peak in the presence of preserved function, but despite increased mass (p <0.001) and volume (p <0.05). No differences emerged between stages of surgery. Globular shaped LV remnants had the lowest RV diastolic KE compared to slit-like LV remnants (p =0.005). This was also related to the size of the LV remnant with lower KE seen in those with larg-

er median LV size (LV >2.4mls; p =0.016).

Conclusions: In HLHS, the RV displays incomplete physiological adaptations to its role as a systemic ventricle with diastolic KE limited by the inherent RV morphology. This is further influenced by larger, globular LV remnants acting as stiff piggy-back ventricles with adverse effects on diastolic momentum.

4.2 Exploring kinetic energy as a new marker of function in the single ventricle circulation

4.2.1 Background

In Chapter 3.2 ventricular contractility and stroke work were studied in patients with HLHS through a range of heart rates. The work of the heart rose dramatically at higher heart rates. The contractility was preserved and well matched to the arterial system. Continuing with the theme of energetics we examined a different component of the useful work that the heart performs - the kinetic work imparted to blood as momentum. We examined the kinetic work in a range of patients with HLHS in Chapter 4.1 using a non-invasive MRI technique. The previous section demonstrated that KE is altered in those with HLHS compared to healthy hearts. Here 4D flow MRI derived KE is used to derive and investigate its use as a potential new marker of function. Two approaches are examined. The first approach assessed peak instantaneous KE and was named the *kinetic energy ejection fraction* (KE EF). This is the maximum energy exerted onto the whole blood volume. The second approach used a novel particle-based assessment and was named the *particle energy ejection fraction* (PE EF). This is the maximum energy exerted onto individual particles. It utilises the ability of 4D flow to study fluid dynamics using a Lagrangian method. We compared each technique in those with single ventricle circulations to those with established LV dysfunction and used healthy control sub-

jects across the age spectrum to determine normal ranges and act as comparisons. We hypothesized that as metrics based on kinetic energy are related to the useful work of the heart they could act as an improved marker of function for assessing cardiac performance compared to VV EF.

4.2.2 Results

Accuracy of 4D flow measurements

Four dimensional flow was compared to 2D flow. The peak velocity measurements showed a mean bias of -0.06 m/s with the 95% limits of agreement ranging from -0.305 m/s to +0.186 m/s. There was no statistical difference in 2D and 4D peak velocity measurements between the different patient groups (healthy LV vs. single ventricle vs. LV dysfunction, p = 0.163) (see Figure 26). A mean of 4.8% of particles were discarded due to leakage across the myocardial border. This did not significantly differ between groups (ANOVA p =0.09).

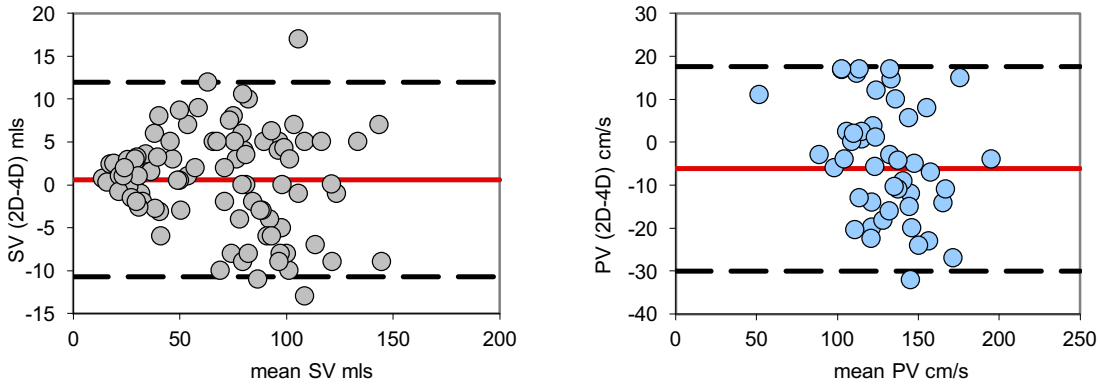

Figure 26: Bland Altman plots of 2D PC and 4D PC flow stroke volume and peak velocity measurements

Reproducibility of ventricular volumes and aortic flow

Intra-class coefficient (95th confidence interval) was 0.97 (0.86 - 0.99) for aortic SV, 0.97 (0.80 - 0.99) for end diastolic volume (EDV), 0.95 (0.82 - 0.980) for ESV, 0.95 (0.82 - 0.98) for SV and 0.89 (0.58 - 0.97) for VV EF.

Demographics

The demographic data for each patient group is shown in Table 13. As expected from the disease aetiology those from the single ventricle circulation group were younger than those from the LV dysfunction group.

		Healthy controls	Single ventricle hearts	LV dysfunction	ANOVA P value
Gender		22F:21M	12F:29M	5F:9M	
Median age	**[range] (years)**	31 (1.5 – 62)	5 (0.6 – 28) *	50 (28 – 79) *	<0.001
BSA	**[range] (m^2)**	1.7 (0.5 – 2.2)	0.9 (0.5 – 2.2) *	1.9 (1.3 – 2.5)	<0.001
Median HR	**[range] (bpm)**	71 (48 – 138)	77 (43 -110)	64 (45 – 80)	0.055
Median BP systolic	**(± SD) (mmHg)**	118 (± 10)	97 (± 21) *	122 (± 22)	<0.001
Median BP diastolic	**(± SD) (mmHg)**	74 (± 10)	54 (±12) *	79 (± 10)	<0.001
***p* value compared to healthy LV**		*p < 0.01	†p < 0.05		

Table 13: Kinetic energy function study: patient demographics. F = female, M = male, BSA = body surface area, HR = heart rate, BP = blood pressure, LV = left ventricle

Distribution of systolic kinetic energy

The percentage of particles at peak velocity during each systolic time point were plotted against the fraction of systole (see Figure 27) to permit

comparison between subjects with different heart rates. Visually those with single ventricle circulations appeared negatively skewed. The Q-Q plots are shown in Figure 28. Surprisingly despite the visual skewedness, particularly in those with single ventricle circulations, when tested all groups demonstrated a normal distribution (Healthy LV p = 0.127; SV p = 0.132; LV dysfunction p = 0.262). In all groups, a maximum of 10% of ejected particles were at peak velocity (and therefore peak KE) at any time with the remainder of particles still gaining or already losing velocity.

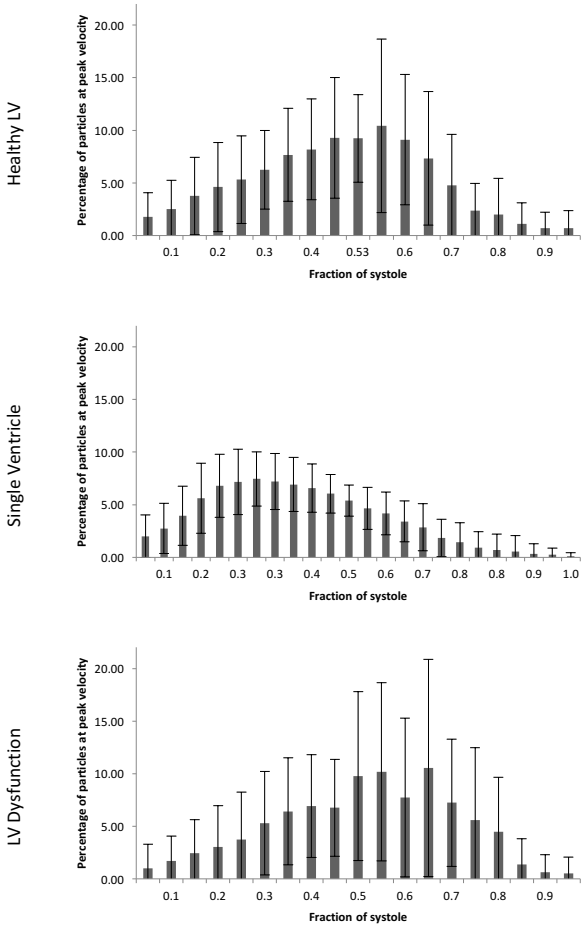

Figure 27: Percentage of particles at peak velocity at each point through systole.

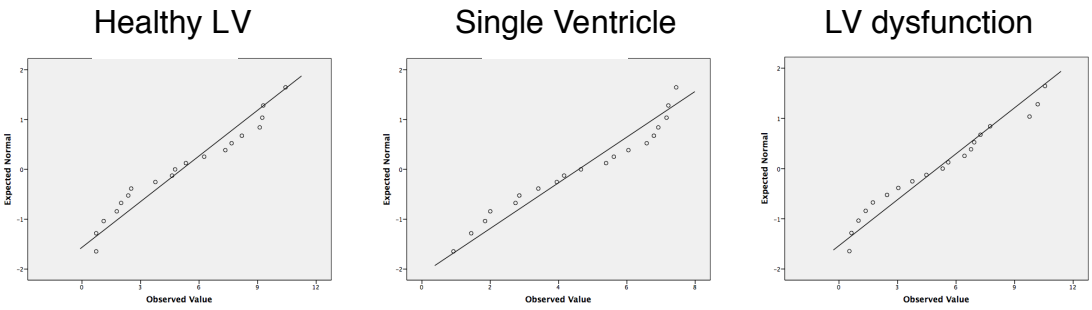

Figure 28: Quantile-Quantile plots of expected vs observed values for percentage of particles at peak velocity during systole.

Streamline data showed maximal velocities occurred in the outflow. The effect of the size of the outflow tract on the peak systolic KE showed a weakly positive correlation (R^2 = 0.204, p <0.001) indicating that smaller outflows were not associated with a greater velocity and, or KE (see Figure 29).

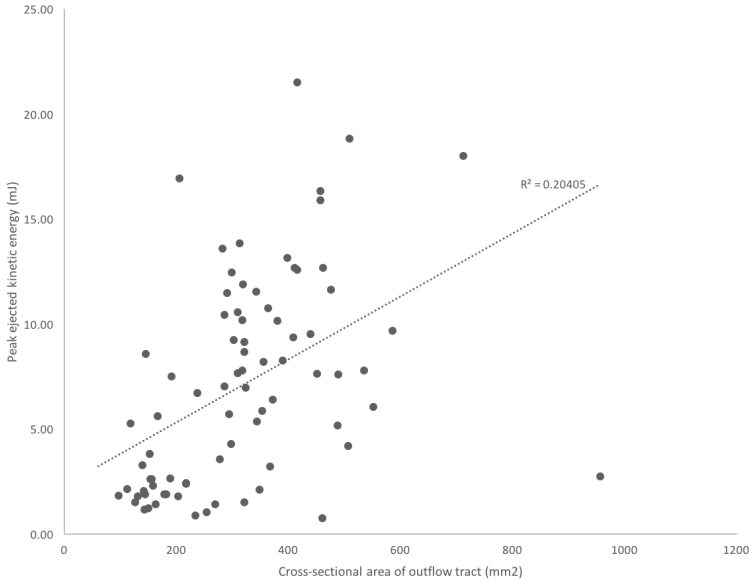

Figure 29: Peak ejected kinetic energy against outflow tract size. Smaller outflows are not associated with increased velocity or KE.

Comparison between healthy children and adults

Table 14 shows the volumetric and KE indices for healthy children and adults. Cardiac volumes display an exponential allometric change in size with patient age. There were no differences between healthy adults and children for VV EF ($p = 0.52$), KE EF ($p = 0.7$) or PE EF ($p = 0.3$) allowing them to be combined into one group of healthy controls. This point and the differences in age range between our study population, healthy controls and positive controls with heart failure are discussed further in the limitations section.

		Adult LV n = 35	Child LV n = 8	*p* value
iEDV (± SD)	ml/m^2	84 (± 11.8)	69 (± 9.6)	0.002
iESV (± SD)	ml/m^2	33 (± 7.5)	28 (± 2.3)	0.05
iSV (± SD)	ml/m^2	50 (± 6.9)	41 (± 7.1)	0.002
VV EF (± SD)	%	60.3 (± 5.5)	59.0 (± 3.3)	0.5
iKEej (± SD)	mcgJ/ml	110.9 (± 39.5)	108.7 (± 37.4)	0.8
iKEres (± SD)	mcgJ/ml	3.6 (± 1.4)	3.8 (± 2.6)	0.7
KE EF (± SD)	%	97.9 (± 0.8)	97.9 (± 0.9)	0.7
iPEej (± SD)	mJ/ml	0.247 (± 0.078)	0.216 (± 0.080)	0.31
iPEres (± SD)	mJ/ml	0.010 (± 0.003)	0.008 (± 0.005)	0.11
PE EF (± SD)	%	97.3 (± 0.8)	97.6 (± 0.5)	0.3

Table 14: Kinetic energy function study: MRI derived volume indices for healthy adults and children. iEDV = indexed end diastolic volume, iESV = indexed end systolic volume, iSV = indexed stroke volume, VV EF = ventricular volumetric ejection fraction, iKEej = kinetic energy density for ejected blood, iKEres = kinetic energy density for residual blood, KE EF = kinetic energy ejection fraction, iPEej = particle energy density for ejected blood, iPEres = particle energy density for residual blood, PE EF = particle energy ejection fraction

Comparison between the single ventricle group and control groups

Volumetric and kinetic energy data for the three different study groups is shown in Table 15, and Figure 30. For VV EF, patients with single ventricle circulation exhibited values that were very similar to healthy controls (GLM adjusted mean 60.1% vs. 60.1%, $p = 0.99$), which were both very dissimilar to patients with LV dysfunction (GLM adjusted mean 39.6%; $p < 0.001$ for both

comparisons). This was in stark contrast to the values for kinetic energy ejection fraction and particle energy ejection fraction, where single ventricle patients now yielded results similar to the diseased left ventricle group and both of which were lower than healthy controls.

		Healthy controls	Single ventricle	LV dysfunction	ANOVA or GLM
		n = 43	n = 41	n =18	P values
iEDV (± SD)	ml/m^2	81 (±13)	93 (± 23) †	105 (± 25) *	<0.0001
iESV (± SD)	ml/m^2	33 (± 7)	38 (± 16)	64 (± 24) *	<0.0001
iSV (± SD)	ml/m^2	49 (± 8)	55 (± 11) †	41 (± 10) †	<0.0001
VV EF (± SD)	%	60.1 (± 5.2)	60.1 (± 8.5)	40.4 (± 10.7) *	<0.0001
GLM adjusted VV EF	%	60.1	60.1	39.6 *	<0.001
iKEej (± SD)	mcgJ/ml	111.0 (± 38.7)	73.7 (± 27.5) *	101.0 (± 36.9)	<0.0001
iKEres (± SD)	mcgJ/ml	3.6 (± 1.7)	3.8 (± 2.5)	2.8 (± 1.1)	0.2
KE EF (± SD)	%	97.9 (± 0.8)	96.4 (± 2.6) †	95.1 (± 4.3) *	<0.0001
GLM adjusted KE EF	%	97.9	96.4 *	95.1 †	<0.001
iPEej (± SD)	mcJ/ml	241.6 (± 78.3)	166.9 (± 81.4) *	214.7 (± 66.0)	<0.0001
iPEres (± SD)	mcJ/ml	9.9 (± 3.6)	36.2 (± 68.5) †	17.9 (± 2.7)	0.029
PE EF (± SD)	%	97.3 (± 0.8)	90.9 (± 7.9) *	90.1 (± 6.9) *	<0.0001
GLM adjusted PE EF	%	97.3	90.9 *	90.3 *	<0.001
Particles discarded	%	4.2 (± 3.5)	4.4 (± 4.1)	6.7 (± 4.6)	0.086
***p* value compared to healthy LV**		*p < 0.01	†p < 0.05		

Table 15: Kinetic energy function study: MRI derived volumetric and kinetic energy indices for healthy control, single ventricle and left ventricle dysfunction groups. GLM = generalised linear model

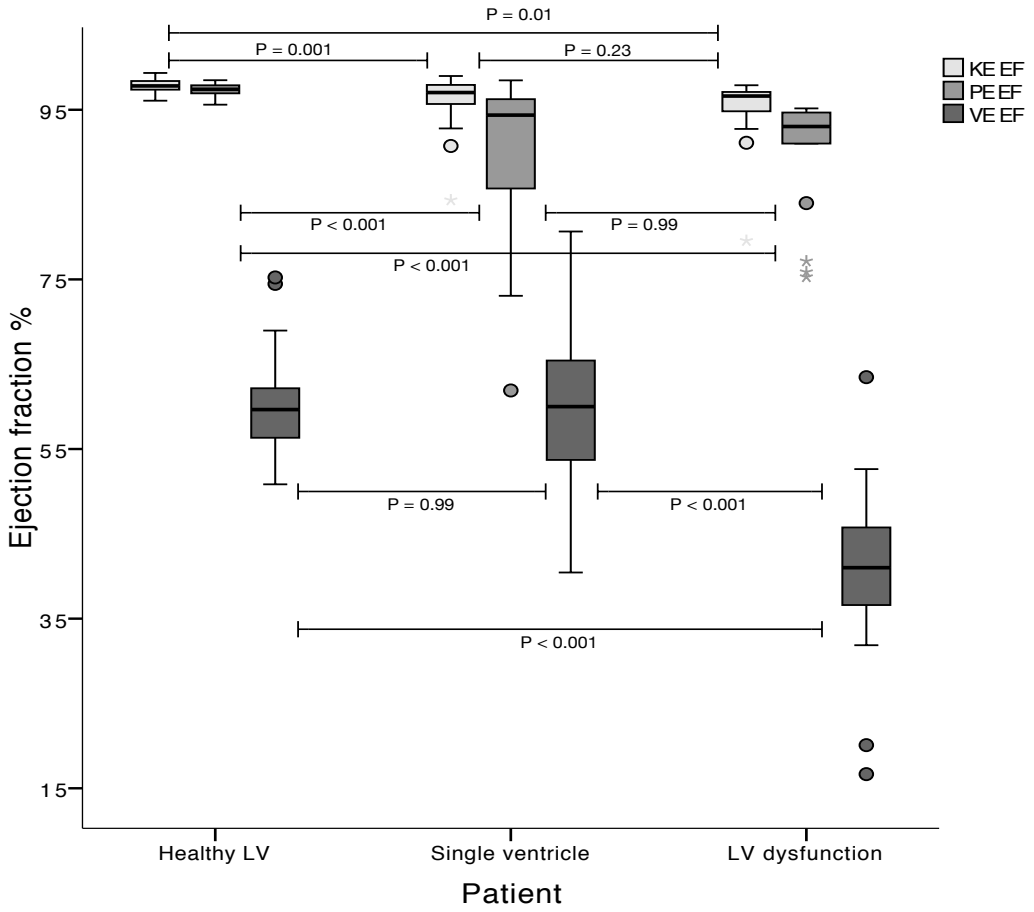

Figure 30: Box and whisker plots showing relationship between patient group and ejection fraction (kinetic and volumetric) for all patients. P values are shown for inter-group comparisons, and are calculated post hoc from the Generalized Linear Model using the Bonferroni adjustment.

The role of single ventricle morphology

Table 16 shows the morphology of those from the single ventricle circulation group including the degree of atrio-ventricular valve regurgitation (AVVR). Subjects with moderate or severe AVVR (regurgitation fraction > 25%; n = 5) had a significantly worse PE EF than those with none or only mild regurgitation (79.3 ± 12.0% vs. 92.5 ± 5.8%; p = 0.0002) with no detected differences when

comparing KE EF or VV EF. There were no differences between the group with a systemic RV and the group with a systemic LV. Both had similar sized hearts with equivalent VV EF ($p = 0.22$), PE EF ($p = 0.49$) and KE EF ($p = 0.5$).

Estimates of functional status were made in 40 of the 41 subjects (Table 20). One child was not included as they were too young (6 months old) for a reliable estimate to be made. There was no clear relationship between NHYA status and VV EF and KE EF; however, this was not the case for PE EF, which demonstrated a fall as NHYA status worsened. Figure 8 shows VV EF and PE EF across the three NYHA sub-groups within the single ventricle patients. There was no significant correlation between VV EF and PE EF in the single ventricle patients ($r = 0.23$, $p = 0.15$) (Figure 31).

Normal atrial situs	39/41
Apex to left	33/41
Systemic Right Ventricle	14HF:17F
Mitral atresia/Aortic atresia	12
Mitral stenosis/Aortic stenosis	15
ccTGA with Mitral atresia/Pulmonary atresia	2
DORV	2
Tricuspid regurgitation	
None (<15%)	16
Mild (15 – 25%)	10
Moderate (25 - 40%)	2
Severe (>40%)	3
Mean APC % cardiac output (± SD)	13 (±15)%
VSD	2/31
Systemic Left Ventricle	3HF:7F
Tricuspid atresia	5
Pulmonary atresia/IVS	2
DILV + Pulmonary stenosis	2
DILV + Pulmonary atresia	1
Atrio-ventricular valve regurgitation	
None (< 15%)	8
Mild (15 – 25%)	2
Moderate (25 - 40%)	0
Severe (> 40%)	0
Mean APC % cardiac output (± SD)	13 (±14)%
VSD	7/10
NYHA Status	40/41
NYHA I	24
NYHA II	11
NYHA III	5
NYHA IV	0
Blood density	
Haemoglobin (mean ± SD)	13.8 ± 2.1 g/dL
Haematocrit (mean ± SD)	0.418 ± 0.06

Table 16: Kinetic energy function study: single ventricle morphology and functional status.. Where HF = Hemifontan, F = Fontan, ccTGA = congenitally corrected transposition of the great arteries, DORV = double outlet right ventricle, IVS = intact ventricular septum, DILV = double inlet left ventricle, APC = aorto-pulmonary collateral vessels, VSD = ventricular septal defect, NHYA = New York Heart Association functional class

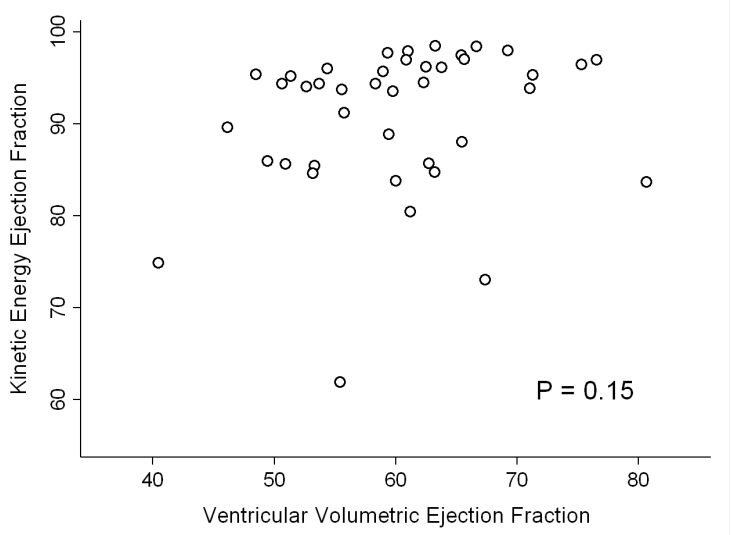

Figure 31: Scatter plot single comparing kinetic energy and ventricular volumetric ejection fractions for single ventricle patients

4.2.3 Discussion

Patients with single ventricle circulations have poor long-term outcomes [48] making accurate assessment of ventricular function a crucial tool in picking up early signs of deterioration. However, our standard way of grading ventricular function, VV EF, is often preserved despite reduced maximal oxygen consumption (VO2 max) on exercise testing. [5, 54, 68] Recently there has been interest in measuring ventricular kinetic energy with a focus on patterns of intra-cardiac kinetic energy in health and disease to see if this could provide an additional tool in the assessment of ventricular function. [203, 208] In this paper we proposed two new measures of ventricular systolic function based conceptually on kinetic energy, the KE EF and PE EF, and assessed their usefulness in patients with single ventricle circulation.

The results of this study showed that markers of function based on KE displayed a small but significant difference in values between health and disease. The KE EF and PE EF in healthy individuals had a very small variance (±0.8% for each respectively). In contrast, in patients with single ventricle physiology, both the KE EF and PE EF values were significantly decreased (96.4 ± 2.6% and 90.9 ± 7.9% respectively), with a broader range suggesting a spectrum of impaired function. The magnitude of the difference was small, only 1.5% lower in KE EF and 6.4% in PE EF but the small variance involved in both figures is in marked contrast to VE EF which had a broad range in health and furthermore showed no differences in values between the two groups. The positive control group represented by subjects with LV dysfunction, where we would expect abnormalities in kinetic energy, [137] showed a reduction in both KE EF and PE EF similar to the single ventricle group indicating that metrics based around systolic kinetic energy indices may offer a new tool for functional assessment across a spectrum of cardiac diseases.

Existing studies [137] on KE in patients with compensated DCM demonstrate preserved stroke volume compared to healthy controls. However the proportion of blood that enters the heart in diastole and is then ejected in the following systolic contraction - direct flow - is significantly reduced. Comparably we note that our LV dysfunction population also had identical stroke volumes to our healthy control group. Although we did not measure

direct flow we were able to demonstrate a significantly reduced peak early diastolic KE value.

Comparing differences in ventricular and kinergetic assessment

The broad range of VV EF in health makes detection of abnormalities in cardiac function more challenging with larger numbers needed to separate healthy hearts from those with reduced function. This is in part due to our method of assessing ventricular volumes. Standard CMR protocols recommend planning stacks of slices in the short axis plane parallel to the atrio-ventricular valve plane for assessment of VV EF. [209] Whilst CMR is the gold standard for volumetric assessment this process can be prone to errors that may increase the variability in measurements. [77, 78] Stacks of transverse slices offer less variability [85, 210] but not necessarily a more accurate volume. An inconsistent breath-holding position between slices leads to loss of contiguity further contributing to increased margins of error. Indeed, the large range and variability in VV EF [211] may be responsible for its poor gradation of risk in those with only mildly reduced ejection fraction. [212] The physiological adaptations undergone by those with a single ventricle circulation further contributes to the difficulty in accurate assessment of function using VV EF. Single ventricles are dilated, hypertrophic and hypocontractile. [7] They undergo dramatic changes in loading conditions during early operative procedures that leave VV EF sensitized to preload and relatively insensitive to detecting mild cardiac dysfunction. [72] We found that as a group although patients with single ventricle

physiology had an increased end diastolic volume (EDV), they also had an increased SV which led to a VV EF that was similar to the control group. The preservation of VV EF was at odds with patient reported symptomology. Whilst 16 out of 40 assessed patients with single ventricle physiology described symptoms of exercise intolerance (NYHA class II or greater) we found no relationship between VV EF and NYHA class. In contrast, KE EF and PE EF values were significantly depressed in single ventricle patients, indicating the presence of an underlying abnormality in the dynamics of energy transfer from myocardium to blood. Furthermore, PE EF fell in tandem with subjectively reported symptoms of heart failure. Those describing significant limitations in function had the lowest PE EF values. PE EF allowed stratification of function that appeared to match with reported symptomology in a way that is not permitted by VV EF or KE EF. These results are from a small sample size but warrant further work in assessing particle based measures of kinetic energy as a potential new functional biomarker.

The role of single ventricle morphology and valvular regurgitation on energetics

The reduction in KE EF and PE EF seen in those with single ventricle physiology is a multifactorial process. We assessed the impact of left and right single ventricular morphology and found no apparent differences. We additionally assessed if the severity of AVVR played a part and found a significant fall in PE EF. The severity of AVVR is correlated to the degree of volume loading on the ventricle. More AVVR results in an increase in the end diastolic and end sys-

tolic volume of the ventricle. Those with only modestly dilated hearts frequently demonstrate compensatory changes leading to preserved function. This does not reflect the increased work performed by the heart in ejecting the recirculating regurgitant blood volume and the additional KE imparted to the larger residual volume of blood. Altered energy efficiency has been demonstrated in computational models [9] and the changes in PE EF may reflect this altered energy efficiency.

Relevance to previous studies

Previous studies performed using 4D flow MRI have assessed the intracardiac KE in healthy hearts [10, 118, 204], established normal values through a range of ages [200] and also investigated the impact of heart failure on normal kinergetics. [137, 213, 214] In one study KE was used to assess function in Tetralogy of Fallot, a form of congenital heart disease, with mixed results. Importantly these studies have all assessed the peak kinetic energy of the total blood volume. This study used a previously validated method to derive KE [200] Two different measures of energetic ejection fraction were then assessed. The KE EF used a similar principle of measuring peak total KE as compared to the existing body of published work. However, a second method based on a particle-by-particle analysis was also evaluated. The use of PE EF represented a novel approach to assessing kinetic energy in the heart. It utilised the advantages of particle analysis afforded by 4D flow MRI, with advances in computational processing to permit detailed kinematic analysis of blood flow. The importance of a

Lagrangian approach to assessing particle energetics and fluid dynamics becomes clear when considering that at any instance a maximum of 10% of particles are ever at peak velocity. Assessing whole blood volumes in this way may underestimate the total work of the heart. The area of energetics is an emerging topic and further work is currently being performed to compare energetics in healthy hearts to those with heart failure [201, 213–215] and there is much potential to expand this into congenital heart disease to help us better understand these conditions.

4.2.4 Limitations

The large majority of the patients with single ventricle physiology in our study were children, but it was difficult to match a healthy volunteer cohort with similar ages with only eight of our normal volunteers being children. However when analysed as separate groups, the energetic parameters in our adult and children healthy volunteers were similar, including their KE EFs with a narrow range in both children and adults. For our positive controls we were unable to include any children in the heart failure group as none underwent cardiac MRI during the study period. However as there were no differences between the adults and children in the healthy control group then we would expect our positive controls to be a reasonable comparative group.

4D flow MRI was acquired using a free-breathing technique only during expiration, which loses the normal respiratory variation in flow. There was no signifi-

cant difference between the peak velocities of different groups measured by signal averaged free breathing 2D or 4D flow indicating no systematic bias caused by patient size or morphology. The highly accelerated 4D flow sequence allowed us to acquire at an isotropic spatial resolution of 2.0-3.0mm and a true temporal resolution of <35milliseconds falling within previously defined recommendations for accurate flow acquisitions. This resolution was comparable to other published 4D flow literature

Although MRI 4D flow is now becoming increasingly available on scanners with the latest generation software, the technical expertise to perform detailed post-processing to calculate kinetic energy is less generally available. As familiarity grows with this concept we hope that our work to improve post-acquisition and processing analysis [216] may prove invaluable for increasing accuracy and reliability of such sequences and lead to increased clinical integration. In addition, in the future it may be possible to acquire the 4D flow data using novel echocardiographic techniques that would make data acquisition much simpler and possible at the bedside or in the clinic. [119]

The density of blood taken was assumed to be 1060gm/mm^3 for all cases. This can alter in those with cyanotic heart disease. The haematocrit for the single ventricle group was measured prior to anaesthesia and was within the normal range for all but three patients. The literature suggests a large change in haematocrit from 0.30 to 0.60 is required to cause a small 1.9% increase in the

blood density from 1040gm/mm^3 to 1060gm/mm^3 permitting the use of a mean blood density value. [217]

4.2.5 Conclusions

Kinetic energy parameters offer new insight into the function of the heart. They are consistent in health and show deviation in cardiac disease particularly in conditions such as single ventricle physiology where standard ejection fraction values are often normal. Particle based analysis seems sensitive towards detecting dysfunction and may be a new biomarker of disease if the computational cost of the analysis can be improved in future.

4.2.6 Summary

Background: VV EF is often normal in patients with single ventricle circulations despite them experiencing symptoms related to circulatory failure. We sought to determine if KE could be a better marker of ventricular performance.

Method and Results: KE was prospectively quantified using 4D flow MRI in 41 patients with a single ventricle circulation (0.5 - 28 years) and compared to 43 healthy volunteers (1.5 – 62 years) and 14 patients with LV dysfunction (28 – 79 years). Intraventricular end-diastolic blood was tracked through systole and divided into ejected and residual blood components. Two ejection fraction (EF) metrics were devised based on the KE of the ejected component over the total of both the ejected and residual components using: (1) instantaneous peak KE to assess *KE EF* or; (2) summating individual peak PE to assess *PE EF*.
KE EF and PE EF had a smaller range than VV EF in healthy subjects (97.9 ± 0.8% vs. 97.3 ± 0.8% vs. 60.1 ± 5.2%). LV dysfunction caused a fall in KE EF (p =0.01) and PE EF (p =0.0001). VV EF in healthy LVs and single ventricle hearts was equivalent however KE EF and PE EF were lower (p <0.001) with a wider range indicating a spectrum of severity. Those reporting the greatest symptomatic impairment (NYHA II) had lower PE EF than asymptomatic subjects (p =0.0067).

Conclusions: KE metrics are markers of healthy cardiac function. PE EF may be useful in grading dysfunction.

5. Characterising ventricular function: Shape and Strain

5.1 Right ventricular morphology and function following stage I palliation with a modified Blalock-Taussig shunt versus a right ventricle-to-pulmonary artery conduit

European Journal of Cardio-Thoracic Surgery (2016) 1–8

5.1.1 Background

In Chapter 1.3.7 the two different type of Norwood operation were described. Briefly, the modified Blalock-Taussig (MBT) shunt involves a connection between the innominate or subclavian artery and one of the branch pulmonary arteries allowing blood to shunt from the systemic circulation into the pulmonary circulation. The MBT shunt has been associated with haemodynamic instability [218] and sudden death [219] in the postoperative period. The right ventricle-to-pulmonary artery (RVPA) conduit was developed to offset this risk. [39] Following a ventriculotomy, a tube is inserted between the RV and the main pulmonary artery to act as a conduit. This results in volume loading from conduit regurgitation and a scar on the systemic ventricle predispose the patient to an increased risk of arrhythmias or aneurysmal dilatation of the outflow tract. [220, 221] At present, the direct impact of the ventriculotomy scar on the growth and motion of the systemic RV remains incompletely understood. [222, 223]

In this study we performed a dual centre retrospective analysis of cine imaging to investigate the differences in shape and motion of the ventricle after each procedure. Datasets from Boston Children's hospital were used as Evelina hospital preferentially performs the mBT shunt based Norwood procedure. Computational anatomical analysis of CMR images was used to create detailed 3D cardiac atlases and to detect small differences in ventricular geometry. [103, 105] Using traditional two-dimensional (2D) measurements such as length and diameter to assess a complex 3D shape does not capture subtle variations in topology. Strain analysis captured the motion of the ventricle and these were used to examine the impact of the RVPA conduit on the function of the systemic RV in patients with HLHS. The ventriculotomy scar would be expected to cause adverse remodelling and motion of the ventricle and alter the shape and motion in those with RVPA conduits.

5.1.2 Results

There were a total of 93 CMR datasets from the two congenital centres. 34 underwent RVPA conduit and 59 underwent MBT shunt. The MBT shunt population comprised 30 Stage I scans and 29 Stage II scans. The RVPA conduit population comprised 20 Stage I scans and 14 Stage II scans. Demographic data is shown in Table 17. A more limited ventriculotomy scar was introduced in those undergoing RVPA conduit after 2009. 5 Stage I scans and 3 Stage II scans had the more limited incision.

	MBT shunt	RVPA conduit	P value
Number	59	34	
Birth weight	3.2 ± 0.4 kg	3.0 ± 0.5 kg	0.22
Re-coarctation	4/59	7/34	0.06
Occlusion of collateral vessels	8/59	33/34	**0.0001**
Stage 1 scans	30	20	
Age at Stage I	7.1 ± 6.7 days	5.3 ± 2.8 days	0.28
Age at MRI scan	103 ± 24 days	141 ± 57 days	**0.0007**
BSA	0.40 ± 0.04 m^2	0.44 ± 0.06 m^2	**0.0087**
Stage 2 scans	29	14	
Age at Norwood	7.1 ± 6.7 days	7.3 ± 3.8 days	0.98
Age at Stage II	172 ± 38 days	177 ± 65 days	0.72
Age at MRI scan	30.6 ± 8.2 months	27 ± 11 months	0.16
BSA	0.67 ± 0.23 m^2	0.70 ± 0.11 m^2	0.53

Table 17: Shape and strain study: demographic data showing means and standard deviations

There were no significant differences in birth weight or age at Norwood procedure between groups. Stage I scans for the RVPA conduit group tended to be performed later than the MBT shunt group and, as expected, these patients were larger in size. Table 18 shows the MRI derived data.

	MBT shunt	RVPA conduit	P value
Total	n = 59	n = 34	
iEDV ml/ $BSA^{1.3}$	80 ± 20	106 ± 33	**0.0001**
iESV ml/ $BSA^{1.3}$	34 ± 13	47 ± 24	**0.001**
iSV ml/ $BSA^{1.3}$	46 ± 11	59 ± 15	**0.0001**
EF %	57.9 ± 8.3	56.5 ± 8.5	0.43
Stage 1	n = 30	n = 20	
iEDV ml/ $BSA^{1.3}$	83 ± 23	110 ± 32	**0.001**
iESV ml/ $BSA^{1.3}$	38 ± 15	48 ± 24	0.087
iSV ml/ $BSA^{1.3}$	44 ± 10	62 ± 13	**0.0001**
EF %	55.1 ± 7.6	58.3 ± 9.1%	0.18
TR			0.75
None	14	9	
Mild	13	8	
Moderate	3	3	
Severe	0	1	
LV shape			0.92
Globular	17	17	
Slit-like	10	8	
Borderline	3	3	
Stage 2	n = 29	n = 14	
iEDV ml/ $BSA^{1.3}$	77 ±17	98 ± 33	**0.014**
iESV ml/ $BSA^{1.3}$	30 ± 9	47 ± 19	**0.001**
iSV ml/ $BSA^{1.3}$	47 ± 13	51 ± 17	0.38
EF %	60.6 ± 8.7	53.4 ± 6.6	**0.006**
TR			0.31
None	17	6	
Mild	10	7	
Moderate	2	0	
Severe	0	1	
LV shape			0.30
Globular	18	9	
Slit-like	8	2	
Borderline	2	3	

Table 18: Shape and strain study: MRI derived data for systemic RV global function following either a MBT shunt or RVPA conduit. Values are indexed to BSA.

Compared with the MBT shunt group, patients with RVPA conduit had more dilated hearts at all stages of surgery (Stage I, $p = 0.001$; Stage II, $p = 0.014$). Indexed end-diastolic volume decreased following volume off-loading Stage II surgery in both groups. There were no differences in tricuspid regurgitation. There were no differences in the range of LV morphology between the two groups.

Geometric analysis

All 93 computational shapes were successfully created reaching a sub-voxel accuracy (average fitting error 1.43 mm). Average cardiac shapes for the MBT shunt and RVPA conduit groups at each stage are illustrated in Figure 32.

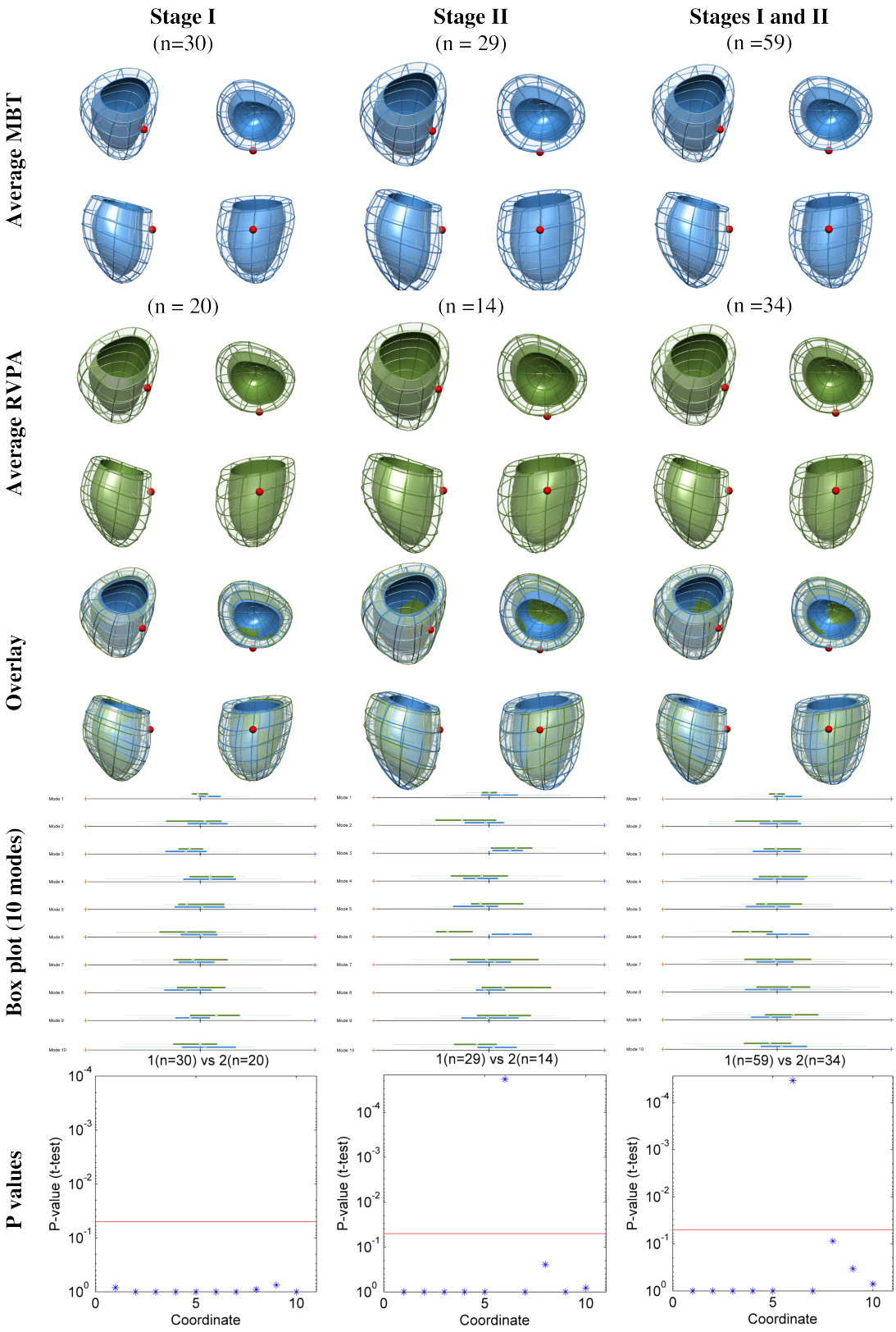
Stage I
(n=30)
Stage II
(n = 29)
Stages I and II
(n =59)
Average MBT
(n = 20)
(n =14)
(n =34)
Average RVPA
Overlay
Box plot (10 modes)
1(n=30) vs 2(n=20)
1(n=29) vs 2(n=14)
1(n=59) vs 2(n=34)
P values
P-value (t-test)
Coordinate

Figure 32: Ventricular shape difference between RVPA and MBT shunt groups in the entire HLHS population. The top row shows average ventricular shape for MBT shunts at each surgical stage and then an overall ventricular shape for both stages. The second row shows the equivalent average ventricular shape for RVPA shunts. The third row shows an overlay of the two averaged shapes for MBT and RVPA shunt groups. The solid colour represents the endocardial surface whilst the mesh represents the epicardial surface. The position of the LV remnant is marked with a red dot. Boxplots for each of the first ten *Modes* **are shown in the fourth row, with their corresponding p-values in the fifth row, showing a significant difference in shape in Mode 6 occurring only at Stage II (p-values before Bonferroni correction).**

The statistical atlas was built, and 10 cardiac atlases representing 79.0% of the variance in shape within the population were selected for analysis. A comparison between all RVPA and MBT groups revealed a significant difference in the mean of Mode 6 (p <0.001) (Figure 32). A statistical difference in Mode 6 was not apparent between a comparison of RVPA vs. MBT groups after Stage I surgery but then became statistically significant following Stage II surgery ($p < 0.001$). This corresponded to the removal of the conduit. Figure 33 shows a visualisation of the extreme shape variations (i.e. ±3 standard deviations) for Mode 6.

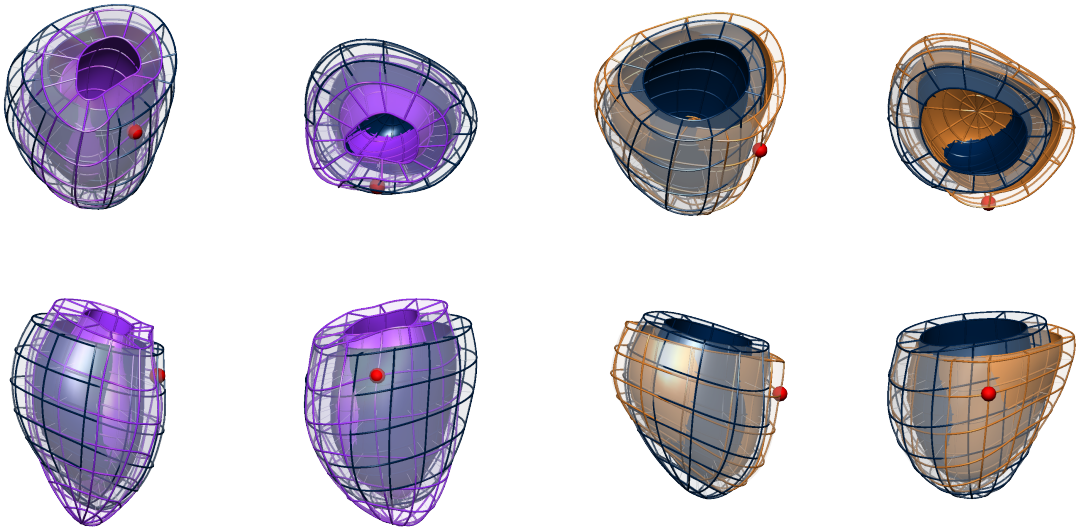

Mean -3 standard deviations

MBT shunt tendancy

Mean +3 standard deviations

RVPA conduit tendancy

Figure 33: Changes in ventricular shape described by the anatomical Mode 6. Dark blue mesh represents the average ventricle of the 93 cases, and the brown and purple meshes illustrate the ± 2 standard deviations of the range in shape variation described by Mode 6. MBT shunt shows a positive (brown) tendency, and RVPA shunt a negative (purple) tendency. The shell represents the endocardial surface and the mesh is the epicardial surface, and the position of the LV remnant is marked with a small red sphere.

The traditional geometrical measures in Table 19 revealed that the RVPA conduit group had a more spherical-shaped heart (1.35 ± 0.25 vs. 1.49 ± 0.25; p = 0.007), increased indexed RV cavity diameter (59 ± 13mm/$\sqrt{m^2}$ vs. 53 ± 9mm/$\sqrt{m^2}$;p = 0.006), and a larger indexed EDV (106 ± 33ml/$BSA^{1.3}$ vs. 80 ± 20ml/$BSA^{1.3}$; p <0.0001, Table 18). However the models in Figure 33 additionally demonstrated subtle differences in size at the base of the ventricle and orientation of the apex. These topological differences were not captured by parameters in Table 19.

		MBT shunt	RVPA conduit	P value
Total				
Myocardial mass	$gm/BSA^{1.3}$	104.4 ± 31.0	91.6 ± 50.5	0.12
Length	$mm/\sqrt{m^2}$	77.8 ± 10.1	78.3 ± 14.2	0.82
Maximum ventricular cavity diameter	$mm/\sqrt{m^2}$	53.0 ± 8.9	59.2 ± 13.3	**0.006**
Maximum ventricular epicardial diameter	$mm/\sqrt{m^2}$	71.4 ± 7.2	74.5 ± 15.3	0.17
Sphericity ratio		1.49 ± 0.25	1.35 ± 0.25	**0.007**
Maximum wall thickness	$mm/\sqrt{m^2}$	8.9 ± 2.4	7.9 ± 2.8	**0.044**
Standard deviation of septal wall thickness	$mm/\sqrt{m^2}$	2.45 ± 0.76	2.76 ± 1.06	0.10
Stage I				
Myocardial mass	$gm/\sqrt{m^2}$	115.9 ± 32.1	99.3 ± 56.0	0.17
Length	$mm/\sqrt{m^2}$	81.0 ± 10.5	78.1 ± 11.3	0.31
Maximum ventricular cavity diameter	$mm/\sqrt{m^2}$	55.4 ± 7.6	56.6 ± 10.9	0.63
Maximum ventricular epicardial diameter	$mm/\sqrt{m^2}$	74.8 ± 6.5	70.3 ± 7.4	**0.020**
Sphericity ratio		1.47 ± 0.15	1.41 ± 0.28	0.29
Maximum wall thickness	$mm/\sqrt{m^2}$	9.4 ± 2.4	7.8 ± 2.9	**0.021**
Standard deviation of septal wall thickness	$mm/\sqrt{m^2}$	2.67 ± 0.86	2.65 ± 1.03	0.94
Stage II				
Myocardial mass	$gm/\sqrt{m^2}$	91.7 ± 24.6	77.2 ± 33.7	0.11
Length	$mm/\sqrt{m^2}$	74.2 ± 8.6	78.9 ± 18.9	0.27
Maximum ventricular cavity diameter	$mm/\sqrt{m^2}$	50.3 ± 9.6	64.0 ± 16.3	**0.001**
Maximum ventricular epicardial diameter	$mm/\sqrt{m^2}$	67.5 ± 5.8	81.2 ± 21.6	**0.003**
Sphericity ratio		1.52 ± 0.35	1.24 ± 0.19	**0.006**
Maximum wall thickness	$mm/\sqrt{m^2}$	8.4 ± 2.4	8.0 ± 2.8	0.64
Standard deviation of septal wall thickness	$mm/\sqrt{m^2}$	2.24 ± 0.56	2.97 ± 1.13	**0.006**

Table 19: Two-dimensional traditional geometrical measurements of the systemic right ventricle. Values are derived from personalised computational meshes, following either a modified Blalock-Taussig shunt or right ventricle to pulmonary artery conduit. Values show mean and standard deviations and are indexed to BSA.

Functional Analysis

There were no differences in global systolic function between the MBT shunt and the RVPA conduit groups. Initially EF was equivalent between groups at Stage I surgery but after Stage II surgery was significantly lower in those receiving a RVPA conduit (p =0.014), although the mean value was within the normal range.

Table 20 shows the results of the strain analysis using feature tracking. Compared to the MBT shunt group, subjects from the RVPA conduit group had reduced longitudinal systolic function (strain p =0.023, strain rate p <0.0001). Furthermore, at the midventricular level, the RVPA conduit group displayed a reduced circumferential strain (p <0.006) and radial strain (p <0.0001). Diastolic strain rates in the RVPA conduit group were reduced on assessment of longitudinal function (strain rate p <0.0001), midventricular radial function (strain rate p =0.011), and apical radial function (p =0.029). Typical strain curves are shown in Figure 34.

Reproducibility of ventricular volumes

Intra-class correlation (95% confidence interval) was 0.97 (0.80-0.99) for EDV, 0.95 (0.82-0.980) for ESV, 0.95 (0.82-0.98) for SV, and 0.89 (0.58-0.97) for EF.

	MBT shunt	RVPA conduit	P value
Ejection fraction %	57.9 ± 8.3	56.5 ± 8.5	0.44
Systolic Function			
Longitudinal			
Strain %	-14.78 ± 5.68	-12.23 ± 4.52	**0.023**
Strain rate % s^{-1}	-1.37 ± 0.61	-0.92 ± 0.28	**0.0001**
Circumferential			
Basal strain %	-12.53 ± 4.80	-10.44 ± 3.56	0.15
Basal strain rate % s^{-1}	-0.82 ± 0.34	-0.73 ± 0.22	0.19
Mid strain %	-16.90 ± 5.14	-12.97 ± 4.63	**0.006**
Mid strain rate % s^{-1}	-1.17 ± 1.11	-0.94 ± 0.34	0.22
Apical strain %	-17.28 ± 9.54	-18.03 ± 6.98	0.070
Apical strain rate % s^{-1}	-1.30 ± 0.84	-1.38 ± 0.50	0.35
Radial			
Basal strain %	16.11 ± 12.45	15.82 ± 7.47	0.38
Basal strain rate % s^{-1}	1.16 ± 0.52	1.10 ± 0.41	0.25
Mid strain %	24.76 ± 11.89	16.22 ± 8.05	**0.0001**
Mid strain rate % s^{-1}	1.32 ± 0.69	1.17 ± 0.44	0.14
Apical strain %	11.08 ± 8.32	9.95 ± 7.72	0.15
Apical strain rate % s^{-1}	1.31 ± 0.78	1.14 ± 0.75	0.12
Diastolic Function			
Longitudinal			
Strain rate % s^{-1}	1.82 ± 0.91	1.32 ± 0.61	**0.0001**
Circumferential			
Basal strain rate % s^{-1}	1.04 ± 0.40	0.99 ± 0.36	0.63
Mid strain rate % s^{-1}	1.46 ± 0.52	1.27 ± 0.50	0.054
Apical strain rate % s^{-1}	1.63 ± 1.10	1.94 ± 0.75	0.12
Radial			
Basal strain rate % s^{-1}	-1.22 ± 0.59	-1.11 ± 0.49	0.11
Mid strain rate % s^{-1}	-1.74 ± 0.94	-1.39 ± 0.68	**0.011**
Apical strain rate % s^{-1}	-1.42 ± 0.82	-1.24 ± 0.87	**0.029**

Table 20: Systolic and diastolic function of the systemic right ventricle following either a modified Blalock-Taussig shunt or right ventricle to pulmonary artery conduit.

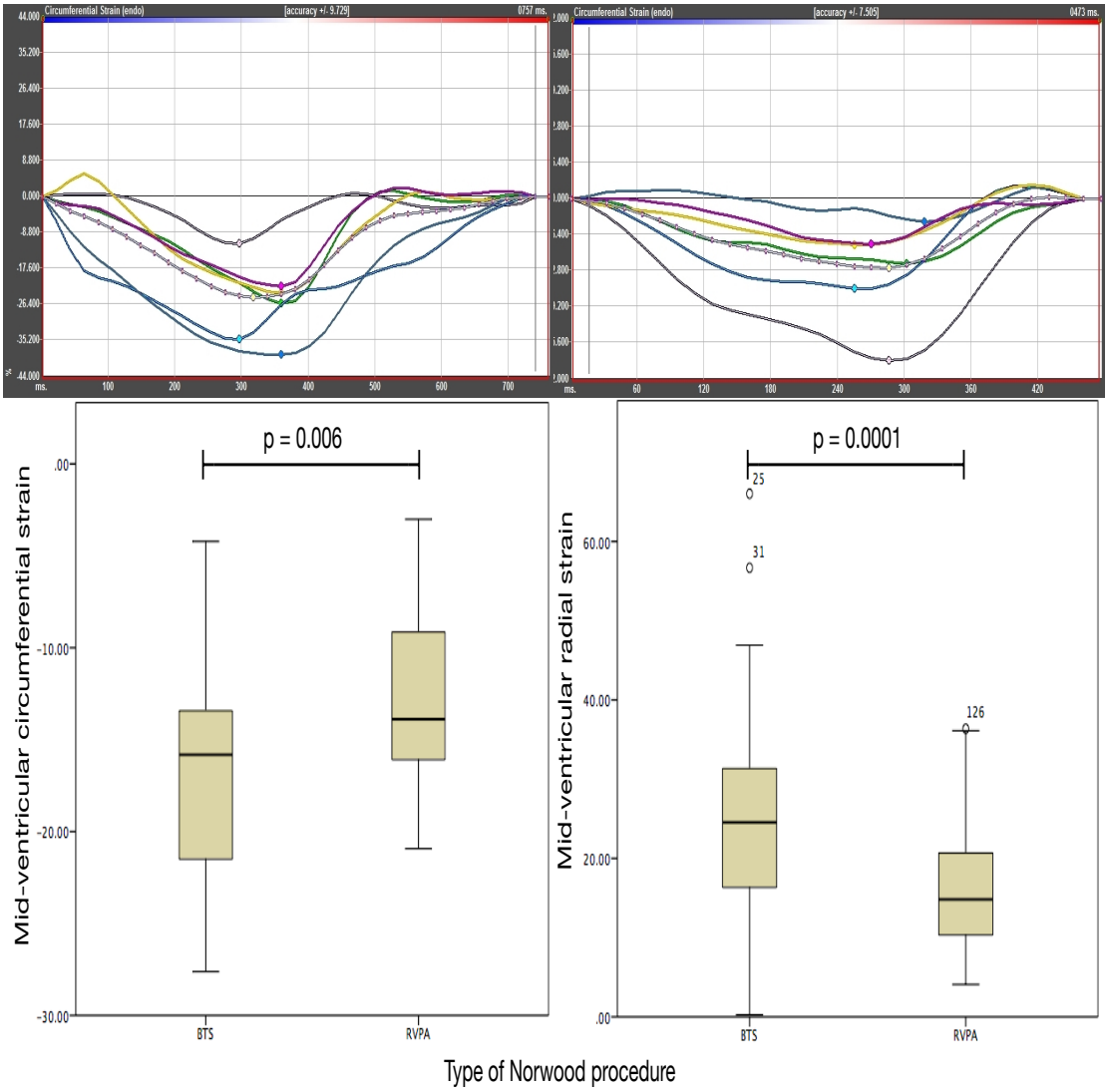

Figure 34: Feature tracking derived MR strain. Top panel shows the feature tracking for the mid ventricular short axis slice in diastole (left) and systole (right). The strain curves are shown in the middle panel. Typical circumferential strain for the MBT shunt is on the left and RVPA shunt is on the right. Segmental analysis is represented by each colour and white is the mean global strain. The bottom panel shows a box and whisker plot comparing circumferential strain (left) and radial strain (right). Circumferential strain is a negative value representing a shortening whilst radial strain is a positive value representing a lengthening.

5.1.3 Discussion

Interest in outcomes following a RVPA conduit is due to concern about the impact of a residual scar at the site of the conduit insertion on the systemic RV. Post-mortem studies have shown the scar remains stable in size irrespective of patient age and consists of fibrosis and ventricle wall thinning. [96] Echocardiographic studies have found wall motion abnormalities localised to the ventriculotomy site [95] with altered contractility occurring only after removal of the conduit and formation of a scar. Recent studies have compared survival rates, rates of intervention, and transplant free survival between the 2 types of shunt used in Stage I operation. [41, 42] Survival at 3 years was comparable but longer-term prognoses remain uncertain. We hypothesised that the focal scarring following a RVPA conduit would adversely affect the shape and motion of the RV and, through computational shape analysis and strain analysis of MRI data, we would be able to detect differences between the Norwood groups. The major results of this study demonstrated that those receiving a RVPA conduit tend to have a more spherical-shaped and dilated ventricle, and, despite preserved EF, have reduced longitudinal systolic and diastolic strain values compared to those receiving a MBT shunt.

The use of computational modelling, [103] allowed the creation of a 3D computational atlas of ventricular anatomy accounting for characteristic variation in the HLHS population. Creating a cardiac atlas has the advantage of not having to assume any typical shape or dimension. Instead variations in a

structure are described and analysed in 3D terms rather than being subject to the constraints of applying 2D measurements to try and describe a 3D space. This is illustrated in Figure 33 where differences in the orientation of the apex and shape at the base of the ventricle are seen but not easily measured. Similar techniques have been used to study the LV in adults who were born prematurely [105] and we were able to apply this to accurately capture the geometry of the systemic RV. In this study, one of the ten cardiac modes captured the shape remodelling differences between the RVPA conduit and MBT shunt groups, and corresponded to increased sphericity and dilatation of the heart. The formation of the fibrotic scar after Stage II surgery might cause reduced regional growth in the scar region relative to the remote myocardial wall, as previously described in echocardiographic and post-mortem studies, [96] leading to the observed change in the shape of the ventricle. The effects of pulmonary regurgitation through a non-valved conduit may also contribute to this difference in shape in comparison to those with mBT shunts where blood is not able to regurgitate back into the ventricle.

The results demonstrated that those receiving RVPA conduits had more dilated ventricles at Stage I than those receiving MBT shunts. This differs from that reported in the literature using echocardiography [224] and may reflect that CMR more accurately records ventricular volumes [71] without the echocardiographic limitations of acoustic windows. EF has a prognostic value in those with HLHS and a decline in EF has been shown in those with RVPA conduits compared to

MBT shunts at 3 years of age. [42] We found EF was lower in the RVPA conduit group compared to the MBT shunt group but still within normal range. This might reflect the smaller sample size of this study but may also be influenced by the method of assessment, as there is increased variability in measurement between echocardiography techniques and the CMR used in this study. [71] Interestingly despite the preserved EF, comparison of feature tracking based strain analysis between the 2 Norwood groups showed that the RVPA conduit group had significantly reduced strain in multiple ventricular axes. The CMR strain data is the first to be analysed for HLHS. As would be expected from the altered RV geometry, systemic RV strain values were markedly different from the healthy LV [105] and healthy RV. [102] Values were comparable to existing measures taken in those with HLHS via echocardiography. [37] The altered strain in the RVPA conduit group may represent dyskinesia caused by the scar, though increased volume loading from pulmonary regurgitation through the RVPA conduit may also play a role. Abnormal strain has been linked to an increased risk of adverse events in adults with LV dysfunction [99] and correlates to the risk of developing heart failure in adults with anatomically normal hearts. As such, strain analysis in the systemic RV may be a useful early marker of those that might have a poorer prognosis, particularly when the primary benefits of feature tracking are considered, namely: it is able to rapidly extract measures of strain from conventional MR imaging techniques; it is not limited by acoustic windows and it does not require new sequences or time consuming post-processing.

5.1.4 Limitations

Differences in clinical management certainly exist between the two groups as they were recruited from two centres. Some such as interventional coil occlusion rate can be accounted for, but many subtle factors affecting the RV shape cannot be fully quantified. This may lead to centre specific bias however single centre recruitment would not remove this potential bias either. The RVPA cohort undergoing primary CMR represented those with “best-physiology” as patients with less than ideal physiology underwent primary cardiac catheterisation. Despite this bias, marked differences in shape and function existed between the two groups after Stage II surgery with those undergoing BTS having better strain values across multiple axes.

The discrepancy in population size between the 2 groups is a consequence of the development of surgical techniques. The MBT shunt has been the standard approach for 30 years. The RVPA conduit has gained popularity during the past 10 years. Recent refinements including a reduction in the size of the ventriculotomy are becoming more commonplace. We advocate increasing the database size to include more subjects as they become available allowing improved sensitivity to abnormalities. Further work would include an analysis of how the more recent limited ventriculotomy affects growth and function. Prospectively collected data on serial MRI scans from the same subject would make this a more powerful study.

Patients receiving a RVPA conduit were older when they underwent Stage I CMR with consequent greater exposure to the effects of a higher Qp:Qs through the shunt. Qp:Qs was not routinely measured in either centre. This might have provided useful additional information on how the shunt affects ventricular volume. There was no difference in age at which each group underwent Stage II surgery with the continued presence of increased ventricular dilatation in the RVPA group indicating a major proportion of the volume loading may be a consequence of the type and size of shunt rather than its duration.

The addition of catheterization pressure data would have added further information on the loading effects on the ventricle. Unfortunately, this was not comprehensively available to permit analysis.

The construction of the computational atlas is limited to the available image resolution. Full 3D resolution images would provide greater anatomical detail. The automatic 3D mesh reconstruction of the systemic RV achieved a tolerable accuracy compared to the adult healthy LV (average fitting error divided by average length: 1.43mm/78mm vs. 1.28mm/95mm), [105] despite the greater difficulty for manual segmentation and automatic reconstruction of a structure with thinner walls and larger shape variability.

MRI feature tracking is susceptible to inter-user variability particularly for longitudinal and radial regional segmental assessments. [98, 101] Comparison of global circumferential strain to the gold standard of MR-tagged sequences does show good correlation. Regional strain analysis in the right ventricular outflow tract region would be desirable, but the current analysis technique does not provide reliable data and requires further refinement.

5.1.5 Conclusions

Utilising computational tools to create a cardiac atlas of ventricular geometry allows detection of subtle deviations in 3D shape that may not be adequately captured using 2D measurements. Alterations in the shape of the ventricle following RVPA conduit palliation are associated with abnormal function, which may have adverse effects on intra-ventricular blood flow energetics. Although the current evidence on short-term outcomes is equivocal, the results of this study warrant continued surveillance to assess the long-term outcomes in this vulnerable group of patients.

5.1.6 Summary

Background: The Norwood procedure for hypoplastic left heart syndrome (HLHS) is performed either via a right ventricle-to-pulmonary artery (RVPA) conduit or a modified Blalock-Taussig (MBT) shunt. The effects of the ventriculotomy associated with RVPA conduit on ventricular shape and function are assessed.

Methods and Results: A retrospective analysis of 93 cardiac magnetic resonance scans in subjects with HLHS was performed (59 MBT shunt, 34 RVPA shunt) incorporating data from two congenital centres at varying stages of surgery. Longitudinal and short-axis cine images were used to create a computational cardiac atlas and assess global strain. Those receiving RVPA conduit had significant differences (p <0.0001) in the shape of the RV corresponding to increased ventricular dilatation (p = 0.001) and increased sphericity (p = 0.006). Differences were evident only following completion of Stage II surgery. Despite preserved ejection fraction in both groups, functional strain in the RVPA shunt group compared to the MBT shunt group was reduced across multiple ventricular axes, including reduced systolic longitudinal strain rate (p < 0.0001), reduced diastolic longitudinal strain rate (p = 0.0001), and reduced midventricular systolic circumferential strain (p < 0.0001).

Conclusions: Computational modelling analysis reveals subtle differences in ventricular remodelling in those with HLHS undergoing a RVPA conduit with fo-

cal scarring potentially leading to altered functional markers of strain. Although comparative early outcome data shows no differences in survival, the need for continued surveillance is warranted, as deleterious effects may not become apparent until later years.

6. Overall Discussion

6.1 Overview

The aim of this thesis was to use CMR to characterise the function of the systemic RV in those with HLHS in terms of energy, shape and motion.

Chapter 3 described efforts to understand the external work performed by the ventricle using multi-modality CMR imaging and to explore the constraints imposed on the systemic RV during simulated exertion. Although pharmacological stimulation cannot mimic all of the physiological changes experienced during true exercise, a literature review suggested that it might offer useful insights. Surprisingly the load independent measures of contractility and relaxation of the ventricle were normal in this group of patients despite patients being symptomatic. Simultaneous measurements of volume and pressure demonstrated a 50% fall in preload, unrelated to PVR, was found to contribute to the plateau of cardiac index seen during pharmacological stress. The characteristics of the ventricle were described in energetic terms and it was found to be well coupled to the circulation although a dramatic increase in ventricular work was noted due primarily to a heart rate mediated increase in cardiac output. Determining the limitation to exercise in this group of patients provides important information on potential treatment strategies. Measures to improve preload could be explored as ways to alleviate symptoms of reduced functional capacity whilst trying to modulate PVR in the younger age group is less likely to be successful unless altered resistance is proven. Since this work was pub-

lished the data has been useful in guiding clinical decision making for this group of patients at Evelina. Seeing the translation of this work into the clinical realm, albeit in highly specialised practice, has been particularly rewarding.

The energetic theme was then developed further by using MRI to non-invasively assess another energetic parameter of external work - kinetic work. The progression towards assessing kinetic work was described in Chapter 2.6. A translational approach was used to answer the question "can a non-invasive measure of kinetic work be used in the clinical environment?" As a collaboration, a highly accelerated 4D flow MRI sequence was validated for clinical applicability and accuracy. Simultaneously, an approach to measuring intra-ventricular kinetic energy was developed. Clinical acquisition of data then completed the translation (Chapter 4). Kinetic energy profiles both in health and through a range of ages, were described. These normal values were compared to a cohort with established ventricular dysfunction and finally to a group with single ventricle physiology. The KE profiles were unchanged from the healthy RV. This was surprising as although the systemic RV demonstrates both volume-loading and hypertrophy there were no KE adaptations. This is also different to pressure-volume loops in patients with HLHS which show the systemic RV loop resembles a healthy LV loop. It was noted that subjects with larger and likely stiffer LV remnants had the greatest reductions in diastolic KE profiles. This preliminary work demonstrated that KE appeared to be a sensitive marker to pathology and led to the possibility of using markers based

around KE as potential new measures of ventricular function. Novel markers of systolic ventricular performance based on KE were developed and evaluated. The remainder of the chapter set out to explore the impact of function and morphology on KE EF and PE EF values. KE EF and PE EF in health had a very narrow range. In those with LV dysfunction, they were both significantly decreased suggesting they might be useful as a marker of function. In those with HLHS, KE EF and PE EF were also found to be decreased and additionally had a broader range than in those with healthy LVs suggesting they measured a spectrum of function. Comparatively VV EF remained within the very broad range of what is considered normal. The interesting finding was that PE EF was also associated with worsening AVVR and worsening NYHA status. These early results indicate that PE EF appears to be a marker of systolic ventricular function and may even be useful in grading dysfunction. Comparing these to objective clinical measures of exercise tolerance would be a useful next step. Exploring the use of KE to assess diastology would also be interesting. Both measuring total intra-ventricular KE and using the developed KE metrics provided some useful insights into the ventricle. However both were computationally intensive and the magnitude of the values whilst seeming significant were quite small. It will be interesting to see if other groups are able to reproduce these findings in other subjects or if the computation can be sped up. For the moment both methods will appear to be confined to the research realm.

In Chapter 6, a collaborative approach was used to bring the thesis to a con-

clusion through characterisation of the shape, motion and function of the ventricle following Norwood palliation. Single institution datasets for rare clinical conditions such as HLHS may be statistically underpowered. Sharing expertise, processing and datasets between institutions can allow important insights to be made. In conjunction with Boston Children's Hospital a retrospective computational analysis of shape and motion of the systemic RV was undertaken using CMR. Those undergoing MBT shunts and RVPA conduits demonstrated distinct 3D differences in shape. The dilated shape in those receiving a RVPA conduit was only partially captured using traditional metrics of length and volume indicating the increased sensitivity for 3D shape analyses. Measures of ventricular motion showed decreased strain indices in those undergoing a RVPA conduit. Either the ventriculotomy scar on the systemic RV or the effect of shunt regurgitation on the ventricle caused deleterious effects on function. The results warrant further surveillance and support the need for ongoing studies to assess the longer term impact in older patients.

The process of completing this thesis has raised and answered and then raised further questions. Using pressure-volume loop analyses of the systemic single RV allowed us to understand that preload is a major factor for symptoms. The RV in HLHS appeared to adapt as a pressure loaded ventricle and the pressure-volume loop resembled that of a healthy LV. The stroke work, a useful measure of ventricular work, was seen to be grossly elevated during higher heart rates. This led to the question of whether the work of the heart could be

investigated non-invasively. A 4D flow sequence was used to measure kinetic energy. Kinetic energy and stroke work are part of the useful work that the heart performs in ejecting blood. Surprisingly the intra-cardiac KE profile resembled a RV. There was no adaptation. It would have been useful to examine and compare single RV to single LV datasets but unfortunately there were not enough subjects available. Although the KE and PV loop results appear contrasting, one showing no energetic adaptation and the other showing a complete adaptation I think these ideas complement each other. They measure different aspects of the useful work the heart performs in pumping blood and show how the adaptation that the RV undergoes in HLHS is not complete. It is still inherently a morphological RV and as such when asked to pump at systemic pressures it is less efficient and uses more energy. It is able to eject a given volume at a set pressure however the work of pumping the blood and transferring energy to the blood is altered. Over time this cumulative load could be costly. Finally an investigation into the shape and motion of the ventricle was performed confirming our thoughts about the RVPA conduit causing dilatation and reduced motion presumably from scar and regurgitation. However these values have not yet been shown to have any clinical impact. It would also be useful in future to understand how shape and motion correlate to work. At the end of this process some questions are answered and some unexpected insights were gained but what is certain is that we are still only a small part of the way to understanding the pathophysiology of this condition.

6.2 Limitations

Limitations to each study have been discussed at the end of the relevant chapter. However three over-arching themes span the breadth of this work. The first is that the majority of scans are performed on anaesthetised patients. The second is the relatively small numbers in each study and the third is a sparsity of clinical correlates. The effect these have on the context of this work will be assessed in turn.

The majority of patients with HLHS within the institution where these studies were performed are of a young age. Opportunistic scanning and ethical considerations meant recruitment occurred at the time of scheduled clinical visits. The majority of the CMR studies then represent pre-surgical scans. The age of the recruited patients therefore tended to be between 3 to 10 years of age. Institutional preference dictated scans be performed under a general anaesthetic to facilitate acquisition of high quality clinical data. In those with a Fontan circulation, positive pressure ventilation represents a reversal of respiratory physiology. [206, 207] Furthermore those with Fontan circulations rely on the actions peripheral muscle pump to contribute towards systemic venous return. Ethical considerations did not allow younger patients to be scanned awake, and technological limitations prevented scanning in an upright or active position. However with the increasing population of patients with HLHS surviving into early teenage years and beyond these may become available options in the future. Furthermore work on developing supine exercise is underway and may offer

further insights. [61]

HLHS is a rare condition and the number of patients available and suitable for study recruitment reflects this. The largest studies to-date have come from the Single Ventricle Reconstruction trial involving the recruitment of 549 patients through multiple North American centres. [41, 42, 218] Through similar collaborations such as this, or smaller partnerships such as demonstrated in chapter 6, our understanding of the limitations faced by the systemic RV can be advanced more completely.

The population of subjects with HLHS remains skewed towards the younger age range. This limits their ability to successfully complete objective measures of function such as cardio-pulmonary exercise testing as they are often too young or too small to run on a treadmill or reach the pedals on a bike. Subjective clinical correlates were used as a substitute where possible but these cannot replace objective data. However the translational work performed in this thesis does draw interesting preliminary conclusions that can be followed up with robust objective measures of function in future studies.

6.3 Future directions

In better characterising the single RV, further questions emerge leading to new avenues of research. The development of supine exercise bikes that can be used whilst a patient is within the bore of the CMR scanner offer new opportu-

nities for better understanding changes in physiology during exertion. [61] Dual VENC 4D flow sequences are being developed and require validation. [225] These will pave the way for improved flow data sampling particularly in low velocity areas of the heart where a single higher VENC sequence can miss subtleties in blood flow dynamics. Further work in the field of KE may include the development of echocardiographic assessment of KE using 3D flow [119] or the application of indices of KE to study other congenital cardiac conditions. The increasing use of Lagrangian particle-by-particle based analysis offers the possibility of understanding kinematics in new ways. [202, 213, 214, 226] The use of cardiac atlases offer the opportunity to understand and compare a wide variety of conditions and could include, how the hybrid procedure can alter the shape of the ventricle. This technique could also be applied to other forms of CHD to assess the impact of different treatment strategies on the same cohort of patients. Developing 3D CMR tagging would provide more robust measures of regional ventricular wall motion.

This thesis focused on those with HLHS as they have the worst outcomes. Future work could include expanding these techniques to incorporate other patients with single ventricle circulations to compare and contrast their haemodynamics.

6.4 Final Conclusions

This thesis has sought to characterise distinctive features typical of the sys-

temic RV in relation to energy, shape, motion and function. The objectives set out in the introduction have been met but in doing so have raise new questions for further investigation. Ultimately in trying to characterise the systemic RV, the hope is that this thesis will provide some insights that lead to improvements in the delivery of care for those living with this difficult condition.

7. References

1. Noonan JA, Nadas AS. The hypoplastic left heart syndrome; an analysis of 101 cases. *Pediatric Clinics of North America*. 1958;5:1029.

2. Norwood WI, Lang P, Hansen DD. Physiologic repair of aortic atresia-hypoplastic left heart syndrome. *N Engl J Med*. 1983;308:23-26.

3. Moodie DS, Gallen WJ, Friedberg DZ. Congenital aortic atresia. Report of long survival and some speculations about surgical approaches. *J Thorac Cardiovasc Surg*. 1972;63:726-731.

4. Erikssen G, Aboulhosn J, Lin J, Liestøl K, Estensen ME, Gjesdal O, Skulstad H, Døhlen G, Lindberg HL. Survival in patients with univentricular hearts: the impact of right versus left ventricular morphology. *Open Heart*. 2018;5:e000902.

5. Ohuchi H, Yasuda K, Hasegawa S, Miyazaki A, Takamuro M, Yamada O, Ono Y, Uemura H, Yagihara T, Echigo S. Influence of ventricular morphology on aerobic exercise capacity in patients after the Fontan operation. *J Am Coll Cardiol*. 2001;37:1967-1974.

6. Takken T, Tacken MHP, Blank AC, Hulzebos EH, Strengers JLM, Helders PJM. Exercise limitation in patients with Fontan circulation: a review. *Journal of Cardiovascular Medicine*. 2007;8:775-781.

7. Gewillig M, Brown SC, Eyskens B, Heying R, Ganame J, Budts W, La Gerche A, Gorenflo M. The Fontan circulation: who controls cardiac output? *Interact Cardiovasc Thorac Surg*. 2010;10:428-433.

8. Fontan F, Baudet E. Surgical repair of tricuspid atresia. *Thorax*. 1971;26:240-248.

9. de Vecchi A, Nordsletten DA, Remme EW, Bellsham-Revell H, Greil G, Simpson JM, Razavi R, Smith NP. Inflow typology and ventricular geometry determine efficiency of filling in the hypoplastic left heart. *Ann Thorac Surg*. 2012;94:1562-1569.

10. Fredriksson AG, Zajac J, Eriksson J, Dyverfeldt P, Bolger AF, Ebbers T, Carlhall CJ. 4-D blood flow in the human right ventricle. *Am J Physiol Heart Circ Physiol*. 2011;301:H2344-50.

11. Kilner PJ, Yang GZ, Wilkes AJ, Mohiaddin RH, Firmin DN, Yacoub MH. Asymmetric redirection of flow through the heart. *Nature*. 2000;404:759-761.

12. Watanabe H, Sugiura S, Hisada T. The looped heart does not save energy by maintaining the momentum of blood flowing in the ventricle. *Am J Physiol Heart Circ Physiol*. 2008;294:H2191-6.

13. Barron DJ, Kilby MD, Davies B, Wright JG, Jones TJ, Brawn WJ. Hypoplastic left heart syndrome. *Lancet*. 2009;374:551-564.

14. Redington AN, Rigby ML, Shinebourne EA, Oldershaw PJ. Changes in the pressure-volume relation of the right ventricle when its loading conditions are modified. *Heart*. 1990;63:45-49.

15. *Nadas' Pediatric Cardiology*. Hanley & Belfus; 1992.

16. Hoffman JI, Kaplan S. The incidence of congenital heart disease. *J Am Coll Cardiol*. 2002;39:1890-1900.

17. Burn J, Brennan P, Little J, Holloway S, Coffey R, Somerville J, Dennis NR, Allan L, Arnold R, Deanfield JE, Godman M, Houston A, Keeton B, Oakley C, Scott O, Silove E, Wilkinson J, Pembrey M, Hunter AS. Recurrence risks in offspring of adults with major heart defects: results from first cohort of British collaborative study. *Lancet*. 1998;351:311-316.

18. Connor JA, Thiagarajan R. Hypoplastic left heart syndrome. *Orphanet J Rare Dis*. 2007;2:23.

19. Norwood WI, Kirklin JK, Sanders SP. Hypoplastic left heart syndrome: experience with palliative surgery. *The American journal of cardiology*. 1980;45:87-91.

20. Bogaard HJ, Abe K, Noordegraaf AV, Voelkel NF. The right ventricle under pressurecellular and molecular mechanisms of right-heart failure in pulmonary hypertension. *Chest Journal*. 2009;135:794-804.

21. Nagel E, Stuber M, Hess OM. Importance of the right ventricle in valvular heart disease. *European heart journal*. 1996;17:829-836.

22. Redington AN, Gray HH, Hodson ME, Rigby ML, Oldershaw PJ. Characterisation of the normal right ventricular pressure-volume relation by biplane angiography and simultaneous micromanometer pressure measurements. *British heart journal*. 1988;59:23-30.

23. Sheehan F, Redington A. The right ventricle: anatomy, physiology and clinical imaging. *Heart*. 2008;94:1510-1515.

24. Fourie PR, Coetzee AR, Bolliger CT. Pulmonary artery compliance: its role in right ventricular-arterial coupling. *Cardiovascular research*. 1992;26:839-844.

25. Redington AN, Rigby ML, Shinebourne EA, Oldershaw PJ. Changes in the pressure-volume relation of the right ventricle when its loading conditions are modified. *British heart journal*. 1990;63:45-49.

26. Henning RJ. Effects of positive end-expiratory pressure on the right ventricle. *J Appl Physiol (1985)*. 1986;61:819-826.

27. Tan JL, Prati D, Gatzoulis MA, Gibson D, Henein MY, Li W. The right ventricular response to high afterload: comparison between atrial switch procedure, congenitally corrected transposition of the great arteries, and idiopathic pulmonary arterial hypertension. *Am Heart J*. 2007;153:681-688.

28. de Vroomen M, Cardozo RHL, Steendijk P, van Bel F, Baan J. Improved contractile performance of right ventricle in response to increased RV afterload in newborn lamb. *American Journal of Physiology-Heart and Circulatory Physiology*. 2000;278:H100-H105.

29. Leeuwenburgh BPJ, Helbing WA, Steendijk P, Schoof PH, Baan J. Biventricular systolic function in young lambs subject to chronic systemic right ventricular pressure overload. *American Journal of Physiology-Heart and Circulatory Physiology*. 2001;281:H2697-H2704.

30. Presbitero P, Somerville J, Rabajoli F, Stone S, Conte MR. Corrected transposition of the great arteries without associated defects in adult patients: clinical profile and follow up. *British heart journal*. 1995;74:57-59.

31. Graham TP, Bernard YD, Mellen BG, Celermajer D, Baumgartner H, Cetta F, Connolly HM, Davidson WR, Dellborg M, Foster E. Long-term outcome in congenital-

ly corrected transposition of the great arteriesa multi-institutional study. *Journal of the American College of Cardiology*. 2000;36:255-261.

32. Feneley MP, Gavaghan TP, Baron DW, Branson JA, Roy PR, Morgan JJ. Contribution of left ventricular contraction to the generation of right ventricular systolic pressure in the human heart. *Circulation*. 1985;71:473-480.

33. Fogel MA, Weinberg PM, Gupta KB, Rychik J, Hubbard A, Hoffman EA, Haselgrove J. Mechanics of the single left ventricle: a study in ventricular-ventricular interaction II. *Circulation*. 1998;98:330-338.

34. Fogel MA, Weinberg PM, Fellows KE, Hoffman EA. A study in ventricular–ventricular interaction single right ventricles compared with systemic right ventricles in a dual-chamber circulation. *Circulation*. 1995;92:219-230.

35. Furck AK, Uebing A, Hansen JH, Scheewe J, Jung O, Fischer G, Rickers C, Holland-Letz T, Kramer HH. Outcome of the Norwood operation in patients with hypoplastic left heart syndrome: a 12-year single-center survey. *J Thorac Cardiovasc Surg*. 2010;139:359-365.

36. Sugiyama H, Yutani C, Iida K, Arakaki Y, Yamada O, Kamiya T. The relation between right ventricular function and left ventricular morphology in hypoplastic left heart syndrome: angiographic and pathological studies. *Pediatric cardiology*. 1999;20:422-427.

37. Schlangen J, Fischer G, Steendijk P, Petko C, Scheewe J, Hart C, Hansen JH, Ahrend F, Rickers C, Kramer HH, Uebing A. Does left ventricular size impact on intrin-

sic right ventricular function in hypoplastic left heart syndrome? *Int J Cardiol*. 2013;167:1305-1310.

38. Feinstein JA, Benson DW, Dubin AM, Cohen MS, Maxey DM, Mahle WT, Pahl E, Villafane J, Bhatt AB, Peng LF, Johnson BA, Marsden AL, Daniels CJ, Rudd NA, Caldarone CA, Mussatto KA, Morales DL, Ivy DD, Gaynor JW, Tweddell JS, Deal BJ, Furck AK, Rosenthal GL, Ohye RG, Ghanayem NS, Cheatham JP, Tworetzky W, Martin GR. Hypoplastic left heart syndrome: current considerations and expectations. *J Am Coll Cardiol*. 2012;59:S1-42.

39. Sano S, Ishino K, Kawada M, Arai S, Kasahara S, Asai T, Masuda Z-i, Takeuchi M, Ohtsuki S-i. Right ventricle–pulmonary artery shunt in first-stage palliation of hypoplastic left heart syndrome. *The Journal of Thoracic and Cardiovascular Surgery*. 2003;126:504-509.

40. Tweddell JS, Ghanayem NS, Mussatto KA, Mitchell ME, Lamers LJ, Musa NL, Berger S, Litwin SB, Hoffman GM. Mixed venous oxygen saturation monitoring after stage 1 palliation for hypoplastic left heart syndrome. *Ann Thorac Surg*. 2007;84:1301-10; discussion 1310.

41. Ohye RG, Sleeper LA, Mahony L, Newburger JW, Pearson GD, Lu M, Goldberg CS, Tabbutt S, Frommelt PC, Ghanayem NS. Comparison of shunt types in the Norwood procedure for single-ventricle lesions. *New England Journal of Medicine*. 2010;362:1980-1992.

42. Newburger JW, Sleeper LA, Frommelt PC, Pearson GD, Mahle WT, Chen S, Dunbar-Masterson C, Mital S, Williams IA, Ghanayem NS, Goldberg CS, Jacobs JP, Krawczeski CD, Lewis AB, Pasquali SK, Pizarro C, Gruber PJ, Atz AM, Khaikin S,

Gaynor JW, Ohye RG. Transplantation-free survival and interventions at 3 years in the single ventricle reconstruction trial. *Circulation*. 2014;129:2013-2020.

43. Bellsham-Revell HR, Tibby SM, Bell AJ, Witter T, Simpson J, Beerbaum P, Anderson D, Austin CB, Greil GF, Razavi R. Serial magnetic resonance imaging in hypoplastic left heart syndrome gives valuable insight into ventricular and vascular adaptation. *J Am Coll Cardiol*. 2013;61:561-570.

44. Fiore AC, Turrentine M, Rodefeld M, Vijay P, Schwartz TL, Virgo KS, Fischer LK, Brown JW. Fontan operation: a comparison of lateral tunnel with extracardiac conduit. *Ann Thorac Surg*. 2007;83:622-9; discussion 629.

45. d'Udekem Y, Iyengar AJ, Galati JC, Forsdick V, Weintraub RG, Wheaton GR, Bullock A, Justo RN, Grigg LE, Sholler GF, Hope S, Radford DJ, Gentles TL, Celermajer DS, Winlaw DS. Redefining expectations of long-term survival after the Fontan procedure: twenty-five years of follow-up from the entire population of Australia and New Zealand. *Circulation*. 2014;130:S32-8.

46. Robbers-Visser D, Miedema M, Nijveld A, Boersma E, Bogers AJ, Haas F, Helbing WA, Kapusta L. Results of staged total cavopulmonary connection for functionally univentricular hearts; comparison of intra-atrial lateral tunnel and extracardiac conduit. *Eur J Cardiothorac Surg*. 2010;37:934-941.

47. Meadows J, Lang P, Marx G, Rhodes J. Fontan fenestration closure has no acute effect on exercise capacity but improves ventilatory response to exercise. *J Am Coll Cardiol*. 2008;52:108-113.

48. Khairy P, Poirier N, Mercier LA. Univentricular heart. *Circulation*. 2007;115:800-812.

49. van den Bosch AE, Roos-Hesselink JW, Van Domburg R, Bogers AJ, Simoons ML, Meijboom FJ. Long-term outcome and quality of life in adult patients after the Fontan operation. *Am J Cardiol*. 2004;93:1141-1145.

50. Feldt RH, Driscoll DJ, Offord KP, Cha RH, Perrault J, Schaff HV, Puga FJ, Danielson GK. Protein-losing enteropathy after the Fontan operation. *J Thorac Cardiovasc Surg*. 1996;112:672-680.

51. Moller P, Weitz M, Jensen KO, Dubowy KO, Furck AK, Scheewe J, Kramer HH, Uebing A. Exercise capacity of a contemporary cohort of children with hypoplastic left heart syndrome after staged palliation. *Eur J Cardiothorac Surg*. 2009;36:980-985.

52. Durongpisitkul K, Driscoll DJ, Mahoney DW, Wollan PC, Mottram CD, Puga FJ, Danielson GK. Cardiorespiratory response to exercise after modified Fontan operation: determinants of performance. *Journal of the American College of Cardiology*. 1997;29:785-790.

53. Sundareswaran KS, Kanter KR, Kitajima HD, Krishnankutty R, Sabatier JF, Parks WJ, Sharma S, Yoganathan AP, Fogel M. Impaired power output and cardiac index with hypoplastic left heart syndrome: a magnetic resonance imaging study. *Ann Thorac Surg*. 2006;82:1267-75; discussion 1275.

54. Anderson PA, Sleeper LA, Mahony L, Colan SD, Atz AM, Breitbart RE, Gersony WM, Gallagher D, Geva T, Margossian R, McCrindle BW, Paridon S, Schwartz

M, Stylianou M, Williams RV, Clark BJ. Contemporary outcomes after the Fontan procedure: a Pediatric Heart Network multicenter study. *J Am Coll Cardiol*. 2008;52:85-98.

55. Redington A. The physiology of the Fontan circulation. *Progress in Pediatric Cardiology*. 2006;22:179-186.

56. Khambadkone S, Li J, de Leval MR, Cullen S, Deanfield JE, Redington AN. Basal pulmonary vascular resistance and nitric oxide responsiveness late after Fontan-type operation. *Circulation*. 2003;107:3204-3208.

57. Presson RGJ, Baumgartner WAJ, Peterson AJ, Glenny RW, Wagner WWJ. Pulmonary capillaries are recruited during pulsatile flow. *J Appl Physiol (1985)*. 2002;92:1183-1190.

58. Stickland MK, Welsh RC, Petersen SR, Tyberg JV, Anderson WD, Jones RL, Taylor DA, Bouffard M, Haykowsky MJ. Does fitness level modulate the cardiovascular hemodynamic response to exercise? *J Appl Physiol (1985)*. 2006;100:1895-1901.

59. Goldberg DJ, French B, McBride MG, Marino BS, Mirarchi N, Hanna BD, Wernovsky G, Paridon SM, Rychik J. Impact of oral sildenafil on exercise performance in children and young adults after the fontan operation: a randomized, double-blind, placebo-controlled, crossover trial. *Circulation*. 2011;123:1185-1193.

60. Giardini A, Balducci A, Specchia S, Gargiulo G, Bonvicini M, Picchio FM. Effect of sildenafil on haemodynamic response to exercise and exercise capacity in Fontan patients. *Eur Heart J*. 2008;29:1681-1687.

61. Van De Bruaene A, La Gerche A, Claessen G, De Meester P, Devroe S, Gillijns H, Bogaert J, Claus P, Heidbuchel H, Gewillig M, Budts W. Sildenafil improves exercise hemodynamics in Fontan patients. *Circ Cardiovasc Imaging*. 2014;7:265-273.

62. Stamm C, Anderson RH, Ho SY. The morphologically tricuspid valve in hypoplastic left heart syndrome. *European journal of cardio-thoracic surgery*. 1997;12:587-592.

63. Elmi M, Hickey EJ, Williams WG, Van Arsdell G, Caldarone CA, McCrindle BW. Long-term tricuspid valve function after Norwood operation. *The Journal of thoracic and cardiovascular surgery*. 2011;142:1341-1347. e4.

64. Ohye RG, Gomez CA, Goldberg CS, Graves HL, Devaney EJ, Bove EL. Tricuspid valve repair in hypoplastic left heart syndrome. *J Thorac Cardiovasc Surg*. 2004;127:465-472.

65. Ugaki S, Khoo NS, Ross DB, Rebeyka IM, Adatia I. Tricuspid valve repair improves early right ventricular and tricuspid valve remodeling in patients with hypoplastic left heart syndrome. *J Thorac Cardiovasc Surg*. 2013;145:446-450.

66. Altmann K, Printz BF, Solowiejczyk DE, Gersony WM, Quaegebeur J, Apfel HD. Two-dimensional echocardiographic assessment of right ventricular function as a predictor of outcome in hypoplastic left heart syndrome. *The American journal of cardiology*. 2000;86:964-968.

67. Hughes ML, Tsang VT, Kostolny M, Giardini A, Muthurangu V, Taylor AM, Brown K. Lessons from inter-stage cardiac magnetic resonance imaging in predicting

survival for patients with hypoplastic left heart syndrome. *Cardiology in the Young*. 2011;21:646-653.

68. Takken T, Hulzebos HJ, Blank AC, Tacken MH, Helders PJ, Strengers JL. Exercise prescription for patients with a Fontan circulation: current evidence and future directions. *Neth Heart J*. 2007;15:142-147.

69. Voelkel NF, Quaife RA, Leinwand LA, Barst RJ, McGoon MD, Meldrum DR, Dupuis J, Long CS, Rubin LJ, Smart FW, Suzuki YJ, Gladwin M, Denholm EM, Gail DB. Right ventricular function and failure: report of a National Heart, Lung, and Blood Institute working group on cellular and molecular mechanisms of right heart failure. *Circulation*. 2006;114:1883-1891.

70. Bell A, Rawlins D, Bellsham-Revell H, Miller O, Razavi R, Simpson J. Assessment of right ventricular volumes in hypoplastic left heart syndrome by real-time three-dimensional echocardiography: comparison with cardiac magnetic resonance imaging. *Eur Heart J Cardiovasc Imaging*. 2014;15:257-266.

71. Margossian R, Schwartz ML, Prakash A, Wruck L, Colan SD, Atz AM, Bradley TJ, Fogel MA, Hurwitz LM, Marcus E, Powell AJ, Printz BF, Puchalski MD, Rychik J, Shirali G, Williams R, Yoo SJ, Geva T. Comparison of echocardiographic and cardiac magnetic resonance imaging measurements of functional single ventricular volumes, mass, and ejection fraction (from the Pediatric Heart Network Fontan Cross-Sectional Study). *Am J Cardiol*. 2009;104:419-428.

72. Gewillig M. The Fontan circulation. *Heart*. 2005;91:839-846.

73. Friedberg MK, Silverman NH. The systolic to diastolic duration ratio in children with hypoplastic left heart syndrome: a novel Doppler index of right ventricular function. *J Am Soc Echocardiogr*. 2007;20:749-755.

74. Williams RV, Ritter S, Tani LY, Pagotto LT, Minich LL. Quantitative assessment of ventricular function in children with single ventricles using the Doppler myocardial performance index. *The American journal of cardiology*. 2000;86:1106-1110.

75. Bellsham-Revell HR, Tibby SM, Bell AJ, Miller OI, Razavi R, Greil GF, Simpson JM. Tissue Doppler time intervals and derived indices in hypoplastic left heart syndrome. *Eur Heart J Cardiovasc Imaging*. 2012;13:400-407.

76. Tsai-Goodman B, Geva T, Odegard KC, Sena LM, Powell AJ. Clinical role, accuracy, and technical aspects of cardiovascular magnetic resonance imaging in infants. *The American journal of cardiology*. 2004;94:69-74.

77. Mistry N, Halvorsen S, Hoffmann P, Muller C, Bohmer E, Kjeldsen SE, Bjornerheim R. Assessment of left ventricular function with magnetic resonance imaging vs. echocardiography, contrast echocardiography, and single-photon emission computed tomography in patients with recent ST-elevation myocardial infarction. *Eur J Echocardiogr*. 2010;11:793-800.

78. Lorenz CH. The Range of Normal Values of Cardiovascular Structures in Infants, Children, and Adolescents Measured by Magnetic Resonance Imaging. *Pediatr Cardiol*. 2000;21:37-46.

79. Geva T. Is MRI the preferred method for evaluating right ventricular size and function in patients with congenital heart disease?: MRI is the preferred method for

evaluating right ventricular size and function in patients with congenital heart disease. *Circ Cardiovasc Imaging*. 2014;7:190-197.

80. Muthurangu V, Taylor AM, Hegde SR, Johnson R, Tulloh R, Simpson JM, Qureshi S, Rosenthal E, Baker E, Anderson D, Razavi R. Cardiac magnetic resonance imaging after stage I Norwood operation for hypoplastic left heart syndrome. *Circulation*. 2005;112:3256-3263.

81. Dillman JR, Dorfman AL, Attili AK, Agarwal PP, Bell A, Mueller GC, Hernandez RJ. Cardiovascular magnetic resonance imaging of hypoplastic left heart syndrome in children. *Pediatr Radiol*. 2010;40:261-74; quiz 379.

82. Grosse-Wortmann L, Yun TJ, Al-Radi O, Kim S, Nii M, Lee KJ, Redington A, Yoo SJ, van Arsdell G. Borderline hypoplasia of the left ventricle in neonates: insights for decision-making from functional assessment with magnetic resonance imaging. *J Thorac Cardiovasc Surg*. 2008;136:1429-1436.

83. Dickstein K, Cohen-Solal A, Filippatos G, McMurray JJV, Ponikowski P, Poole-Wilson PA, Strömberg A, Veldhuisen DJ, Atar D, Hoes AW. ESC Guidelines for the diagnosis and treatment of acute and chronic heart failure 2008‡. *European journal of heart failure*. 2008;10:933-989.

84. Fratz S, Chung T, Greil GF, Samyn MM, Taylor AM, Buechel ERV, Yoo S-J, Powell AJ. Guidelines and protocols for cardiovascular magnetic resonance in children and adults with congenital heart disease: SCMR expert consensus group on congenital heart disease. *Journal of Cardiovascular Magnetic Resonance*. 2013;15:1-26.

85. Fratz S, Schuhbaeck A, Buchner C, Busch R, Meierhofer C, Martinoff S, Hess J, Stern H. Comparison of accuracy of axial slices versus short-axis slices for measuring

ventricular volumes by cardiac magnetic resonance in patients with corrected tetralogy of fallot. *The American journal of cardiology*. 2009;103:1764-1769.

86. Kalam K, Otahal P, Marwick TH. Prognostic implications of global LV dysfunction: a systematic review and meta-analysis of global longitudinal strain and ejection fraction. *Heart*. 2014;100:1673-1680.

87. Smiseth OA, Torp H, Opdahl A, Haugaa KH, Urheim S. Myocardial strain imaging: how useful is it in clinical decision making. *Eur Heart J*. 2016;37:1196-1207.

88. Zerhouni EA, Parish DM, Rogers WJ, Yang A, Shapiro EP. Human heart: tagging with MR imaging--a method for noninvasive assessment of myocardial motion. *Radiology*. 1988;169:59-63.

89. Ibrahim E-SH. Myocardial tagging by cardiovascular magnetic resonance: evolution of techniques--pulse sequences, analysis algorithms, and applications. *J Cardiovasc Magn Reson*. 2011;13:36.

90. Moore CC, Lugo-Olivieri CH, McVeigh ER, Zerhouni EA. Three-dimensional systolic strain patterns in the normal human left ventricle: characterization with tagged MR imaging. *Radiology*. 2000;214:453-466.

91. Cupps BP, Taggar AK, Reynolds LM, Lawton JS, Pasque MK. Regional myocardial contractile function: multiparametric strain mapping. *Interact Cardiovasc Thorac Surg*. 2010;10:953-957.

92. Del-Canto I, López-Lereu MP, Monmeneu JV, Croisille P, Clarysse P, Chorro FJ, Bodí V, Moratal D. Characterization of normal regional myocardial function by MRI cardiac tagging. *J Magn Reson Imaging*. 2015;41:83-92.

93. Kawel-Boehm N, Maceira A, Valsangiacomo-Buechel ER, Vogel-Claussen J, Turkbey EB, Williams R, Plein S, Tee M, Eng J, Bluemke DA. Normal values for cardiovascular magnetic resonance in adults and children. *J Cardiovasc Magn Reson*. 2015;17:29.

94. Friedberg MK, Silverman NH, Dubin AM, Rosenthal DN. Right ventricular mechanical dyssynchrony in children with hypoplastic left heart syndrome. *J Am Soc Echocardiogr*. 2007;20:1073-1079.

95. Menon SC, Minich LL, Casper TC, Puchalski MD, Hawkins JA, Tani LY. Regional myocardial dysfunction following Norwood with right ventricle to pulmonary artery conduit in patients with hypoplastic left heart syndrome. *J Am Soc Echocardiogr*. 2011;24:826-833.

96. Menon SC, Erickson LK, McFadden M, Miller DV. Effect of ventriculotomy on right-ventricular remodeling in hypoplastic left heart syndrome: a histopathological and echocardiography correlation study. *Pediatr Cardiol*. 2013;34:354-363.

97. Maret E, Todt T, Brudin L, Nylander E, Swahn E, Ohlsson JL, Engvall JE. Functional measurements based on feature tracking of cine magnetic resonance images identify left ventricular segments with myocardial scar. *Cardiovasc Ultrasound*. 2009;7:53.

98. Hor KN, Gottliebson WM, Carson C, Wash E, Cnota J, Fleck R, Wansapura J, Klimeczek P, Al-Khalidi HR, Chung ES, Benson DW, Mazur W. Comparison of magnetic resonance feature tracking for strain calculation with harmonic phase imaging analysis. *JACC Cardiovasc Imaging*. 2010;3:144-151.

99. Cho G-Y, Marwick TH, Kim H-S, Kim M-K, Hong K-S, Oh D-J. Global 2-dimensional strain as a new prognosticator in patients with heart failure. *Journal of the American College of Cardiology*. 2009;54:618-624.

100. Schuster A, Kutty S, Padiyath A, Parish V, Gribben P, Danford DA, Makowski MR, Bigalke B, Beerbaum P, Nagel E. Cardiovascular magnetic resonance myocardial feature tracking detects quantitative wall motion during dobutamine stress. *J Cardiovasc Magn Reson*. 2011;13:58.

101. Augustine D, Lewandowski AJ, Lazdam M, Rai A, Francis J, Myerson S, Noble A, Becher H, Neubauer S, Petersen SE, Leeson P. Global and regional left ventricular myocardial deformation measures by magnetic resonance feature tracking in healthy volunteers: comparison with tagging and relevance of gender. *J Cardiovasc Magn Reson*. 2013;15:8.

102. Morton G, Schuster A, Jogiya R, Kutty S, Beerbaum P, Nagel E. Inter-study reproducibility of cardiovascular magnetic resonance myocardial feature tracking. *Journal of Cardiovascular Magnetic Resonance*. 2012;14:1-8.

103. Lamata P, Niederer S, Nordsletten D, Barber DC, Roy I, Hose D, Smith N. An accurate, fast and robust method to generate patient-specific cubic Hermite meshes. *Medical image analysis*. 2011;15:801-813.

104. Lamata P, Sinclair M, Kerfoot E, Lee A, Crozier A, Blazevic B, Land S, Lewandowski AJ, Barber D, Niederer S, Smith N. An automatic service for the personalization of ventricular cardiac meshes. *J R Soc Interface*. 2014;11:20131023.

105. Lewandowski AJ, Augustine D, Lamata P, Davis EF, Lazdam M, Francis J, McCormick K, Wilkinson AR, Singhal A, Lucas A, Smith NP, Neubauer S, Leeson P.

Preterm heart in adult life: cardiovascular magnetic resonance reveals distinct differences in left ventricular mass, geometry, and function. *Circulation*. 2013;127:197-206.

106. Bove EL, de Leval MR, Migliavacca F, Balossino R, Dubini G. Toward optimal hemodynamics: computer modeling of the Fontan circuit. *Pediatr Cardiol*. 2007;28:477-481.

107. Dasi LP, Krishnankuttyrema R, Kitajima HD, Pekkan K, Sundareswaran KS, Fogel M, Sharma S, Whitehead K, Kanter K, Yoganathan AP. Fontan hemodynamics: importance of pulmonary artery diameter. *J Thorac Cardiovasc Surg*. 2009;137:560-564.

108. Qian Y, Liu JL, Itatani K, Miyaji K, Umezu M. Computational hemodynamic analysis in congenital heart disease: simulation of the Norwood procedure. *Ann Biomed Eng*. 2010;38:2302-2313.

109. Bossers SS, Cibis M, Gijsen FJ, Schokking M, Strengers JL, Verhaart RF, Moelker A, Wentzel JJ, Helbing WA. Computational fluid dynamics in Fontan patients to evaluate power loss during simulated exercise. *Heart*. 2014;100:696-701.

110. Gatehouse PD, Keegan J, Crowe LA, Masood S, Mohiaddin RH, Kreitner KF, Firmin DN. Applications of phase-contrast flow and velocity imaging in cardiovascular MRI. *Eur Radiol*. 2005;15:2172-2184.

111. Dyverfeldt P, Bissell M, Barker AJ, Bolger AF, Carlhäll CJ, Ebbers T, Francios CJ, Frydrychowicz A, Geiger J, Giese D, Hope MD, Kilner PJ, Kozerke S, Myerson S, Neubauer S, Wieben O, Markl M. 4D flow cardiovascular magnetic resonance consensus statement. *J Cardiovasc Magn Reson*. 2015;17:72.

112. Markl M, Geiger J, Kilner PJ, Foll D, Stiller B, Beyersdorf F, Arnold R, Frydrychowicz A. Time-resolved three-dimensional magnetic resonance velocity mapping of cardiovascular flow paths in volunteers and patients with Fontan circulation. *Eur J Cardiothorac Surg*. 2011;39:206-212.

113. Markl M, Wallis W, Brendecke S, Simon J, Frydrychowicz A, Harloff A. Estimation of global aortic pulse wave velocity by flow-sensitive 4D MRI. *Magn Reson Med*. 2010;63:1575-1582.

114. Ebbers T, Wigstrom L, Bolger AF, Engvall J, Karlsson M. Estimation of relative cardiovascular pressures using time-resolved three-dimensional phase contrast MRI. *Magn Reson Med*. 2001;45:872-879.

115. Petersson S, Dyverfeldt P, Ebbers T. Assessment of the accuracy of MRI wall shear stress estimation using numerical simulations. *J Magn Reson Imaging*. 2012;36:128-138.

116. Dyverfeldt P, Hope MD, Tseng EE, Saloner D. Magnetic resonance measurement of turbulent kinetic energy for the estimation of irreversible pressure loss in aortic stenosis. *JACC Cardiovasc Imaging*. 2013;6:64-71.

117. Bissell MM, Hess AT, Biasiolli L, Glaze SJ, Loudon M, Pitcher A, Davis A, Prendergast B, Markl M, Barker AJ, Neubauer S, Myerson SG. Aortic dilation in bicuspid aortic valve disease: flow pattern is a major contributor and differs with valve fusion type. *Circ Cardiovasc Imaging*. 2013;6:499-507.

118. Carlsson M, Heiberg E, Toger J, Arheden H. Quantification of left and right ventricular kinetic energy using four-dimensional intracardiac magnetic resonance imaging flow measurements. *Am J Physiol Heart Circ Physiol*. 2012;302:H893-900.

119. Gómez A, de V, Adelaide, Pushparajah K, Simpson J, Giese D, Schaeffter T, Penney G. 3D Intraventricular Flow Mapping from Colour Doppler Images and Wall Motion. In: Mori K, Sakuma I, Sato Y, Barillot C, Navab N, eds. *8150*. Springer Berlin Heidelberg; 2013:476-483.

120. Markl M, Kilner PJ, Ebbers T. Comprehensive 4D velocity mapping of the heart and great vessels by cardiovascular magnetic resonance. *J Cardiovasc Magn Reson*. 2011;13:1-22.

121. Uribe S, Beerbaum P, Sorensen TS, Rasmusson A, Razavi R, Schaeffter T. Four-dimensional (4D) flow of the whole heart and great vessels using real-time respiratory self-gating. *Magn Reson Med*. 2009;62:984-992.

122. Walker PG, Cranney GB, Scheidegger MB, Waseleski G, Pohost GM, Yoganathan AP. Semiautomated method for noise reduction and background phase error correction in MR phase velocity data. *Journal of Magnetic Resonance Imaging*. 1993;3:521-530.

123. Bernstein MA, Zhou XJ, Polzin JA, King KF, Ganin A, Pelc NJ, Glover GH. Concomitant gradient terms in phase contrast MR: analysis and correction. *Magnetic Resonance in Medicine*. 1998;39:300-308.

124. Markl M, Bammer R, Alley MT, Elkins CJ, Draney MT, Barnett A, Moseley ME, Glover GH, Pelc NJ. Generalized reconstruction of phase contrast MRI: analysis

and correction of the effect of gradient field distortions. *Magnetic resonance in medicine*. 2003;50:791-801.

125. Hess AT, Bissell MM, Ntusi NA, Lewis AJ, Tunnicliffe EM, Greiser A, Stalder AF, Francis JM, Myerson SG, Neubauer S, Robson MD. Aortic 4D flow: quantification of signal-to-noise ratio as a function of field strength and contrast enhancement for 1.5T, 3T, and 7T. *Magn Reson Med*. 2015;73:1864-1871.

126. Giese D, Schaeffter T, Kozerke S. Highly undersampled phase-contrast flow measurements using compartment-based k-t principal component analysis. *Magn Reson Med*. 2013;69:434-443.

127. Boussel L, Cernicanu A, Geerts L, Gamondes D, Khouatra C, Cottin V, Revel D, Douek P. 4D time-resolved magnetic resonance angiography for noninvasive assessment of pulmonary arteriovenous malformations patency. *J Magn Reson Imaging*. 2010;32:1110-1116.

128. Markl M, Geiger J, Jung B, Hirtler D, Arnold R. Noninvasive evaluation of 3D hemodynamics in a complex case of single ventricle physiology. *J Magn Reson Imaging*. 2012;35:933-937.

129. Bächler P, Valverde I, Pinochet N, Nordmeyer S, Kuehne T, Crelier G, Tejos C, Irarrazaval P, Beerbaum P, Uribe S. Caval blood flow distribution in patients with Fontan circulation: quantification by using particle traces from 4D flow MR imaging. *Radiology*. 2013;267:67-75.

130. Wong J, Mathur S, Giese D, Pushparajah K, Schaeffter T, Razavi R, Greil GF. Analysis of Aortopulmonary Window Using Cardiac Magnetic Resonance Imaging. *Circulation*. 2012;126:e228-e229.

131. Kilner PJ, Gatehouse PD, Firmin DN. Flow measurement by magnetic resonance: a unique asset worth optimising. *J Cardiovasc Magn Reson*. 2007;9:723-728.

132. Greil G, Geva T, Maier SE, Powell AJ. Effect of acquisition parameters on the accuracy of velocity encoded cine magnetic resonance imaging blood flow measurements. *J Magn Reson Imaging*. 2002;15:47-54.

133. Bonow RO, Mann DL, Zipes DP, Libby P. Braunwald's Heart Disease: A Textbook of Cardiovascular Medicine Saunders. *Philadelphia, PA*. 2011

134. Arvidsson PM, Toger J, Heiberg E, Carlsson M, Arheden H. Quantification of left and right atrial kinetic energy using four-dimensional intracardiac magnetic resonance imaging flow measurements. *J Appl Physiol (1985)*. 2013;114:1472-1481.

135. Suga H. Ventricular energetics. *Physiological reviews*. 1990;70:247-277.

136. Prec O, Katz LN, Sennett L, Rosenman… RH. Determination of kinetic energy of the heart in man. *American Journal of Physiology* 1949

137. Eriksson J, Bolger AF, Ebbers T, Carlhall CJ. Four-dimensional blood flow-specific markers of LV dysfunction in dilated cardiomyopathy. *Eur Heart J Cardiovasc Imaging*. 2013;14:417-424.

138. Muthurangu V, Taylor A, Andriantsimiavona R, Hegde S, Miquel ME, Tulloh R, Baker E, Hill DL, Razavi R. Novel method of quantifying pulmonary vascular resis-

tance by use of simultaneous invasive pressure monitoring and phase-contrast magnetic resonance flow. *Circulation*. 2004;110:826-834.

139. Vitiello R, McCrindle BW, Nykanen D, Freedom RM, Benson LN. Complications associated with pediatric cardiac catheterization. *Journal of the American College of Cardiology*. 1998;32:1433-1440.

140. Andreassi MG, Cioppa A, Manfredi S, Palmieri C, Botto N, Picano E. Acute chromosomal DNA damage in human lymphocytes after radiation exposure in invasive cardiovascular procedures. *Eur Heart J*. 2007;28:2195-2199.

141. Andreassi MG, Ait-Ali L, Botto N, Manfredi S, Mottola G, Picano E. Cardiac catheterization and long-term chromosomal damage in children with congenital heart disease. *Eur Heart J*. 2006;27:2703-2708.

142. Modan B, Keinan L, Blumstein T, Sadetzki S. Cancer following cardiac catheterization in childhood. *Int J Epidemiol*. 2000;29:424-428.

143. Bergersen L, Gauvreau K, Marshall A, Kreutzer J, Beekman R, Hirsch R, Foerster S, Balzer D, Vincent J, Hellenbrand W, Holzer R, Cheatham J, Moore J, Lock J, Jenkins K. Procedure-type risk categories for pediatric and congenital cardiac catheterization. *Circ Cardiovasc Interv*. 2011;4:188-194.

144. Shinozaki T, Deane RS, Mazuzan JE. The dynamic responses of liquid-filled catheter systems for direct measurements of blood pressure. *Anesthesiology*. 1980;53:498-504.

145. Tzifa A, Schaeffter T, Razavi R. MR imaging-guided cardiovascular interventions in young children. *Magn Reson Imaging Clin N Am*. 2012;20:117-128.

146. Burkhoff D, Mirsky I, Suga H. Assessment of systolic and diastolic ventricular properties via pressure-volume analysis: a guide for clinical, translational, and basic researchers. *Am J Physiol Heart Circ Physiol*. 2005;289:H501-12.

147. De Tombe PP, Jones S, Burkhoff D, Hunter WC, Kass DA. Ventricular stroke work and efficiency both remain nearly optimal despite altered vascular loading. *American Journal of Physiology*. 1993;264:H1817-H1817.

148. Tanoue Y, Sese A, Ueno Y, Joh K, Hijii T. Bidirectional Glenn Procedure Improves the Mechanical Efficiency of a Total Cavopulmonary Connection in High-Risk Fontan Candidates. *Circulation*. 2001;103:2176-2180.

149. Senzaki H, Masutani S, Ishido H, Taketazu M, Kobayashi T, Sasaki N, Asano H, Katogi T, Kyo S, Yokote Y. Cardiac rest and reserve function in patients with Fontan circulation. *J Am Coll Cardiol*. 2006;47:2528-2535.

150. Schmitt B, Steendijk P, Ovroutski S, Lunze K, Rahmanzadeh P, Maarouf N, Ewert P, Berger F, Kuehne T. Pulmonary vascular resistance, collateral flow, and ventricular function in patients with a Fontan circulation at rest and during dobutamine stress. *Circ Cardiovasc Imaging*. 2010;3:623-631.

151. Schmitt B, Steendijk P, Lunze K, Ovroutski S, Falkenberg J, Rahmanzadeh P, Maarouf N, Ewert P, Berger F, Kuehne T. Integrated assessment of diastolic and systolic ventricular function using diagnostic cardiac magnetic resonance catheterization: validation in pigs and application in a clinical pilot study. *JACC Cardiovasc Imaging*. 2009;2:1271-1281.

152. Suga H. Total mechanical energy of a ventricle model and cardiac oxygen consumption. *American Journal of Physiology-Heart and Circulatory Physiology*. 1979;236:H498-H505.

153. Suga H, Sagawa K. Mathematical interrelationship between instantaneous ventricular pressure-volume ratio and myocardial force-velocity relation. *Annals of biomedical engineering*. 1972;1:160-181.

154. Lang RM, Borow KM, Neumann A, Janzen D. Systemic vascular resistance: an unreliable index of left ventricular afterload. *Circulation*. 1986;74:1114-1123.

155. Burkhoff D, Sagawa K. Ventricular efficiency predicted by an analytical model. *Am J Physiol*. 1986;250:R1021-R1027.

156. Sunagawa K, Maughan WL, Sagawa K. Optimal arterial resistance for the maximal stroke work studied in isolated canine left ventricle. *Circulation Research*. 1985;56:586-595.

157. Chirinos JA. Ventricular-arterial coupling: Invasive and non-invasive assessment. *Artery Res*. 2013;7

158. Chirinos JA, Rietzschel ER, De Buyzere ML, De Bacquer D, Gillebert TC, Gupta AK, Segers P. Arterial Load and Ventricular-Arterial Coupling Physiologic Relations With Body Size and Effect of Obesity. *Hypertension*. 2009;54:558-566.

159. Redfield MM, Jacobsen SJ, Borlaug BA, Rodeheffer RJ, Kass DA. Age- and gender-related ventricular-vascular stiffening: a community-based study. *Circulation*. 2005;112:2254-2262.

160. Takeuchi M, Igarashi Y, Tomimoto S, Odake M, Hayashi T, Tsukamoto T, Hata K, Takaoka H, Fukuzaki H. Single-beat estimation of the slope of the end-systolic pressure-volume relation in the human left ventricle. *Circulation*. 1991;83:202-212.

161. Brimioulle S, Wauthy P, Ewalenko P, Rondelet B, Vermeulen F, Kerbaul F, Naeije R. Single-beat estimation of right ventricular end-systolic pressure-volume relationship. *American Journal of Physiology-Heart and Circulatory Physiology*. 2003;284:H1625-H1630.

162. Kuehne T, Yilmaz S, Steendijk P, Moore P, Groenink M, Saaed M, Weber O, Higgins CB, Ewert P, Fleck E, Nagel E, Schulze-Neick I, Lange P. Magnetic resonance imaging analysis of right ventricular pressure-volume loops: in vivo validation and clinical application in patients with pulmonary hypertension. *Circulation*. 2004;110:2010-2016.

163. Oosterhof T, Tulevski I, Roest A, Steendijk P, Vliegen H, van DW, Ernst, de R, Albert, Tijssen J, Mulder B. Disparity Between Dobutamine Stress and Physical Exercise Magnetic Resonance Imaging in Patients with an Intra-atrial Correction for Transposition of the Great Arteries. *J of Cardiovascular Magnetic Resonance*. 2005;7:383-389.

164. Robbers-Visser D, Luijnenburg SE, van den Berg J, Roos-Hesselink JW, Strengers JL, Kapusta L, Moelker A, Helbing WA. Safety and observer variability of cardiac magnetic resonance imaging combined with low-dose dobutamine stress-testing in patients with complex congenital heart disease. *Int J Cardiol*. 2011;147:214-218.

165. Robbers-Visser D, Jan Ten Harkel D, Kapusta L, Strengers JL, Dalinghaus M, Meijboom FJ, Pattynama PM, Bogers AJ, Helbing WA. Usefulness of cardiac magnetic

resonance imaging combined with low-dose dobutamine stress to detect an abnormal ventricular stress response in children and young adults after fontan operation at young age. *Am J Cardiol*. 2008;101:1657-1662.

166. Parish V, Valverde I, Kutty S, Head C, Qureshi SA, Sarikouch S, Greil G, Schaeffter T, Razavi R, Beerbaum P. Dobutamine stress MRI in repaired tetralogy of Fallot with chronic pulmonary regurgitation: a comparison with healthy volunteers. *Int J Cardiol*. 2013;166:96-105.

167. Strigl S, Beroukhim R, Valente AM, Annese D, Harrington JS, Geva T, Powell AJ. Feasibility of dobutamine stress cardiovascular magnetic resonance imaging in children. *J Magn Reson Imaging*. 2009;29:313-319.

168. Derrick GP, Narang I, White PA, Kelleher A, Bush A, Penny DJ, Redington AN. Failure of stroke volume augmentation during exercise and dobutamine stress is unrelated to load-independent indexes of right ventricular performance after the Mustard operation. *Circulation*. 2000;102:Iii-154.

169. Hjortdal VE, Emmertsen K, Stenbog E, Frund T, Schmidt MR, Kromann O, Sorensen K, Pedersen EM. Effects of exercise and respiration on blood flow in total cavopulmonary connection: a real-time magnetic resonance flow study. *Circulation*. 2003;108:1227-1231.

170. Giese D, Wong J, Greil GF, Buehrer M, Schaeffter T, Kozerke S. Towards highly accelerated Cartesian time-resolved 3D flow cardiovascular magnetic resonance in the clinical setting. *J Cardiovasc Magn Reson*. 2014;16:42.

171. Pedersen H, Kozerke S, Ringgaard S, Nehrke K, Kim WY. k-t PCA: temporally constrained k-t BLAST reconstruction using principal component analysis. *Magn Reson Med*. 2009;62:706-716.

172. Knobloch V, Boesiger P, Kozerke S. Sparsity transform k t principal component analysis for accelerating cine three dimensional flow measurements. *Magnetic Resonance in Medicine*. 2013;70:53-63.

173. Zhang Z, Tendulkar A, Sun K, Saloner DA, Wallace AW, Ge L, Guccione JM, Ratcliffe MB. Comparison of the Young-Laplace law and finite element based calculation of ventricular wall stress: implications for postinfarct and surgical ventricular remodeling. *Ann Thorac Surg*. 2011;91:150-156.

174. Toussaint N, Mansi T, Delingette H, Ayache N, Sermesant M. An integrated platform for dynamic cardiac simulation and image processing: application to personalised tetralogy of fallot simulation. 2008;Proceedings of the First Eurographics conference on Visual Computing for Biomedicine:21-28.

175. Schnabel JA, Rueckert D, Quist M, Blackall JM, Castellano-Smith AD, Hartkens T, Penney GP, Hall WA, Liu H, Truwit CL. A generic framework for non-rigid registration based on non-uniform multi-level free-form deformations. 2001;Medical Image Computing and Computer-Assisted Intervention–MICCAI 2001:573-581.

176. Shi W, Zhuang X, Wang H, Duckett S, Luong DVN, Tobon-Gomez C, Tung K, Edwards PJ, Rhode KS, Razavi RS. A comprehensive cardiac motion estimation framework using both untagged and 3-d tagged mr images based on nonrigid registration. *Medical Imaging, IEEE Transactions on*. 2012;31:1263-1275.

177. Yushkevich PA, Piven J, Hazlett HC, Smith RG, Ho S, Gee JC, Gerig G. User-guided 3D active contour segmentation of anatomical structures: significantly improved efficiency and reliability. *Neuroimage*. 2006;31:1116-1128.

178. Baum CF. Stata tip 63: Modeling proportions. *Stata Journal*. 2008;8:299.

179. Buechel EV, Kaiser T, Jackson C, Schmitz A, Kellenberger CJ. Normal right- and left ventricular volumes and myocardial mass in children measured by steady state free precession cardiovascular magnetic resonance. *J Cardiovasc Magn Reson*. 2009;11:19.

180. Sarikouch S, Peters B, Gutberlet M, Leismann B, Kelter-Kloepping A, Koerperich H, Kuehne T, Beerbaum P. Sex-specific pediatric percentiles for ventricular size and mass as reference values for cardiac MRI: assessment by steady-state free-precession and phase-contrast MRI flow. *Circ Cardiovasc Imaging*. 2010;3:65-76.

181. Sluysmans T, Colan SD. Theoretical and empirical derivation of cardiovascular allometric relationships in children. *J Appl Physiol (1985)*. 2005;99:445-457.

182. Gutgesell HP, Rembold CM. Growth of the human heart relative to body surface area. *The American journal of cardiology*. 1990;65:662-668.

183. Rathod RH, Prakash A, Kim YY, Germanakis IE, Powell AJ, Gauvreau K, Geva T. Cardiac magnetic resonance parameters predict transplantation-free survival in patients with Fontan circulation. *Circulation: Cardiovascular Imaging*. 2014;7:502-509.

184. Bossers SSM, Kapusta L, Kuipers IM, van Iperen G, Moelker A, Kroft LJM, Romeih S, de Rijke Y, ten Harkel ADJ, Helbing WA. Ventricular function and cardiac

reserve in contemporary Fontan patients. *International journal of cardiology*. 2015;196:73-80.

185. Pushparajah K, Wong JK, Bellsham-Revell HR, Hussain T, Valverde I, Bell A, Tzifa A, Greil G, Simpson JM, Kutty S, Razavi R. Magnetic resonance imaging catheter stress haemodynamics post-Fontan in hypoplastic left heart syndrome. *Eur Heart J Cardiovasc Imaging*. 2015

186. Patterson SW, Starling EH. On the mechanical factors which determine the output of the ventricles. *J Physiol*. 1914;48:357-379.

187. Patterson SW, Piper H, Starling EH. The regulation of the heart beat. *The Journal of physiology*. 1914;48:465.

188. Ratshin RA, Rackley CE, Russell RO. Determination of Left Ventricular Preload and Afterload by Quantitative Echocardiography in Man: Calibration of the Method. *Circulation Research*. 1974;34:711-718.

189. Bossers SSM, Helbing WA, Duppen N, Kuipers IM, Schokking M, Hazekamp MG, Bogers AJJC, Ten Harkel ADJ, Takken T. Exercise capacity in children after total cavopulmonary connection: Lateral tunnel versus extracardiac conduit technique. *The Journal of thoracic and cardiovascular surgery*. 2014;148:1490-1497.

190. Starling MR. Left ventricular-arterial coupling relations in the normal human heart. *American heart journal*. 1993;125:1659-1666.

191. Kouatli AA, Garcia JA, Zellers TM, Weinstein EM, Mahony L. Enalapril does not enhance exercise capacity in patients after Fontan procedure. *Circulation*. 1997;96:1507-1512.

192. Gewillig MH, Lundström UR, Bull C, Wyse RKH, Deanfield JE. Exercise responses in patients with congenital heart disease after Fontan repair: patterns and determinants of performance. *Journal of the American College of Cardiology*. 1990;15:1424-1432.

193. Driscoll DJ, Danielson GK, Puga FJ, Schaff HV, Heise CT, Staats BA. Exercise tolerance and cardiorespiratory response to exercise after the Fontan operation for tricuspid atresia or functional single ventricle. *Journal of the American College of Cardiology*. 1986;7:1087-1094.

194. Akazawa S, Shimizu R, Kasuda H, Nemoto K, Yoshizawa Y, Inoue S. Effects of sevoflurane on cardiovascular dynamics, coronary circulation and myocardial metabolism in dogs. *J Anesth*. 1988;2:227-241.

195. Kazmaier S, Hanekop GG, Buhre W, Weyland A, Busch T, Radke OC, Zoelffel R, Sonntag H. Myocardial consequences of remifentanil in patients with coronary artery disease. *Br J Anaesth*. 2000;84:578-583.

196. Chanavaz C, Tirel O, Wodey E, Bansard JY, Senhadji L, Robert JC, Ecoffey C. Haemodynamic effects of remifentanil in children with and without intravenous atropine. An echocardiographic study. *Br J Anaesth*. 2005;94:74-79.

197. Janz RF, Ozpetek S, Ginzton LE, Laks MM. Regional stress in a noncircular cylinder. *Biophysical journal*. 1989;55:173-182.

198. Quaife RA, Chen MY, Lynch D, Badesch DB, Groves BM, Wolfel E, Robertson AD, Bristow MR, Voelkel NF. Importance of right ventricular end-systolic regional wall

stress in idiopathic pulmonary arterial hypertension: a new method for estimation of right ventricular wall stress. *European journal of medical research*. 2006;11:214.

199. Lev M. Pathologic anatomy and interrelationship of hypoplasia of the aortic tract complexes. *Laboratory investigation; a journal of technical methods and pathology*. 1952;1:61.

200. Wong J, Chabiniok R, de Vecchi A, Dedieu N, Sammut E, Schaeffter T, Razavi R. Age-related changes in intra-ventricular kinetic energy: a physiological or pathological adaptation. *Am J Physiol Heart Circ Physiol*. 2016ajpheart.00075.2015.

201. Zajac J, Eriksson J, Dyverfeldt P, Bolger AF, Ebbers T, Carlhäll CJ. Turbulent kinetic energy in normal and myopathic left ventricles. *Journal of Magnetic Resonance Imaging*. 2015;41:1021-1029.

202. Steding-Ehrenborg K, Arvidsson PM, Töger J, Rydberg M, Heiberg E, Carlsson M, Arheden H. Determinants of kinetic energy of blood flow in the four-chambered heart in athletes and sedentary controls. *Am J Physiol Heart Circ Physiol*. 2016;310:H113-22.

203. Carlhall CJ, Bolger A. Passing strange: flow in the failing ventricle. *Circ Heart Fail*. 2010;3:326-331.

204. Eriksson J, Dyverfeldt P, Engvall J, Bolger AF, Ebbers T, Carlhall CJ. Quantification of presystolic blood flow organization and energetics in the human left ventricle. *Am J Physiol Heart Circ Physiol*. 2011;300:H2135-41.

205. Giese D, Knobloch V, Schaeffter T, Pedersen H, Kozerke S. Spatio-temporally constrained reconstruction for highly accelerated flow MRI. *J Cardiovasc Magn Reson*. 2010;12:P73.

206. Cordina RL, O'Meagher S, Karmali A, Rae CL, Liess C, Kemp GJ, Puranik R, Singh N, Celermajer DS. Resistance training improves cardiac output, exercise capacity and tolerance to positive airway pressure in Fontan physiology. *International journal of cardiology*. 2013;168:780-788.

207. Shafer KM, Garcia JA, Babb TG, Fixler DE, Ayers CR, Levine BD. The importance of the muscle and ventilatory blood pumps during exercise in patients without a subpulmonary ventricle (Fontan operation). *Journal of the American College of Cardiology*. 2012;60:2115-2121.

208. Foll D, Taeger S, Bode C, Jung B, Markl M. Age, gender, blood pressure, and ventricular geometry influence normal 3D blood flow characteristics in the left heart. *Eur Heart J Cardiovasc Imaging*. 2013;14:366-373.

209. Kramer CM, Barkhausen J, Flamm SD, Kim RJ, Nagel E. Standardized cardiovascular magnetic resonance imaging (CMR) protocols, society for cardiovascular magnetic resonance: board of trustees task force on standardized protocols. *J Cardiovasc Magn Reson*. 2008;10:35.

210. Alfakih K, Plein S, Bloomer T, Jones T, Ridgway J, Sivananthan M. Comparison of right ventricular volume measurements between axial and short axis orientation using steady-state free precession magnetic resonance imaging. *u§ruhtg99k1*. 2003;gt9g9:25-32.

211. Winter MM, Bernink FJ, Groenink M, Bouma BJ, van Dijk AP, Helbing WA, Tijssen JG, Mulder BJ. Evaluating the systemic right ventricle by CMR: the importance of consistent and reproducible delineation of the cavity. *J Cardiovasc Magn Reson*. 2008;10:40.

212. Curtis JP, Sokol SI, Wang Y, Rathore SS, Ko DT, Jadbabaie F, Portnay EL, Marshalko SJ, Radford MJ, Krumholz HM. The association of left ventricular ejection fraction, mortality, and cause of death in stable outpatients with heart failure. *Journal of the American College of Cardiology*. 2003;42:736-742.

213. Kanski M, Arvidsson PM, Töger J, Borgquist R, Heiberg E, Carlsson M, Arheden H. Left ventricular fluid kinetic energy time curves in heart failure from cardiovascular magnetic resonance 4D flow data. *J Cardiovasc Magn Reson*. 2015;17:111.

214. Svalbring E, Fredriksson A, Eriksson J, Dyverfeldt P, Ebbers T, Bolger AF, Engvall J, Carlhäll CJ. Altered Diastolic Flow Patterns and Kinetic Energy in Subtle Left Ventricular Remodeling and Dysfunction Detected by 4D Flow MRI. *PLoS One*. 2016;11:e0161391.

215. Ponzini R, Vergara C, Redaelli A, Veneziani A. Reliable CFD-based estimation of flow rate in haemodynamics measures. *Ultrasound Med Biol*. 2006;32:1545-1555.

216. Chabiniok R, Wong J, Giese D, Nordsletten D, Shi W, Greil G, Rueckert D, Razavi R, Schaeffter T, Smith N. Flow analysis in cardiac chambers combining phase contrast, 3D tagged and cine MRI. eds. *Functional Imaging and Modeling of the Heart*. Springer; 2013:360-369.

217. Hinghofer-Szalkay H. Method of high-precision microsampled blood and plasma mass densitometry. *Journal of Applied Physiology*. 1986;60:1082-1088.

218. Aiyagari R, Rhodes JF, Shrader P, Radtke WA, Bandisode VM, Bergersen L, Gillespie MJ, Gray RG, Guey LT, Hill KD, Hirsch R, Kim DW, Lee KJ, Pelech AN, Ringewald J, Takao C, Vincent JA, Ohye RG, Pediatric HNI. Impact of pre-stage II hemodynamics and pulmonary artery anatomy on 12-month outcomes in the Pediatric Heart Network Single Ventricle Reconstruction trial. *J Thorac Cardiovasc Surg*. 2014;148:1467-1474.

219. McGuirk SP, Stickley J, Griselli M, Stumper OF, Laker SJ, Barron DJ, Brawn WJ. Risk assessment and early outcome following the Norwood procedure for hypoplastic left heart syndrome. *Eur J Cardiothorac Surg*. 2006;29:675-681.

220. Horer J, Malcic I, Schreiber C, Lange R. False aneurysm origination from the proximal anastomosis of a right ventricular to pulmonary artery shunt following staged repair of hypoplastic left heart syndrome. *Interact Cardiovasc Thorac Surg*. 2011;12:487-489.

221. Januszewska K, Kozlik-Feldmann R, Dalla-Pozza R, Greil S, Abicht J, Netz H, Reichart B, Malec E. Right ventricle-to-pulmonary artery shunt related complications after Norwood procedure. *Eur J Cardiothorac Surg*. 2011;40:584-590.

222. Tanoue Y, Kado H, Shiokawa Y, Fusazaki N, Ishikawa S. Midterm Ventricular Performance After Norwood Procedure With Right Ventricular–Pulmonary Artery Conduit. *The Annals of thoracic surgery*. 2004;78:1965-1971.

223. Graham EM, Atz AM, Bradley SM, Scheurer MA, Bandisode VM, Laudito A, Shirali GS. Does a ventriculotomy have deleterious effects following palliation in the

Norwood procedure using a shunt placed from the right ventricle to the pulmonary arteries? *Cardiology in the young*. 2007;17:145-150.

224. Frommelt PC, Guey LT, Minich LL, Bhat M, Bradley TJ, Colan SD, Ensing G, Gorentz J, Heydarian H, John JB, Lai WW, Levine JC, Mahle WT, Miller SG, Ohye RG, Pearson GD, Shirali GS, Wong PC, Cohen MS. Does initial shunt type for the Norwood procedure affect echocardiographic measures of cardiac size and function during infancy?: the Single Vventricle Reconstruction trial. *Circulation*. 2012;125:2630-2638.

225. Giese D, Kabbasch C, Hedderich D, Maintz D, Liebig T, Bunck A. The use of k-t PCA accelerated dual-venc 3D flow MRI to assess hemodynamics before and after flow diverting stent implantation in cerebral aneurysm models. *J Cardiovasc Magn Reson*. 2014;16:W29.

226. Töger J, Kanski M, Carlsson M, Kovács SJ, Söderlind G, Arheden H, Heiberg E. Vortex ring formation in the left ventricle of the heart: analysis by 4D flow MRI and Lagrangian coherent structures. *Ann Biomed Eng*. 2012;40:2652-2662.